Towards more sustainable materials for boat decking:

Novel fillers for light-weighting and enhanced recyclability

Michael Donald Pittaway

2023

Towards more sustainable materials for boat decking:

Novel fillers for light-weighting and enhanced recyclability

Michael Donald Pittaway

A thesis submitted in fulfilment of the requirements of the Manchester Metropolitan University for the degree of Master of Science by Research.

School of Science and the Environment

Faculty of Science and Engineering

Manchester Metropolitan University

2023

Dedication

I offer my sincerest thanks to both my parents for their continued and vital support. Without this I could not have completed this project.

Acknowledgements

Firstly, a humble thank you to Manchester Metropolitan University and Flexiteek (industrial Sponsor) for providing the opportunity, facilities, and crucial support, during these uncertain times (during the Covid period), for me to undertake my MSc (Research) project.

Special thanks to my principal supervisor, Dr Ian Ingram, for providing much needed support and guidance, throughout project duration. I would also like to thank Dr Michele Edge and Dr Lubomira Tosheva, who have also provided excellent support and invaluable expertise, during project duration. Dr Edge who, although retired and a visiting fellow, has spent considerable time assisting my understanding of key areas of polymer science and writing skills.

Finally, a tremendous thank you, to all MMU Technical Staff, for their amazing contributions toward instrumental analysis and support, throughout project progression.

Acronyms/Abbreviations (alphabetical listing)

ACC	Amorphous calcium carbonate

ASTM D638	American Society for Testing and Materials (ASTM) Standard Test Method for Tensile Properties of Plastics (D638) specifies methods for testing the tensile strength of plastics and for calculating mechanical properties, and outlines accuracy requirements for the test frames and accessories used.
BS2782 320A	British Standard (BS) Method of testing plastics (BS2782 320A) Mechanical properties, Tensile strength, elongation and elastic modulus
CFRP	Carbon fibre reinforced polymer
CTAB	Cetyltrimethylammonium bromide
DSC	Differential Scanning Calorimetry
E	Young's (Elastic) modulus
FEG	Field emission gun
HDT	Heat deflection temperature
GCC	Ground (coarse) calcium carbonate
GFRP	Glass fibre reinforced polymer
HGS	Hollow glass spheres
iM30K	Engineered hollow microspheres made of soda-lime borosilicate glass with a true density of 0.60 g/cm³
iM16K	Engineered hollow microspheres made of soda-lime borosilicate glass with a true density of 0.46 g/cm³
κ (or λ)	Thermal conductivity (units: W.m.K)
K-value	Indicator of molecular weight and degree of polymerization of a PVC polymer. K70-75 are high K value resins which gives best mechanical properties but are more difficult to process
PCC	Precipitated (fine) calcium carbonate
ρ	Density (units: g/cm^3 or kg/m^3)
SDS	Sodium Dodecyl Sulfate (= surfactant)
SEM	Scanning electron microscopy
TEM	Transmission electron microscopy
W/O	Water-in-oil
XRD	X-ray diffraction

Polymer Acronyms

ABS	Acrylonitrile butadiene styrene

CA	Cellulose acetate
CPE	Chlorinated polyethylene
CPVC	Chlorinated polyvinyl chloride
EPDM	Ethylene propylene diene monomer
EVA	Ethylene vinyl actetate
LAO	Linear alpha-olefin
PAA	Polyacrylic acid
PC	Polycarbonate
PDADMAC	Polydiallyldimethylammonium chloride (PDDA)
PE	Polyethylene
PEEK	Polyether ether ketone
PEG	Polyethylene glycol
PEO	Polyethylene oxide
PET	Polyethyelene terephthalate
PMMA	Polymethyl methacrylate
POE	Polyolefin elastomers
POM	Polyoxymethylene
POP	Polyolefin plastomers
PP	Polypropylene
PS	Polystyrene
PSMA	Styrene-maleic anhydride copolymers
PTFE	Polytetrafluoroethylemne
PVC	Polyvinyl chloride
PVC-P	Polyvinyl chloride, plasticised
PVC-U	Polyvinyl chloride, unplasticized
PVP	Polyvinylpyrrolidine
TPE	Thermoplastic elastomer
TPU	Thermoplastic polyurethane

Abstract

In this study selected hollow fillers in several polymers and polymer blends have been evaluated for use in composite boat decking. Traditionally teak has been the material of choice for boat decking, but there are now concerns regarding sustainable management of this material. Synthetic polymers now dominate the market, due largely to easier installation and maintenance; with PVC being the polymer frequently used in boat decking. The decking takes the form of strips, rolls or prefabricated panels. A particular focus of recent development has been to enhance thermal insulation (reduce temperature underfoot) and lower the density of the material. Although hollow glass microspheres tend to be the material of choice to achieve these properties, they can be abrasive on processing equipment and difficult to recycle. Hence the focus of this work has centred on hollow calcium carbonate in PVC, because calcium carbonate is used as a filler throughout the PVC industry. The rationale is that end-of-life decking could be more easily close-loop recycled or, regrind directed to a wide-range of alternative PVC applications, thereby enhancing sustainability of the product. At present hollow calcium carbonate is not in widespread commercial production, therefore in this study hollow calcium carbonate was synthesised by templating with a cationic polymer (PDADMAC or PDDA) to direct 3D assembly of hollow structures. The influence of template concentration, mixing time and order of addition of components was evaluated. Both spherical and rhombohedral polymorphs of calcium carbonate were produced. The latter was incorporated in plasticised PVC at filler fractions of 15 wt.% and 24 wt.%. The performance of calcium carbonate was assessed against hollow glass filler in PVC. In addition, predictions using calculations based on volume fraction, for alternative fillers (e.g., cork and expanded microspheres), polymers (epoxy and polyester resins) and polymer blends (PVC/TPU, PVC/Nitrile rubber, PVC/CPE, PVC/CPVC, PE/CPE, PE/CPVC) were undertaken, with a view to optimising product performance.

List of Figures

Figure 3.37 Thermogravimetric weight loss (%) for PVC formulations containing hollow glass spheres (15 wt.% and 24 wt.%) and hollow calcium carbonate (15 wt.% and 24 wt.%), under isothermal conditions at 180°C (ramp rate 100°C/min) for 90 minutes under nitrogen

Figure 3.38 Thermogravimetric weight loss (%) for PVC formulations containing hollow glass spheres (15 wt.% and 24 wt.%) and hollow calcium carbonate (15 wt.% and 24 wt.%), under isothermal conditions at 180°C (ramp rate 100°C/min) under nitrogen, at 10 minutes (a) and 10-90 minutes (b).

Figure 3.39 Thermal conductivity (W/m.K) of PVC composite with filler levels of 15 wt.% and 24 wt.% (Expancel filler at 3 wt.%). Predicted data from a range of sources (commercial specification sheets, matmatch [100], matweb [101])

Figure 3.40 Density (g cm^{-3}) of polymers and polymer blends. Data obtained from a range of sources (commercial specification sheets, matmatch [100], matweb [101])

Figure 3.41 Thermal conductivity (W/m.K) of polymers and polymer blends. Data obtained from a range of sources (commercial specification sheets, matmatch [100], matweb [101])

Figure 3.42 Thermal conductivity (W/m.K) versus density (g cm^{-3}) for composite polymers (listed in **Figs. 3.40 and 3.41**) with filler (IM16K) at 15 wt.%. Predicted data using from a range of sources (commercial specification sheets, matmatch [100], matweb [101])

Figure 3.43 Thermal conductivity (W/m.K) versus density (g cm^{-3}) for composite polymers (listed in **Figs. 3.40 and 3.41**) with filler (IM16K) at 24 wt.%. Predicted data using from a range of sources (commercial specification sheets, matmatch [100], matweb [101])

Figure 3.44 Thermal conductivity (W/m.K) versus density (g cm^{-3}) for composite polymers (listed in **Figs. 3.40 and 3.41**) with filler (spherical, hollow calcium carbonate) at 15 wt.%. Predicted data using from a range of sources (commercial specification sheets, matmatch [100], matweb [101])

Figure 3.45 Thermal conductivity (W/m.K) versus density (g cm^{-3}) for composite polymers (listed in **Figs. 3.40 and 3.41**) with filler (cork) at 15 wt.%. Predicted data using from a range of sources (commercial specification sheets, matmatch [100], matweb [101])

Figure 3.46 Thermal conductivity (W/m.K) versus density (g cm^{-3}) for composite polymers (listed in **Figs. 3.40 and 3.41**) with filler (Expancel (ρ=0.06 g/cm^3) at 3wt.%. Predicted data using from a range of sources (commercial specification sheets, matmatch [100], matweb [101])

List of Tables

Contents

1 Background and General Introduction

1.1 Background

In this thesis materials used as surface covering for the construction and renovation of marine vessels are evaluated. Here the surface covering will be referred to as boat decking in its wider context and, more specifically as yacht decking. This is to distinguish these materials from those labelled marine decking, which includes boardwalk and associated marine applications. It is estimated that there are 6 million boats, owned, within the EU alone and as such the materials that constitute these vessels present a significant environmental footprint.

The choice of materials for boat decking depends mainly on aesthetics (especially those for high-end ocean-going yachts), with the principal driver being the use of wood or synthetic materials that simulate its appearance. While teak has traditionally been the material of choice for boat decking, synthetic polymers have made significant inroads, largely due to easier installation and maintenance. The decking takes the form of strips (teak), rolls (synthetics) or prefabricated panels (plywood, teak, or synthetics). The difficulties of laying a teak deck usually require professional installation, whilst do-it-yourself options are available for synthetic deck by following manufacturers recommendations.

Several properties are key to product performance. The decking material must be non-slip, provide thermal (and sound) insulation, and be resistant to salt water and UV exposure. The collection of water beneath the decking should be prevented and this is normally achieved using adhesives. Also, water run-off channels must be included between adjoining elements, especially around deck fittings. In addition to this, the key driver directing current research and development is to reduce the weight of the decking (in-line with reducing fuel consumption and costs) and improve environmental performance (reduced toxicity, prevention of microplastics and/or enhanced recyclability).

The research presented in this thesis identifies and evaluates materials for boat decking with a view to enhanced sustainability.

1.2 Materials already used in Boat Decking

Materials used in boat decking range are wide-ranging. This section begins with a review of the important classes of materials used, along with their key properties, advantages, and disadvantages. Finally, a window of properties and costs is identified by comparing commercial decking products and the potential for more sustainable options introduced.

1.2.1 Natural Wood and Wood Related Products

Wood has been the traditional material used for boat building, including decking, for centuries. Wood is a composite of polymer fibres (cellulose and hemicellulose) in a polymer matrix (lignin) (**Figure 1.1**(a)**)** [1]**.** Wood is still one of the best engineering materials in current use. The alignment of cellulose nano and microfibrils at approximately 45 degrees produces a fibre that is wound in a similar manner to a rope. When embedded in lignin the fibres result in an anisotropic structure that has high directional strength (depending on whether forces are parallel or perpendicular to the grain) (**Figure 1.1**(b)**)**.

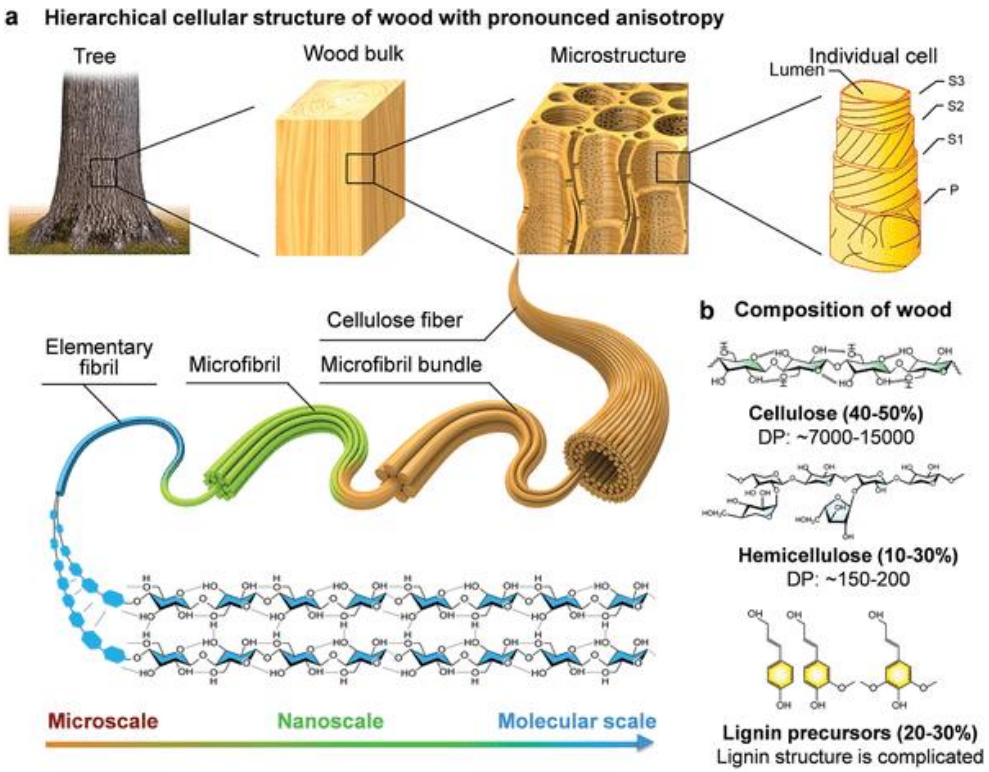

Figure 1.1 The structure (a) and composition (b) of wood (Reproduced from [2])

Hardwood was the early material of choice for boat decking, due to mechanical property requirements and weather resistance. It is important to recognise that the names hardwood and softwood can be misleading: softwood isn't always harder than hardwood and voice-versa. Instead, hardwood (e.g., oak, teak, mahogany) comes from deciduous trees (leaves are shed in winter), while softwood (e.g., pine, spruce) comes from evergreen trees. The comparison of general characteristics between hardwoods and softwoods given in **Table 1.1** below show why hardwoods have been prevalent in boat-decking.

Table 1.1 General comparison of the properties of hardwoods and softwoods important in boat decking

Hardwood	Softwood
• Darker colour • Heavy • More expensive • Lifetime several decades • Natural weather resistance • More environmental impact source material	• Lighter colour • Lighter weight • Less expensive • Lifetime over a decade • Weather resistant when treated • Less environmental impact source material

1.2.1.1 Teak

Teak is a slow-growing tropical hardwood. Because teak is resistant to rot by fungi and mildew, has a low shrinkage ratio to fluctuating moisture levels, high tensile strength, and tight grain, it has been the boat-building material of choice for over 2000 years. Furthermore, it has high levels of teak oil, close to surfaces when planks are cut, providing a natural oiled finish, giving untreated teak an attractive silver-grey appearance on weathering (**Figure 1.2 (a)**). The natural wearing also removes the 'summer' growth bands, resulting in a natural non-slip surface. However, in practice the teak oil is removed during maintenance by sanding and cleaning processes and to facilitate gluing and re-caulking. Treating with finishing agents such as linseed oil or varnish enhances the appearance of the teak (**Figure 1.2 (b)**), but this changes the innate properties and shortens lifetime. Other problems have also driven the

replacement of teak. One of these is that teak absorbs heat making it uncomfortable to walk on in bare feet in hot climates. However, the main issue is, being slow growing, poor forestry practice often negates sustainable management of this important resource. Most of the native teak forests are located, in Myanmar, Laos and India, according to molecular genetics [3].

(a) (b)

Figure 1.2 Appearance of Teak Boat-Deck (Reproduced from [4])

1.2.1.2 Modified Softwood

In contrast to hardwoods, softwoods require treatment before they can be used for any length of time in a harsh ocean environment. Most softwood used is pine (fast growing and sustainably harvested), treated by either acetylation (e.g., Accoya®) or resin (PUF) impregnation (Lignia®) (**Figure 1.3**). These processes improve durability (UV and water and fungal attack) and dimensional stability. It is claimed that these treatments can extend the material lifetime to 50 years. They are also faster to dry when wetted than teak, but the costs associated with laying a deck are similar.

Figure 1.3 Appearance of Lignia® Boat-Deck (22-year-old resin impregnated) Monterey pine boards) (Reproduced from [5])

There has also been significant interest in wood-plastic composites. These products are currently used in boardwalk applications. However, the material composites, in present commercial production, do not meet the stringent property requirements for boat decking (dimensional stability and durability). Furthermore, they offer little in the way of additional engineering benefits. This is not surprising because the addition of wood (short fibres, flour) serves more as a filler, rather than as an embedded (long) fibre offering directional reinforcement.

1.2.1.3 Cork

Although considered a wood product, in contrast to the structure of wood, cork consists of hexagonal (or pentagonal) cells with a highly porous structure, like a honeycomb (**Figure 1.4**). There is a complex cell wall, with the primary layer being abundant in lignin, the secondary layer built from alternating suberin and wax deposits and a thin tertiary layer of polysaccharides. Suberin is a biopolymer based on polyester, which is formed from suberin acids (long-chain fatty acids) and glycerol. The suberin and wax render this material highly impermeable to water. In addition, the cells are filled with an air-like gas mixture. This gives the cork buoyancy (low density), an ability to recover after compression and, good thermal insulation.

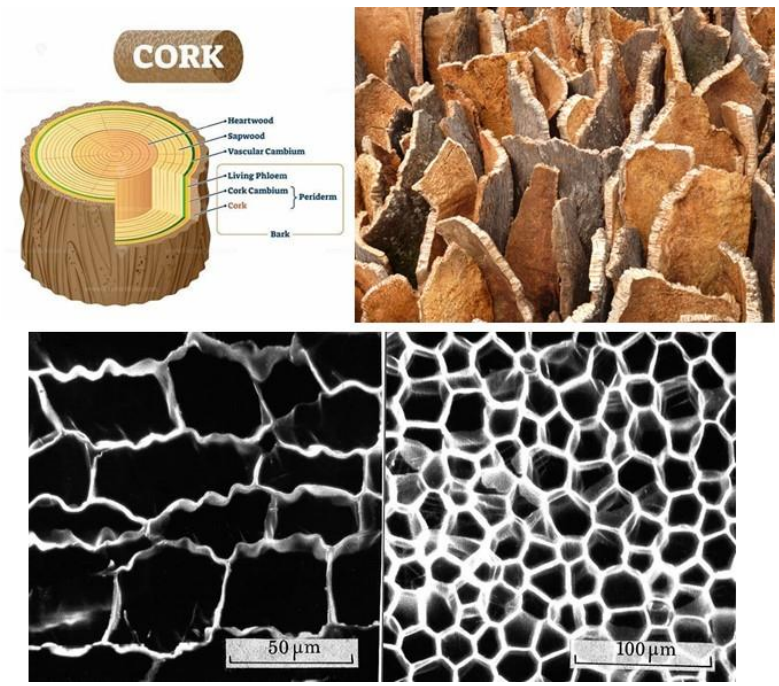

Figure 1.4 Porous, honeycomb structure of cork (Reproduced from [6])

Cork is usually stripped from the trunks of trees every 9 years, after they are 25 years old. Because the cork tree is not cut down, cork is widely regarded as environmentally sustainable [7]. Most cork is found in Portugal (34%) and Spain (27%), but there are about 2.2 million hectares of cork forest worldwide [8].

In practice, the cork used in boat-decks is a composite of cork granules embedded in a synthetic binder (e.g., polyurethane), pressed together under high pressure (see **Figure 1.5**). Cork's inherent resilience means that it is noticeably better than teak at resisting wear and abrasion. As for teak it takes on a grey hue on weathering, but unlike teak it can be sanded back to reveal the original colour with little loss of properties. The size of the cork grains is important though, with larger cork grains offering better impact properties.

Figure 1.5 Appearance of Cork Boat-Deck (polyurethane resin binder) (Reproduced from [9])

1.2.2 Synthetic Polymer-Based Products

1.2.2.1 Closed-Cell (expanded) Foam

The foams used in boat decking typically use PE (polyethylene) and/or EVA (ethylene vinyl acetate). These foams are closed-cell, rather like the cell structure of cork (in **Figure 1.4**). **Figure 1.6** compares the structures of open-cell and closed cell foam. In open-cell foams the connected porous pathways yield a softer, more flexible foam that is more friable and less durable than closed-cell foam. Closed-cell foam is firmer, more rigid and insulating to air.

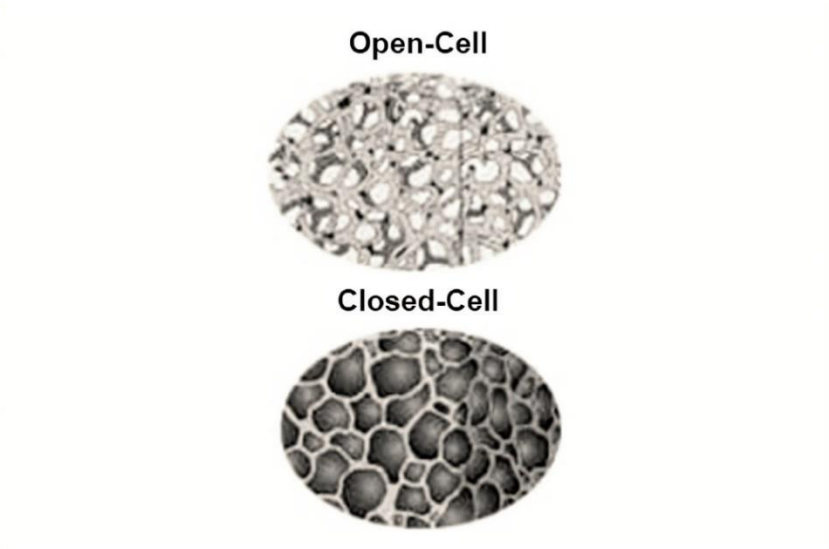

Figure 1.6 Structure of open-cell and closed-cell foam (Reproduced from [10])

The foam structure is partly determined by the base polymer and partly by the method of manufacture. The manufacturing process pumps gas (usually nitrogen) at high pressure into liquid polymer or by adding gas-forming agents (blowing agents) into the polymer. The packing and size of the (irregular) gas bubbles determine the density and rigidity of the foam. Because of the gas-filled closed-cell structure the foam is waterproof, durable, easy to manipulate and cut to required shapes and sizes. It is cushioned underfoot, has good grip and shock absorbing properties. It can be rolled for easy transport, but when affixed to the boat deck gives the appearance of a rigid, wood-based product (**Figure 1.7**).

Figure 1.7 Appearance of EVA and PE Boat-Deck (closed-cell foam) (Reproduced from [11])

1.2.2.2 Thermoset Resins and Resin Composites

Thermosets comprise at least two components; the polymer resin (Part A) and a co-reactant, referred to as hardener or curing catalyst (Part B). The ratio of these two components influences the curing behaviour and properties of the thermoset. The components are liquids or low melting constituents that solidify after mixing when cross-linking reactions take place (curing).

Epoxy-resins are commonly used for this purpose. The oxirane ring in the epoxy structure is strained, so this functionality is highly reactive to network formation by reaction with the hardener (**Figure 1.8**).

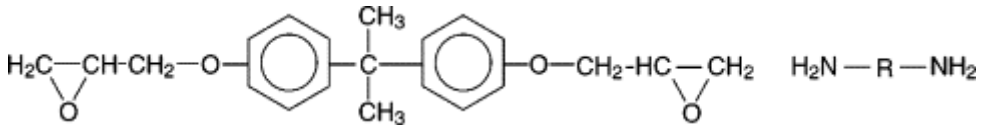

Figure 1.8 Reactive components of an epoxy resin: Epoxy bisphenol A diglycidyl ether and diamine hardener.

Ring-opening of the oxirane generates an OH-group that undergoes nucleophilic attack by the hardener (e.g., amines, anhydrides, phenols) to generate cross-links. This is illustrated in **Figure 1.9** for the NH-group of an amine. Using polyfunctional amines a rigid three-dimensional network is formed.

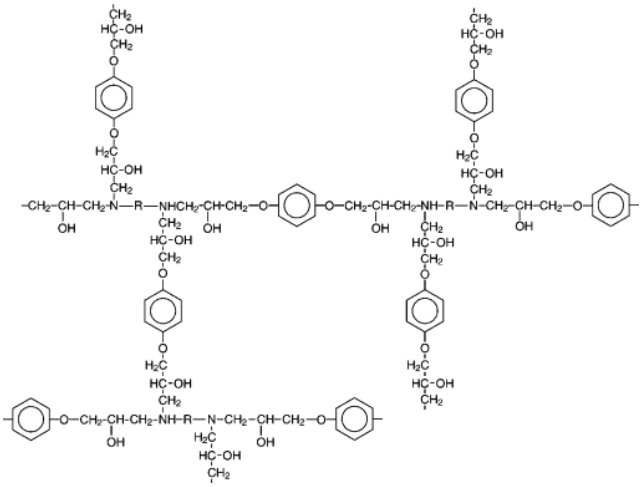

Figure 1.9 Crosslinked network structure of bisphenol A diglycidyl ether and diamine hardener.

Other resins are based on unsaturated polyesters, and polyurethanes. Older resins may be based on phenolic resins (melamine-formaldehyde, urea-formaldehyde).

The advantage of such thermoset resins is that they can be manufactured in a seamless manner, i.e., the caulking doesn't go right through the decking strips, so water resistance (by leakage) is prevented (**Figure 1.10**).

Figure 1.10 Polyurethane resin bound cork granules with caulking in top layer

Due to health and environmental concerns with bisphenol-A and the difficulties of recycling thermosets, recent decking has utilised bio-based resins. The finished appearance of the bio-based thermoset decking is seen in **Figure 1.11**.

Figure 1.11 Appearance of decking based on bio-based thermoset materials

1.2.2.3 Thermoplastics and Thermoplastic Composites

A large part of the market for boat decking is now occupied by PVC and PVC-Based composites. Here plasticised PVC (PVC-P) is used for flexible flooring profile and unplasticized rigid PVC (PVC-U) for rigid planks. The main asset of PVC is that by using only a few types of resin and adding plasticisers, additives, and modifiers, it can be tailored to give a wide range of physical properties (flexibility, elasticity, impact resistance). Typical PVC-P and PVC-U formulations are given in **Table 1.2**.

Table 1.2 Generic compositions of flexible and rigid PVC formulations [12]

	Flexible PVC (PVC-P): %	**Rigid PVC (PVC-U): %**
PVC Polymer	50-95	50-95
Plasticiser	0-50	0
Stabiliser	0.2-5	0.2-5
Lubricant	0.1-2	0.1-2
Filler	1-50	1-50
Reinforcement	0-10	0-10
Pigment	0-5	0-5
Other additives	0-5	0-5

PVC is polarisable (electronegative chlorine substituent on the main chain) and hydrophobic (**Figure 1.12**).

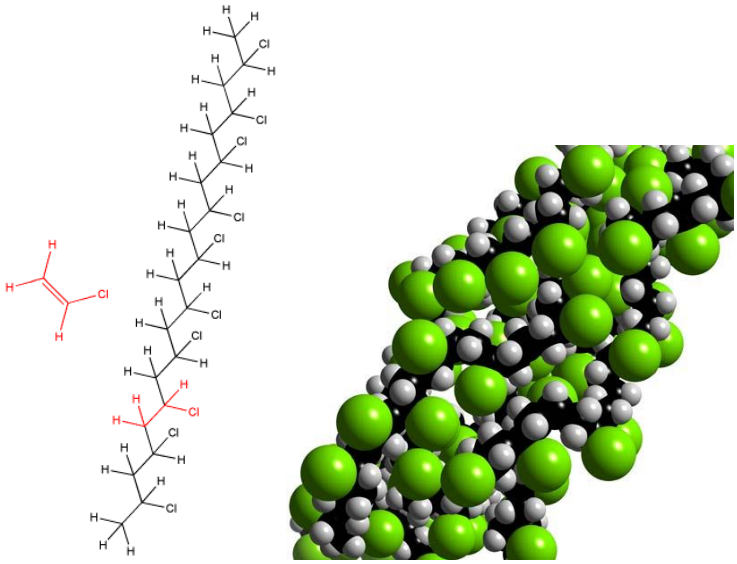

Figure 1.12 Macromolecular chain structure of PVC showing polar chlorine substituent (green spheres)

Its ability to mix well with plasticisers, additives and modifiers is largely due to its amorphous structure (**Figure 1.13**). Because PVC is amorphous with a glass transition of around -50°C, it shows little shrinkage on cooling.

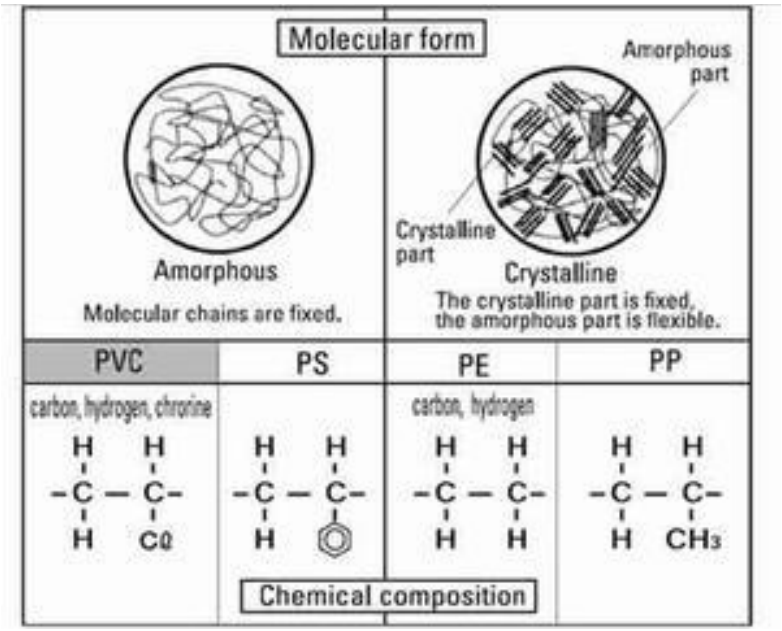

Figure 1.13 Molecular structure of general-purpose polyolefins, including PVC (Reproduced from [13])

The type of PVC resin is determined by its molecular weight and degree of polymerisation which determine its viscosity (K-value). Melt viscosity dictates the processability of a thermoplastic. PVC is selected for extrusion and calendaring because its viscoelastic behaviour is less dependent on temperature.

In addition, PVC lends itself to extensive secondary processes. It can be embossed, and surface treated. Here embossing tools readily create the textured surface that mimics wood grain. On-site workability facilitates laying decking for example, bending, welding and ability to apply adhesives.

1.2.3 Adhesives

The adhesive is not the main consideration in this project, but it does warrant a brief consideration since it is required to prevent water seepage and to stick the deck to the hull. Ideally this needs to compensate for production tolerances, requiring high gap filling. Durability and mechanical resistance to the stress of the join is crucial, i.e.,

balanced optimisation of strength and flexibility, compensating for thermal expansion of different materials and dynamic loads. The elongation at break should be >100%. A fast cure process between 10-60 minutes is also preferable. Typical urethane and epoxy adhesives are used. For flexible EVA/PE foam applications, peel-back pressure sensitive adhesives are often applied to aid layout and can be fitted to GRP, wood, and steel surfaces.

1.3 Fillers used to Modify Properties of Synthetic Polymer-Based Products

1.3.1 Solid Particulate Fillers

Particulate fillers are usually finely ground inorganics, for example chalk, silica, and clay. Originally the purpose of a filler was to act as a bulking agent (extender) to reduce costs, but for today's plastic composites this is a misnomer. Except for calcium carbonate, fillers increase material costs. The addition of a filler changes most of the properties of the base polymer. The key improvements afforded by a 'functional' filler depend on its particle size and aspect ratio, and in this context whether it is isotropic (properties independent of direction) or anisotropic (direction dependent properties). (**Table 1.3**).

Table 1.3 Influence of filler aspect ratio on mechanical properties of selected filler types in a thermoplastic polymer composite [14]

Property	Isotropic	Platy	Fibres
Modulus	↑	↑↑	↑↑↑
Yield Strength	–	↑	↑↑
HDT in amorphous polymer	–	–	–
HDT in semi x-line polymer	↑	↑↑	↑↑↑
Impact resistance	↑ or ↓	↓	↓
Elongation to break	↓	↓↓	↓↓↓
Permeability	↓	↓↓	↓

HDT = Heat Defection Temperature

The 'Aspect Ratio' of a particle is the ratio of its longest dimension to shortest dimension, e.g., the Aspect Ratio (L/D) for rod-like particles is the ratio of length (L) to the diameter (D).

Table 1.4 gives the main types and properties of particulate fillers used in thermosets and thermoplastics.

Table 1.4 Aspect Ratio and properties of common particulate fillers used in thermosets and thermoplastics. (Derived from [15]**)**

Filler Type	Density (gcm^{-3})	Mohs hardness	Refractive index	Mean Size (microns)	Aspect Ratio
Calcium carbonate	2.7	3-4	1.48,1.65,1.70	0.02-30	1-3 Blocky
Talc	2.7-2.8	1	1.55,1.57,1.58	0.5-20	5-40 Plate
Mica	2.8-2.9	2.5-4	1.55-1.70	5-1000	20-100 Plate
Wollastonite	2.9	4.5	1.63,1.65	1-500	5-30 Fiber
Silica (precipitated)	1.9-2.1	5.5	1.46	0.005-0.1	~1 Round
Carbon black	1.7-1.9	2-3	black	0.014-0.25	~1 Round
Dolomite	2.85	3.5-4	1.68	1-30	~1 Round
Barium sulfate	4.0-4.5	3-3.5	1.64	0.1-30	~1 Round
Kaolin	2.6	2	1.54,1.56,1.57	0.2-8	10-30 Plate
ATH $Al(OH)_3$	2.42	2.5-3	1.57,1.57,1.59	5-80	1-10 Plate
MDH $Mg(OH)_2$	2.4	2.5-3	1.56, 1.58	0.5-8	1-10 Plate
Diatomaceous earth	2-2.5	5.5-6	1.42-1.48	4-30	2-10 Disc
Magnetite/Hematite	5.2	5.5-6	black/red	1-50	~1 Blocky
Halloysite	2.54	2.5	1.548 (dried)	1-20	5-20 Tube
Zinc oxide	5.6	4.5	2.00	0.05-10	1 Round
Titanium dioxide	4.23	6	2.609	0.1-10	1 Round

For spherical particles (e.g. calcium carbonate or glass spheres) the shape of particle increases stiffness somewhat, decreases strength slightly and has least effect on impact resistance and elongation to break. A key advantage is that properties are altered equally in all three directions (x, y & z), reducing warpage.

Needle shaped (fibrous) particles typified by wollastonite (Table 1.4) can reinforce plastics if the aspect ratio is high enough and if they are well bonded to the surrounding polymer: the higher the aspect ratio the better the reinforcement.

Platy particles for example talc and mica (Table 1.4), can also reinforce and the higher the aspect ratio, the more effective they are. They reinforce along both the long dimensions of the plate, whereas a fibre only reinforces along its one long dimension. That is, plates are more effective than fibres with the same aspect ratio. Platy fillers also lead to more isotropic shrinkage, i.e., less warpage. However, high aspect ratio leads to poor impact resistance and lower elongation to break. This implies that fibres and plates act as imperfections. The reason is the long dimension is likely to be over the 10-20 micron limit, where stress concentrations are high, facilitating crack initiation and failure.

Finally, the aspect ratio that matters is not the one from the datasheet which describes the as-supplied filler. What does matter is the aspect ratio of the particles inside the final composite material because that is what affects mechanical (and other) properties. It is therefore vital to ensure the particles are not broken down, decreasing aspect ratio, during handling and compounding.

An example of the interplay between particle size, aspect ratio and properties, is given for calcium carbonate filled PVC in **Figure 1.14**. The interplay between the physical and chemical properties of the particulate filler and polymer are used to improve processing, mechanical properties, and flame retardancy. However, it should be noted that on addition of a filler some properties may be enhanced at the expense of others.

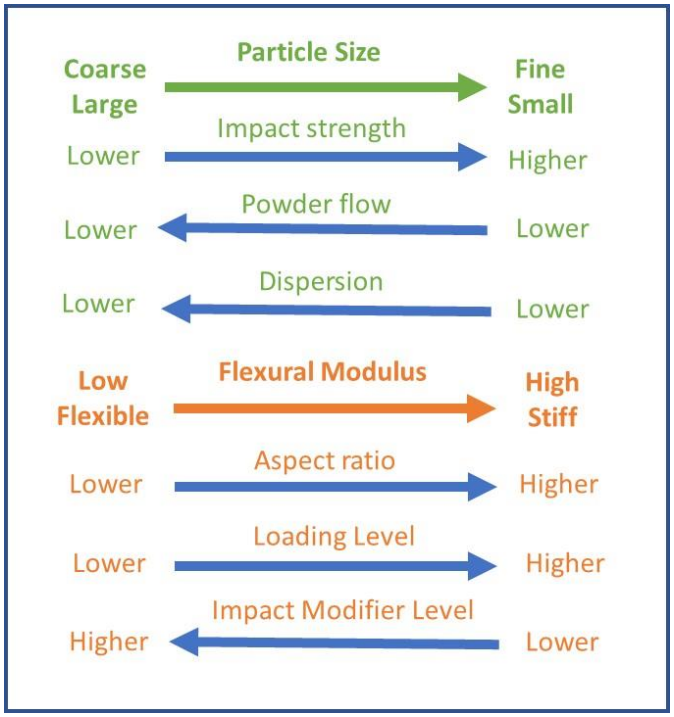

Figure 1.14 Influence of particle size and aspect ratio on properties of calcium carbonate filled PVC (adapted from [16]).

The 'Rule of Mixtures' can be used to predict properties of the filled composite, on the basis that properties are likely to lie between those of the filler and polymer ([17]**, see Section 3.3.5**). Note that when examining the relationship between property changes and amount of filler added, expressing the latter as volume fraction (or percent) rather than weight fraction is more meaningful [18]. Where unexpected interactions between the filler and polymer arise more complex mathematical models are required to predict properties [19].

In the specific case of PVC, ground (GCC) or precipitated (PCC) calcium carbonate, of varying particle size (coarse, fine, ultrafine), is the most used filler (**Table 1.5**). Calcium carbonate improves compounding by dispersion of additives into the PVC powder. Processing is improved because there is more homogeneous flow in the blended powder. To further enhance processing and properties the fillers may be coated (with stearates or coupling agents). By careful selection of these parameters, other costly additives, such as impact modifiers, can be reduced [20].

Table 1.5 Estimated use of calcium carbonate used in PVC in Europe (Derived from [21])

Application	Grade of calcium carbonate	kilo tonnes
PVC Cables	Medium and fine coated and uncoated	250
PVC flooring	**Ultrafine coated, fine, and very fine**	**177**
PVC flexible	Fine, coated, and uncoated	133
PVC-U extrusions	Ultrafine and fine coated	110
PVC-U windows/profiles	Ultrafine coated	80
PVC plastisols	Precipitated, ultrafine coated, fine and coarse	25

Calcium carbonate is already widely used in PVC floor tiles and homogeneous flooring. In the former case, coarse calcium carbonate (GCC) with an average particle size 15 μm and having a broad particle size distribution is used giving better dimensional stability and reduce water uptake. In the latter case, finer calcium carbonate (PCC) is used because its narrower particle size distribution, and fewer large particles, reduces loci that act to concentrate stress in the polymer matrix.

However, most solid particulate fillers increase the density of the final composite material and so have limited value in lightweight applications. Because of this, hollow fillers have made inroads into composite applications.

1.3.2 Hollow Particulate Fillers

Hollow particles (microspheres, also referred to as micro-balloons; or nanospheres) have distinct properties exhibited by low bulk density; high thermal and acoustic insulation; high surface area and surface permeability. With the appearance of fine powders, microspheres range from 12 to 300 μm in diameter. Microspheres are commonly grouped according to their material class: polymers; ceramics; glass. However, it is more useful to characterise them according to their properties (density, crush strength, particle size and shape), which warrants a more detailed inspection.

1.3.2.1 Composition of Commercially Available Microspheres

Several manufacturers produce hollow microspheres that are usually white or grey free-flowing powders in appearance. Of the three main types of microspheres glass and plastic microspheres are the most prevalent in lower cost applications. Hollow glass microspheres are generally produced by using a spray nozzle technique and hollow thermoplastic microspheres are usually manufactured by an emulsion polymerisation process. Glass microspheres can also be produced by processing (expansion of) perlite [22]. In the case of perlite, the hollow structure is multicellular, unlike engineered glass microspheres which consist of a single closed cell.

Hollow glass microspheres are the dominant type of microsphere in commercial markets. **Table 1.6** gives typical properties for the range of hollow glass spheres provided by the manufacturer 3M™

Table 1.6 Typical properties for the range of hollow glass spheres manufactured by 3M™ (Reproduced from [23])

Property	3M™ Glass Bubbles
Shape	Hollow spheres with thin walls
Composition	Soda-lime-borosilicate glass
Color, unaided eye	Off-white, powdery
Crush strength (90% survival)	250–27,000 psi
True density	0.125–0.60 g/cc
Median particle size	18–65 microns
Softening temperature	600°C (1112°F)
Thermal conductivity	0.05–0.20 W•m-1•K-1 @ 20°C
Dielectric constant (@ 100 MHz)	1.2–1.9

It has been reported that polypropylene containing iM30K showed improved material flow, better dimensional stability and a 16.8% reduction in weight for a 50% cost reduction *c.f.* talc filled polypropylene ([24]).

In contrast, plastic microspheres are some of the lightest microspheres available, with densities as low as 0.025 g/cm^3. Although they have lower compressive strength because high pressures cause the spheres to flatten not burst, they are much less susceptible to crushing. Furthermore, when the pressure is removed, they often have sufficient elasticity to recover. This property is also of value in mitigating expansion

and contraction of hollow plastic sphere filled composites when subjected to fluctuating temperatures during winter and summer seasons.

Plastic microspheres are manufactured from a very thin thermoplastic shell (e.g., copolymers of vinylidene chloride, acrylonitrile, or methyl(methacrylate)) that encapsulates a blowing agent (e.g., isopentane or isobutene) that softens and expands (up to 40x) when heated. On removal of the heat the shell stiffens to leave the expanded form as a hollow sphere (20-150 μm). Expansion temperatures lie between 80°C to 190°C, so well within the processing range of polyolefins. Such plastic hollow microspheres can give 38% reductions in density at concentrations as low as 3 wt.%. ([25])

1.3.2.2 Density, Wall Thickness and Crush strength

Because they are hollow, microspheres are susceptible to crushing at high pressures and shear. This is particularly the case during manufacturing processes (e.g., compounding, extrusion). Wall thickness is the main factor controlling the density and crush strength of the microsphere. Generally, the thicker the wall the stronger the sphere. The wall thickness of the particles is about 10% of their diameter ([26]), the latter having dimensions which range between 20 to 100 μm (d50). However, it should be noted that the narrow size distributions of individual product types differ widely. The spherical shape has a uniform curvature so that any applied force causes the least stress concentration provides maximum crush strength. The bulk densities of hollow microspheres generally vary between 0.1 and 0.7 g/cm^3 and thus are clearly below those of conventional fillers. Typical densities by product type are given in **Table 1.7** and crush strength versus density of hollow glass microspheres in **Figure 1.15**.

Table 1.7 Typical densities of hollow microspheres by material class

Microsphere Material	Structure	Density (g cm^{-3})
Glass	hollow	0.15-0.6
Ceramic	hollow	0.7
Plastic	unexpanded	0.1
Plastic	expanded	0.01

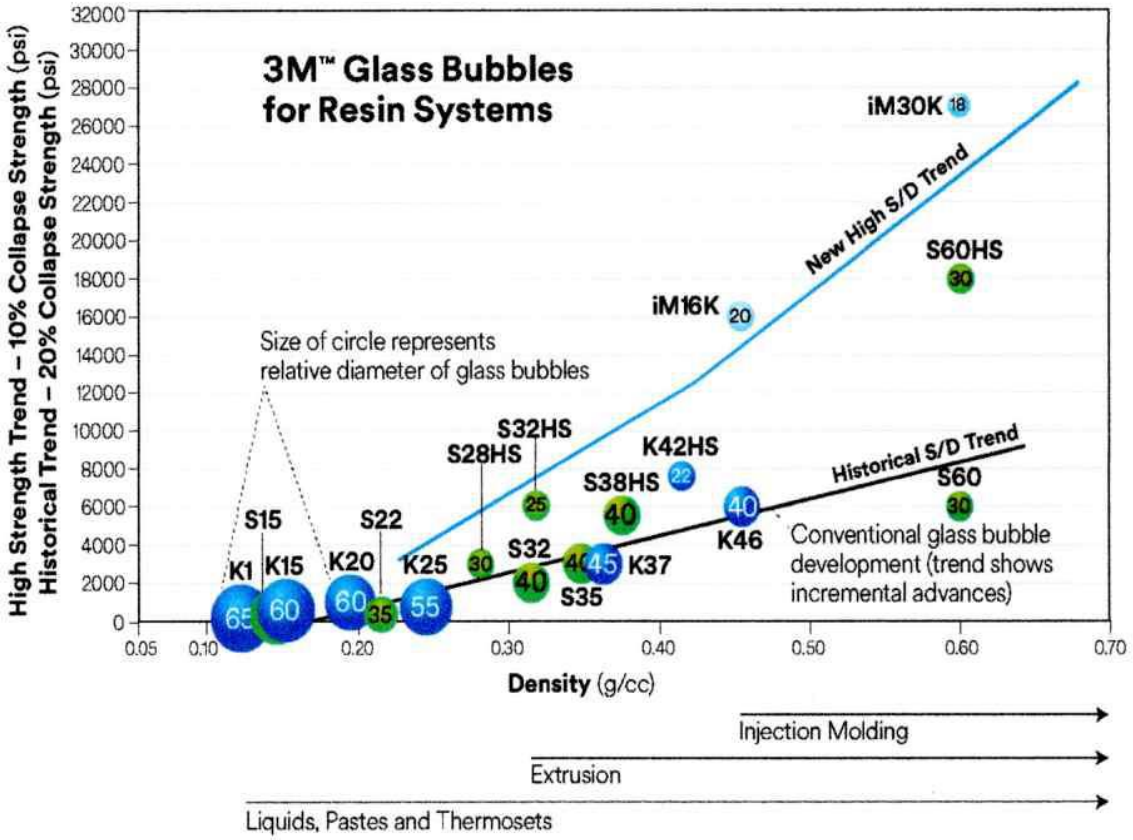

Figure 1.15 Isostatic crush strength versus density of hollow glass spheres (3M™). The number in the coloured circles indicates the average diameter. (Reproduced from [27])

1.3.2.3 Particle Size and Shape

Particle size determines, along with wall thickness, the density of the microsphere. There is an optimisation required between particle size and wall thickness because larger particles are unable to withstand the high shear rates and faster screws in many compounding and extrusion operations. Therefore, smaller particles are more attractive for processing but there may be a trade-off in terms of weight reduction (density).

1.3.2.4 Temperature

The maximum operating temperatures during processing and service-life are important particularly for plastic microspheres. In the case of polyethylene microspheres melting point is in the range 110-130^{o}C, depending on molecular weight. Here the melting phase transition is fast, so spheres could be used as a temporary filler and melted away to create cavities for a 'foam-type' (syntactic) matrix.

Temperature is also important in the selection of expanding plastic microspheres (essentially thermoplastic microspheres encapsulating a gas, which when heated cause the gas to expand while the shell softens giving a dramatic increase in volume (**Figure 1.16**).

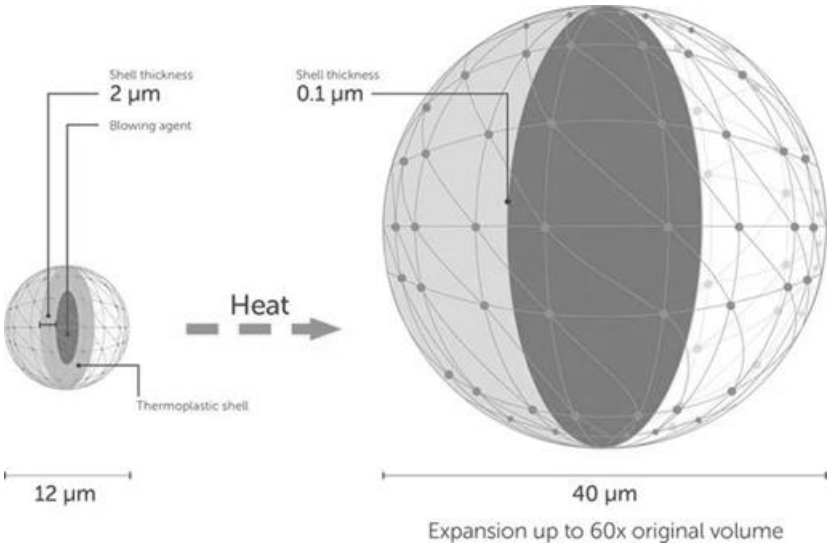

Figure 1.16 Schematic of relative volume change in an expanding plastic microsphere (Reproduced from [28])

1.3.2.5 Cost

In general, expanding polymer microspheres are more costly than glass microspheres which in turn cost two to three times more than chopped glass fibre

However, it should be borne in mind that fillers should really be costed on a per unit volume basis because they can displace a large volume of higher-density material at very low weight. That is, if the microsphere is twice the cost of the existing filler or resin that it is to replace, the considerable reduction in density means that for a given volume the price differential between the two options is negligible. For example, a microsphere with a density of 0.6 g cm^{-3} displacing polymer with a density of 1.15 g cm^{-3}.

There is also the issue of the compatibility of the filler (whether solid or hollow particulate) with the polymer matrix. Poor adhesion with the matrix may necessitate the use of coupling agents, with additional costs for the final compound.

1.4 Comparison of Properties and Costs of Commercial Decking Materials

When planning a new product, selection of suitable materials is based on achieving the best match between properties and design. Once product shape and any fixed dimensions have been decided, constraints on performance must be identified. For example, for boat-decking function constraints include a lightweight, inexpensive material, with good thermal insulation, that is sustainable and recyclable. This section compares the key properties and costs for a range of commercial decking materials. Here Ashby plots ([29]) are used to better define the range of properties and costs of materials currently used, to set a benchmark for further studies (see **Section 3.2.5**). Although this method does not provide the detailed materials engineering performance of CAD-Finite Element Analysis software, it does allow an effective first screening of materials. Here scatter plots are employed to display two (or more) properties and the ratio between properties. The value of this approach is given in **Figure 1.17**. Note that where different classes of materials are compared the wide-range of property values necessitates the use of a log-log scale. However, for materials within a given class this may not be required. After describing the material's function and applying constraints on performance, material indices are defined.

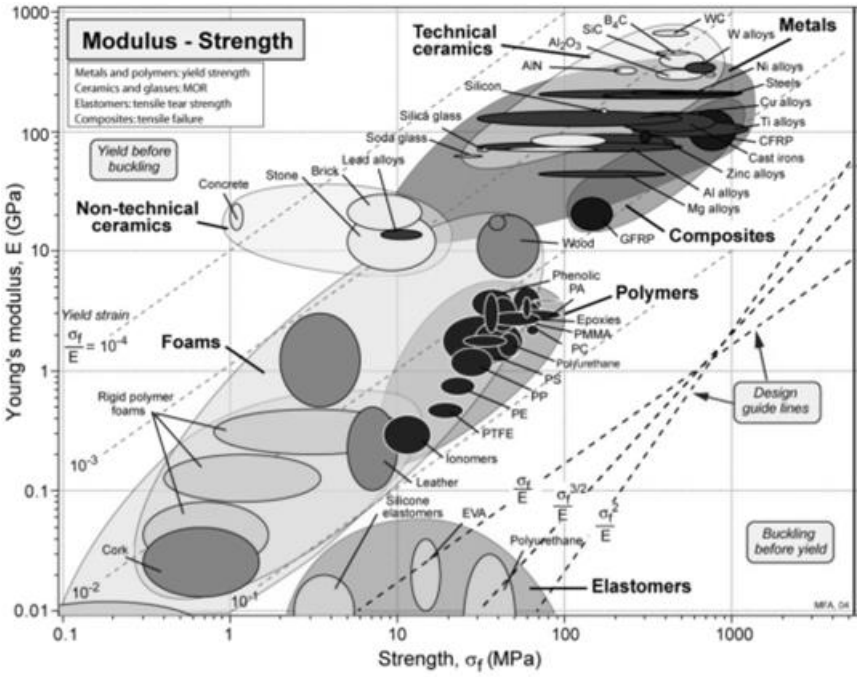

Figure 1.17 Ashby plot for Youngs' modulus, E, (GPa) versus strength, σ_f, (MPa) for common classes of materials. (Reproduced from [30])

1.4.1 Weight

Although decking represents a fraction of the total weight of a boat, it does have a bearing on performance. For sail boats, lower deck weight means lower centre of gravity of the boat (i.e., less weight is sited over the water line), reducing keeling. For motorboats, which have wider decks, it follows that more material is needed, but the main issue is if boats have a flybridge. A lower weight on the flybridge means lower rolling of the boat. **Figure 1.18** illustrates that there are a wide range of densities consistent with the types of materials used in commercially available decking.

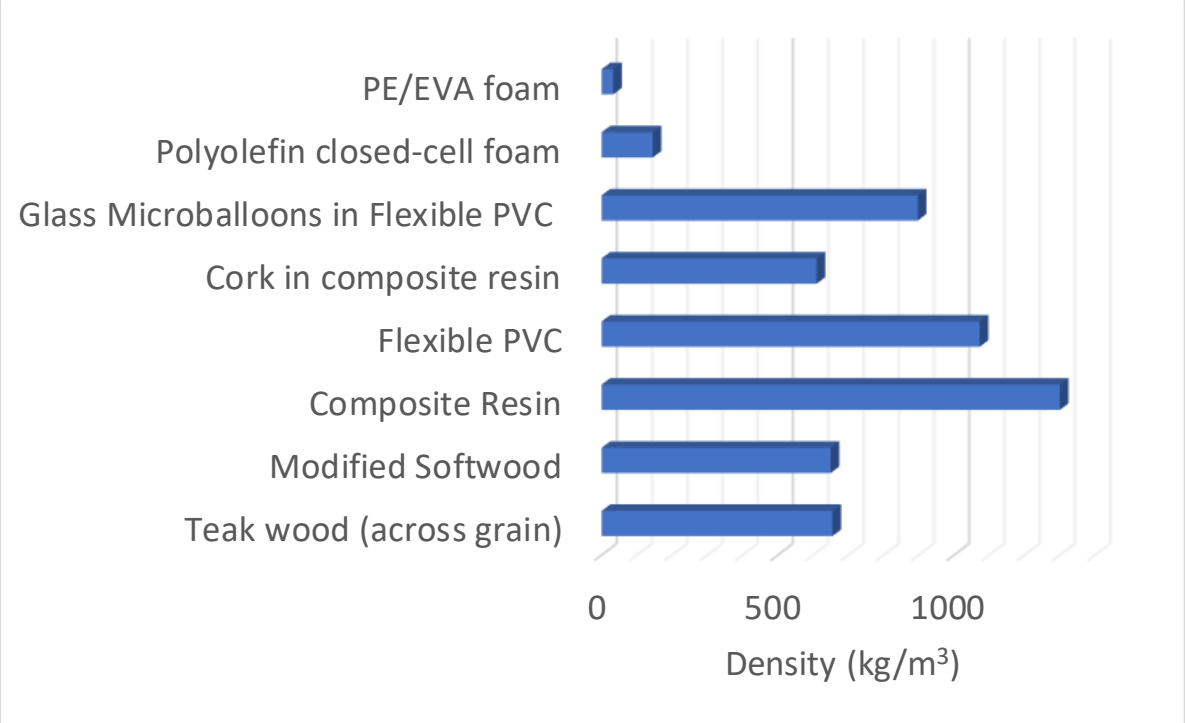

Figure 1.18 Densities of boat decking materials, kg/m^3 (Data averaged, derived from a range of specification sheets of commercial materials, N.B. values are influenced by specific additive formulations)

Figure 1.19 compensates for typical thickness of the decking and uses the more useful weight of boat decking per m^2 of layout. Here it can be seen that there is a reduction in weight when moving from wood to synthetic polymers, but the greatest weight reductions are seen for materials that contain hollow voids within the structure.

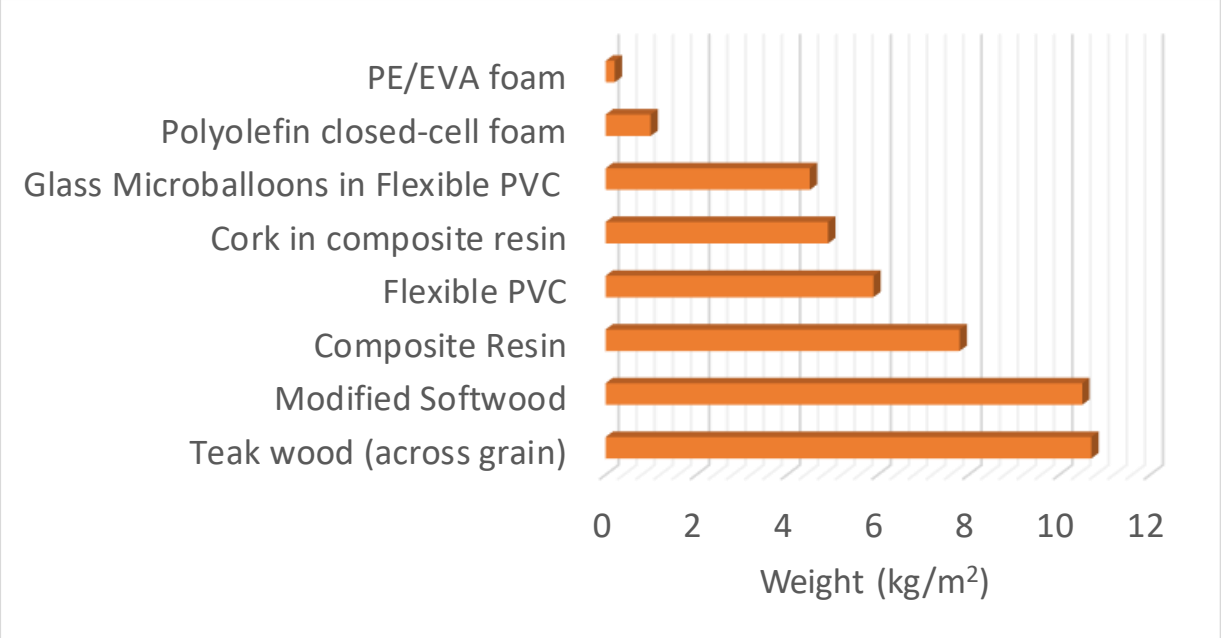

Figure 1.19 Weight of boat decking materials, kg/m^2 (Data average, derived from a range of specification sheets for typical thickness of commercial materials)

The density of decking material also influences fuel consumption during transport between producer and fabricator. Just as important is the influence of density on other factors such as mechanical properties and thermal conductivity.

1.4.2 Mechanical Properties

Although boat decking is usually a 'supported' covering (i.e., adhered to the pre-formed resin deck) the mechanical properties of the material are relevant to its performance. Key general mechanical properties include modulus and strength (**Figure 1.20**). The elastic modulus (*E*) affects how the material deflects (changes it dimensions) under a load, while the strength of the material governs the stress it can withstand before it fails. Prior to the elastic limit the material can deform and return to its original shape. Yielding is a gradual failure going through irreversible plastic deformation which is not usually catastrophic to ultimate failure at fracture. Where non-linear behaviour makes it difficult to define the elastic limit, the offset yield point is calculated as the stress at which 0.2% plastic deformation occurs. Characteristic stress-strain curves for thermosets (brittle plastic), thermoplastics and elastomers are

given in **Figure 1.20** and **Figure 1.21**. [31]. Ashby plots for Youngs' modulus versus density and Strength versus density are given in **Figure 1.22** and **Figure 1.23** respectively. Within the elastic region thermoplastics, elastomers and foams offer acceptable light weight and strength for use in boat decking.

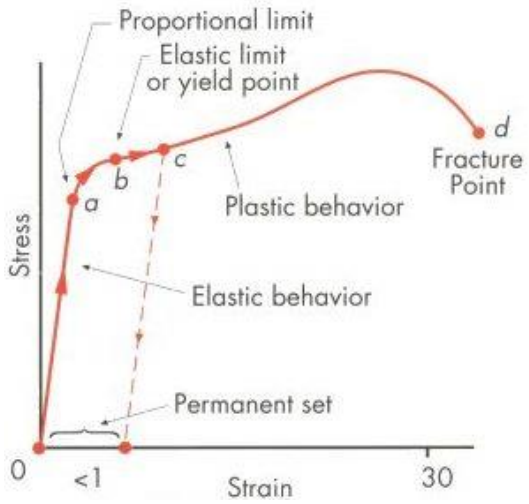

Figure 1.20 Characteristic stress-strain curve for a thermoplastic polymer. (From [32]).

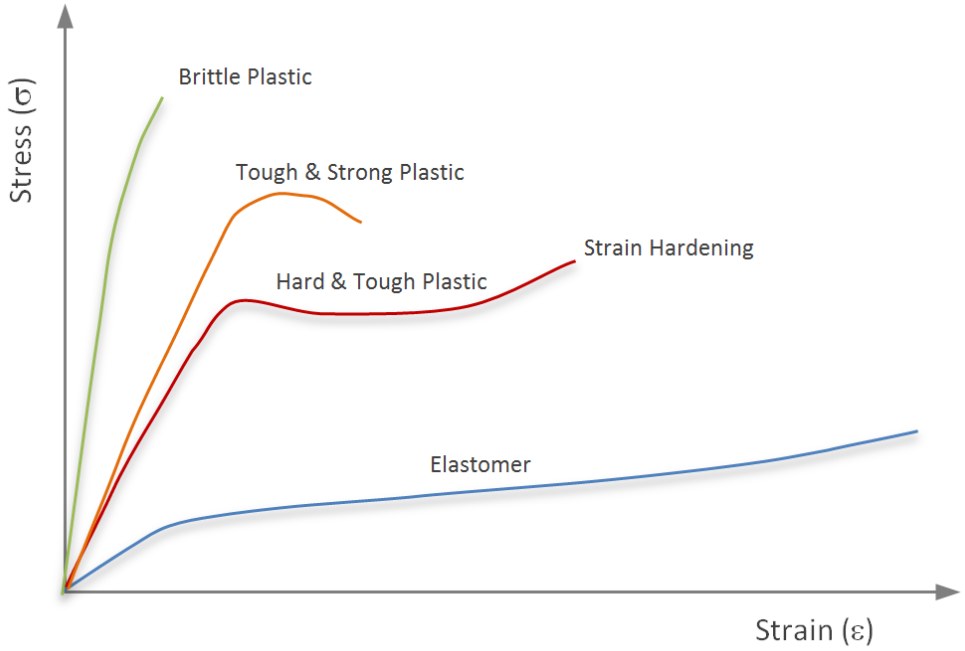

Figure 1.21 Characteristic stress-strain curve for polymer-based materials. (From [33]).

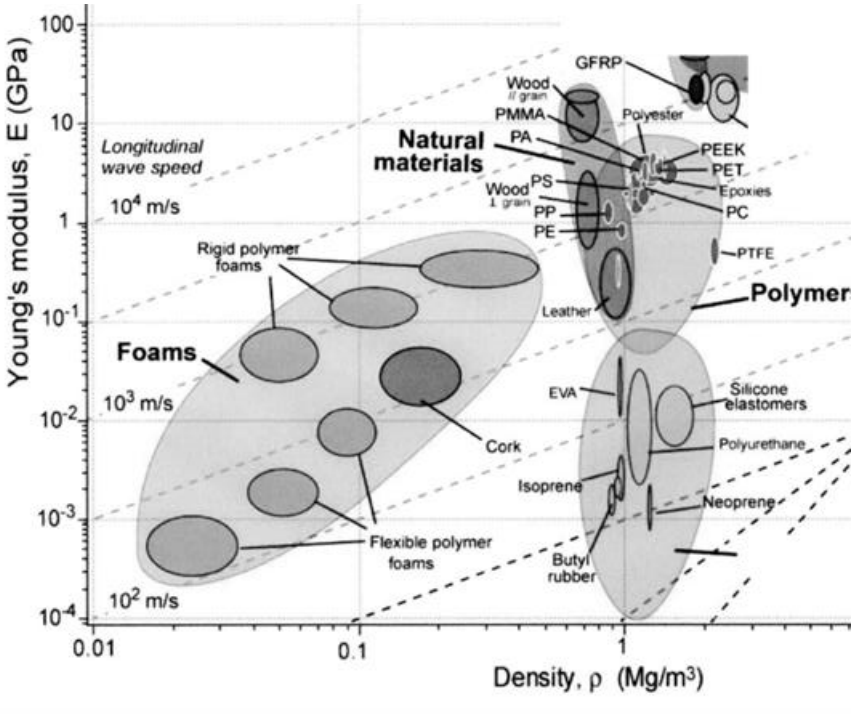

Figure 1.22 Ashby plot for Young's modulus, E, (GPa) versus density, ρ, (g/cm^3) for common classes of materials. (Reproduced from [34])

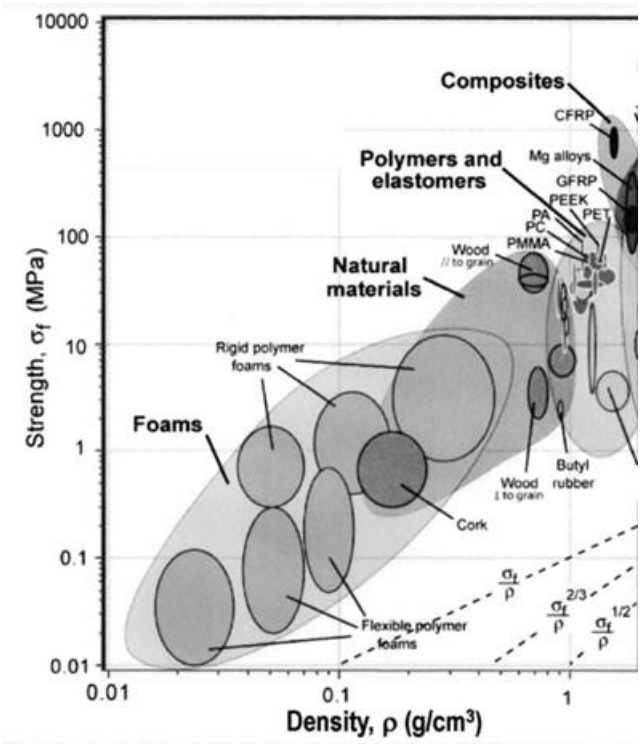

Figure 1.23 Ashby plot for strength, σ_f, (MPa) versus density, ρ, (g/m^3) for common classes of materials. (Reproduced from [35])

1.4.3 Thermal Properties and Surface Temperature Underfoot

Boat decking needs to be cool enough to touch, such that summer heat doesn't burn feet when walking across the floor. The thermal conductivity (**Figure 1.24**) and diffusivity (**Figure 1.25**) of the material selected are therefore important. In addition, the material should show little thermal expansion or contraction during use, which could lead to distortion and the creation of stresses with the underlying adhesive (**Figure 1.26**).

Thermal diffusivity (α) indicates how fast heat diffuses into the material (i.e. the relationship between heat transferred and heat stored), while thermal conductivity (k, λ or κ) indicates the rate of heat transfer per unit area and per unit temperature gradient (i.e., the ability of the material to conduct heat). Materials with low thermal conductivity are insulators and have a cooler feel underfoot.

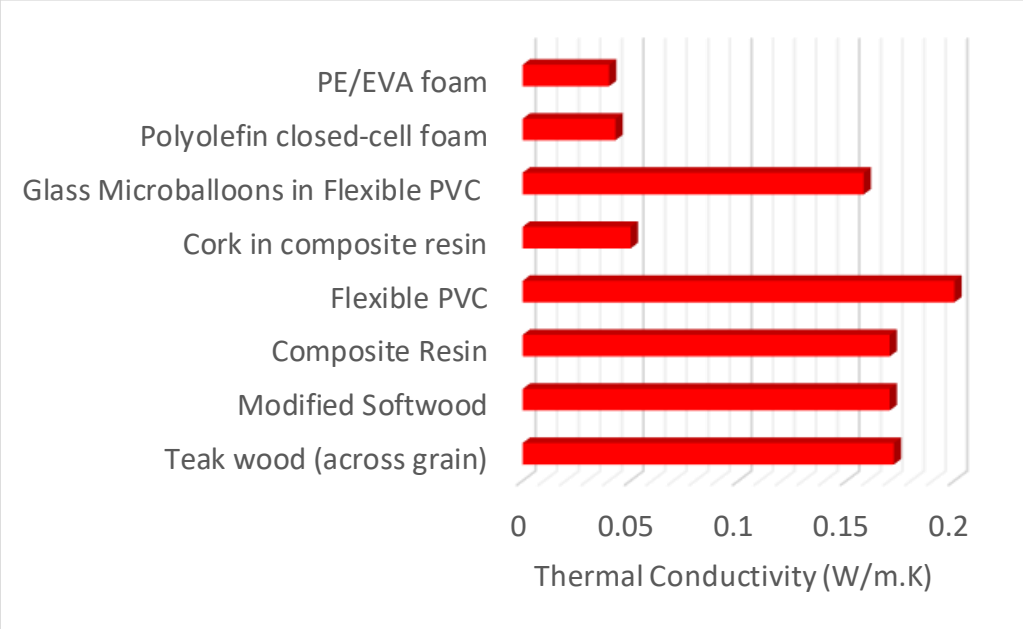

Figure 1.24 Thermal conductivity, λ, (W/m.K) of boat decking materials (Data average, derived from a range of specification sheets for commercial materials, N.B. values are influenced by specific additive formulations)

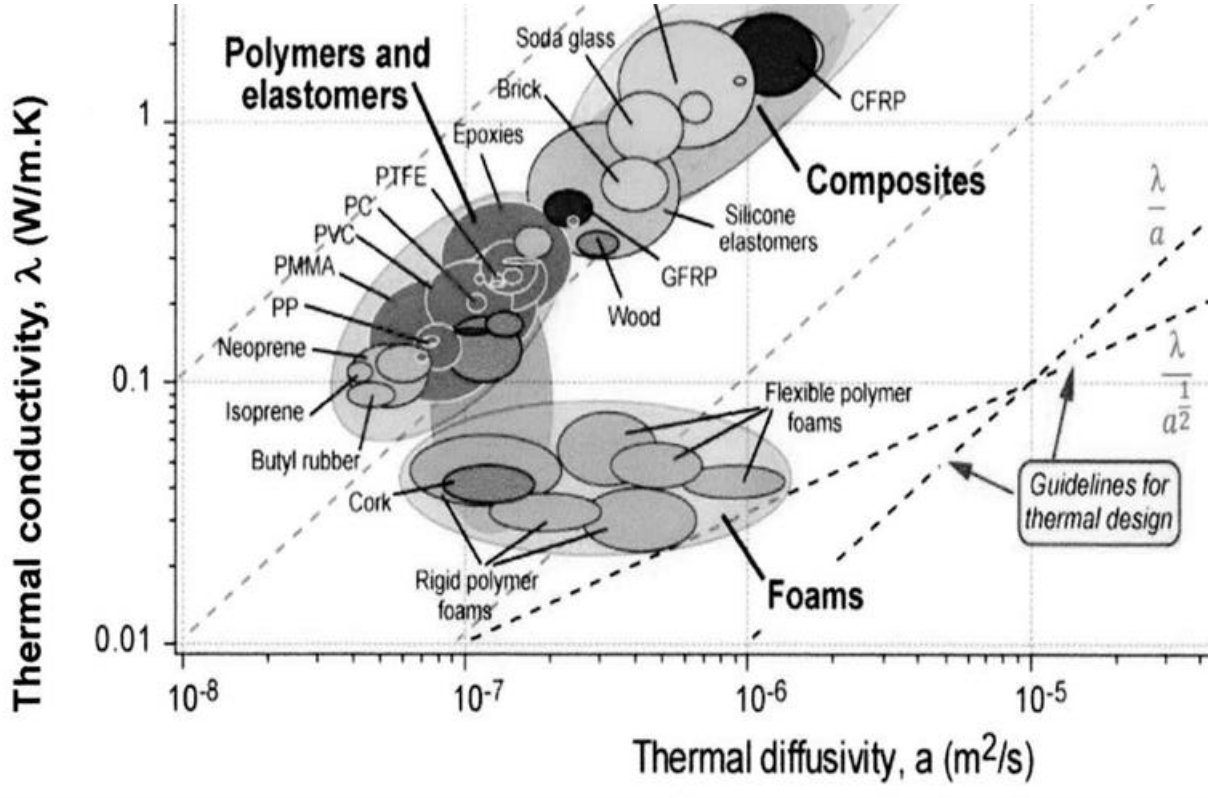

Figure 1.25 Thermal conductivity, λ, (W/m.K) versus thermal diffusivity, *a*, (m^2/s) for natural materials, polymers, elastomers, foams, and composites (Adapted from [36]).

From **Figure 1.24** and **Figure 1.25** more porous materials, especially foams, have the lowest thermal conductivities. Unfortunately, foams have poor mechanical properties. Similar thermal insulation may be afforded by a closed-cell structure like cork in a resin matrix, but this may have issues of wear and recyclability. Composites with hollow sphere fillers therefore present a possible way forward offering thermal insulation with better mechanical properties. However, it should be recognised that the heat transfer process in porous materials is complex, especially for polymer composites. To make an effective selection of filler and polymer (resin) it is important to understand the mechanism of heat transfer. There are three mechanisms of heat transfer for hollow filler polymer composites: thermal conduction between the solid polymer and gas within the sphere; thermal radiation between the hollow microsphere surfaces; and thermal convection of the gas within the microsphere. Several researchers have derived equations to calculate an effective theoretical thermal conductivity of porous composites [37] [38].

Also, the pigments incorporated in a specific formulation are important, darker colours absorb more heat than lighter colours. **Figure 1.26** depicts thermal expansion versus thermal conductivity demonstrating that foams show a relatively high thermal expansion despite their low thermal conductivity. It also suggests that fibrous fillers when embedded in a resin matrix (e.g., wood – cellulose fibres in a lignin resin) can reduce both thermal expansion and thermal conductivity. Although this depends very much on the fibre, exemplified by CFRP (carbon fibre reinforced polymers) versus GFRP (glass fibre reinforced polymers). Such composites are also difficult to close-loop recycle.

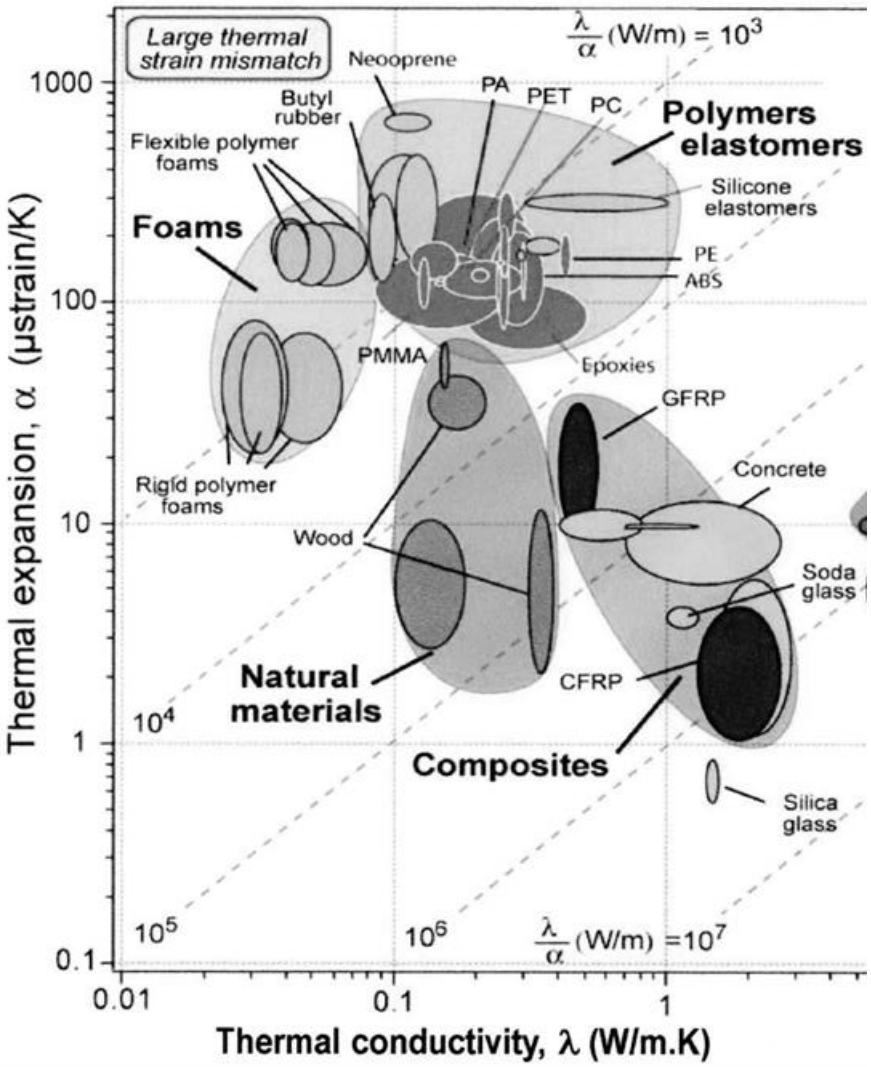

Figure 1.26 Thermal expansion, α, (μstrain/K) versus thermal conductivity, λ, (W/m.K) for natural materials, polymers, elastomers, foams, and composites (Adapted from [39]).

1.4.4 Hardness (or Softness), Wear Rate and Durability

Further to general mechanical properties specific types of mechanical property are important for boat decking materials. During service life the decking is subject to scratching, cutting, abrasion, indentation, or puncture. Here the hardness of the material, which is closely related to strength, and wear resistance are important. In conjunction with this, the texture and softness of the material, along with skid-slip resistance when dry and wet (especially when barefoot) is a vital health and safety measure. **Figure 1.27** illustrates that filled thermoplastics offer the hardest materials with lowest wear rate constant. However, it should be appreciated that a balance must be made between these properties and softness underfoot for boat decking.

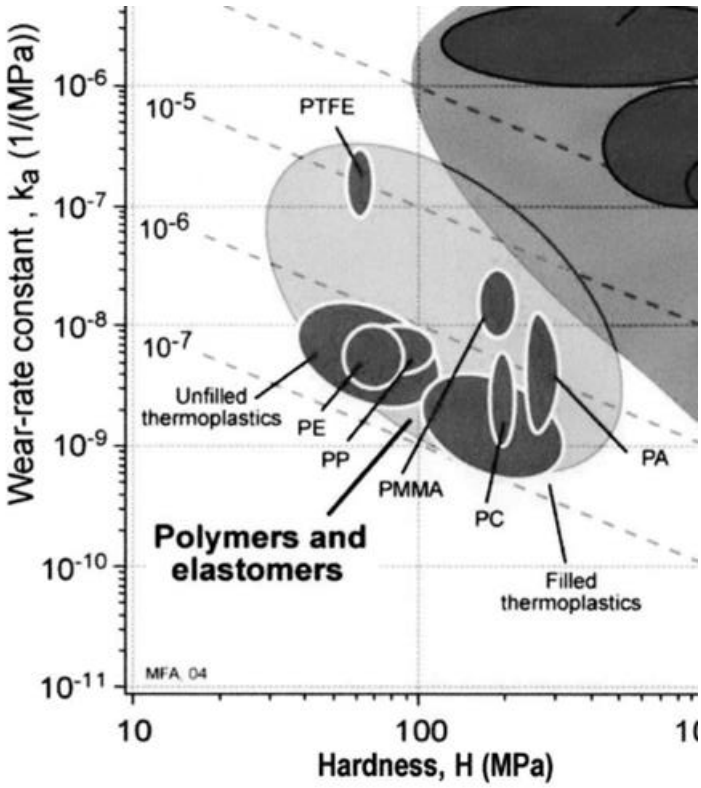

Figure 1.27 Wear-rate constant, K_a, (1/MPa) versus hardness, H, (MPa) for polymers and elastomers (Adapted from [40]).

1.4.5 Costs

Choice of materials is invariably linked to costs, with different materials being selected depending on route to market, e.g., high-end yachts, small boats, large vessels. From **Figure 1.28** polymer resin costs per unit volume are higher for thermoset-based materials (urethane, epoxy) compared to commodity polyolefins (PVC, PE, PP) and butyl rubber.

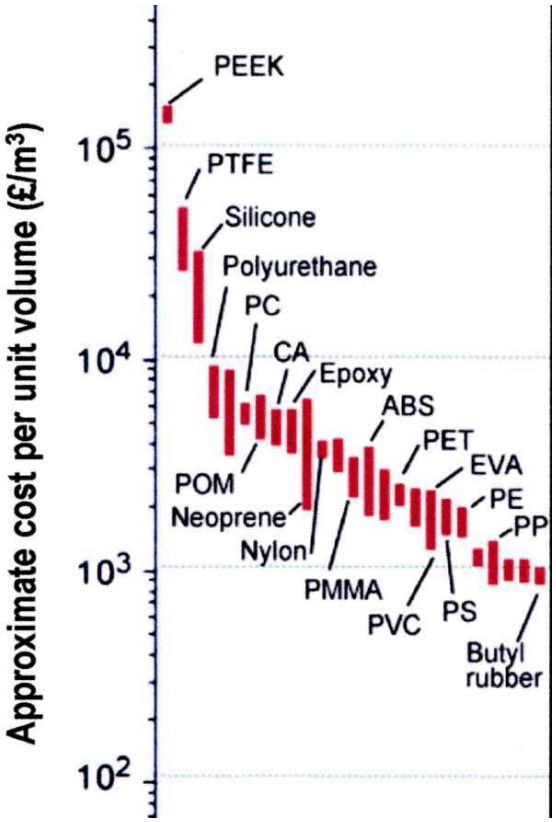

Figure 1.28 Approximate cost per unit volume(£/m^3) for polymers and elastomers, (Adapted from [41]).

The typical (installed) cost of real teak decking is £500-600/m^2, with synthetic teak (e.g., PVC) *ca.* £200-300/m^2. A similar price is given for cork decking (£200-300/m^2), highlighting the fact that the relative costs of filler (cork) and polymer matrix (polyurethane) are important in determining overall price. Foam decking is the cheaper alternative (£150-200/m^2), but it should be borne in mind that longevity is not taken into consideration for the materials quoted [42].

1.5 The drive towards more sustainable materials

Of the materials reviewed in the introduction, natural woods are limited by appropriate sustainable management and, because they are treated (stained, varnished) legislation restricts recycling or incineration at end-of-life. In contrast, for thermoplastics, though PVC, PP and PE have traditionally been produced from fossil oil, novel bio-based products are entering markets and have comparable properties. Bio-based PP and PE are made from natural materials such as corn, sugar cane, vegetable oil and other biomass. Ideally the biomass is utilised from second generation cellulosic or vegetable oil waste, rather than first generation food crops. For PVC the introduction of bio-attributed resources to existing production lines has been driving industry towards recognition of this polymer as an eco-product [43]. Furthermore, PVC, PP and PE have established recycled material markets and the potential to offer closed-loop recycling options. Although it is difficult to recycle thermosets, recently there has been a drive towards fully bio-based high-performance thermosets with closed-loop recyclability [44].

From the overview of the materials used in boat-decking presented in this chapter, clear opportunities exist to produce more sustainable products. Here both the polymer matrix and additives could be derived from bio-based or widely available mineral resources, with the capability of being fully recyclable or undergo natural degradation to generate benign environmental products

Although hollow glass spheres (HGS) are currently in use in numerous composite applications there are difficulties presented by material handling, abrasive wear on equipment during processing and recycling. There is however the potential to replace (wholly or partially) calcium carbonate solid particulate filler with hollow calcium carbonate. As a potential filler material calcium carbonate is attractive because of its global availability (as limestone), low toxicity and biocompatibility. Furthermore, it is already the most widely used filler by the PVC industry, any hollow calcium carbonate based recyclate thus has the potential to feed into a range of PVC products. Although hollow calcium carbonate is not widely available for commercial applications there has been much interest in synthetic methods that are able to be upscaled, with costs that are competitive with solid particulate calcium carbonate. The aim of this project is to

develop such a method and test the product in polymer-based boat-decking formulations.

1.6 Hollow Calcium Carbonate as an Alternative Filler

1.6.1 Overview of Methods to Produce (Hollow) Calcium Carbonate

As stated in **Section 1.3.1** calcium carbonate ($CaCO_3$) is well-established as a filler in PVC applications.

Calcium carbonate can solidify to form chains, needles, flakes, cubes, spheres, and spindles from its four different polymorphs: calcite, aragonite and vaterite and amorphous calcium carbonate (ACC). The crystalline polymorphs are illustrated in **Figure 1.29**.

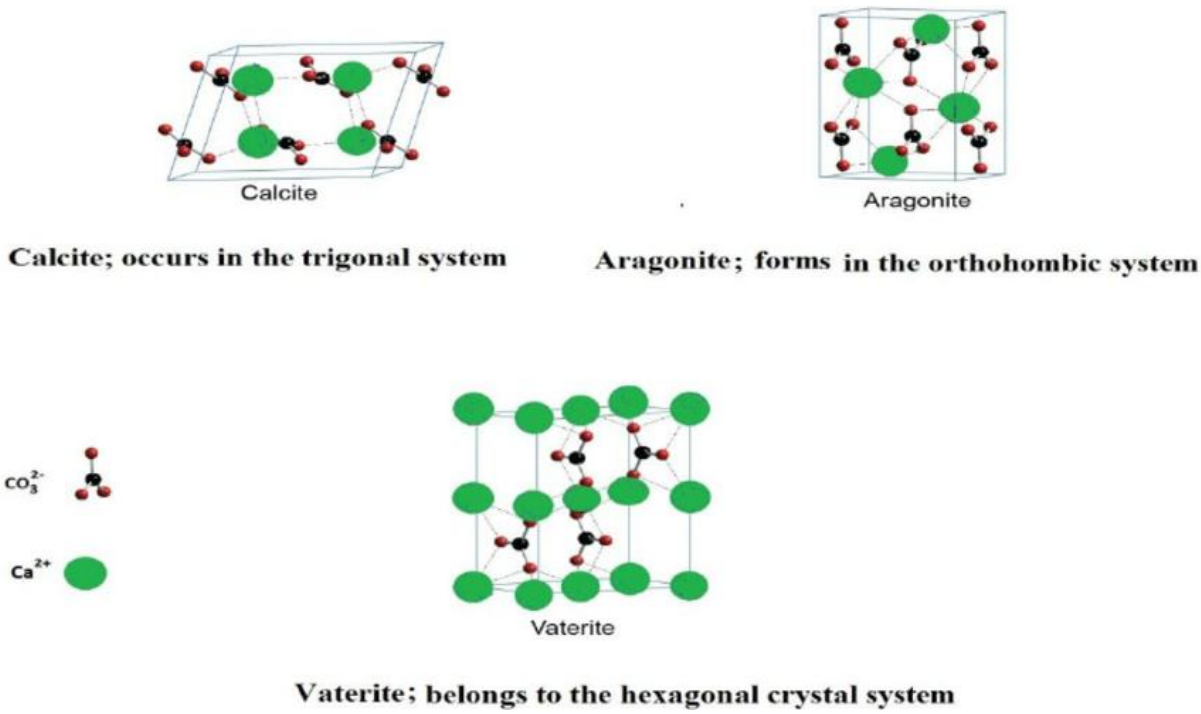

Figure 1.29 Crystal structures of $CaCO_3$: calcite, aragonite and vaterite. (Reproduced from [45])

Compared with the other polymorphs the ACC phase tends to seed crystal growth of the other polymorphs and is unstable (**Figure 1.30)**.

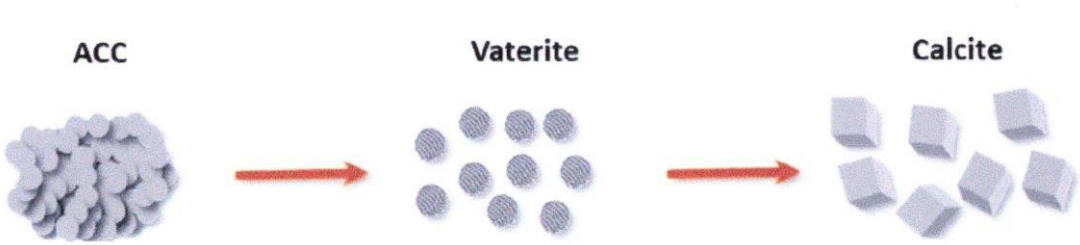

Figure 1.30 Schematic diagram of phase transformations in $CaCO_3$ crystallisation (Reproduced from [46])

The characteristic shapes of calcium carbonate particles are illustrated in **Figure 1.31**.

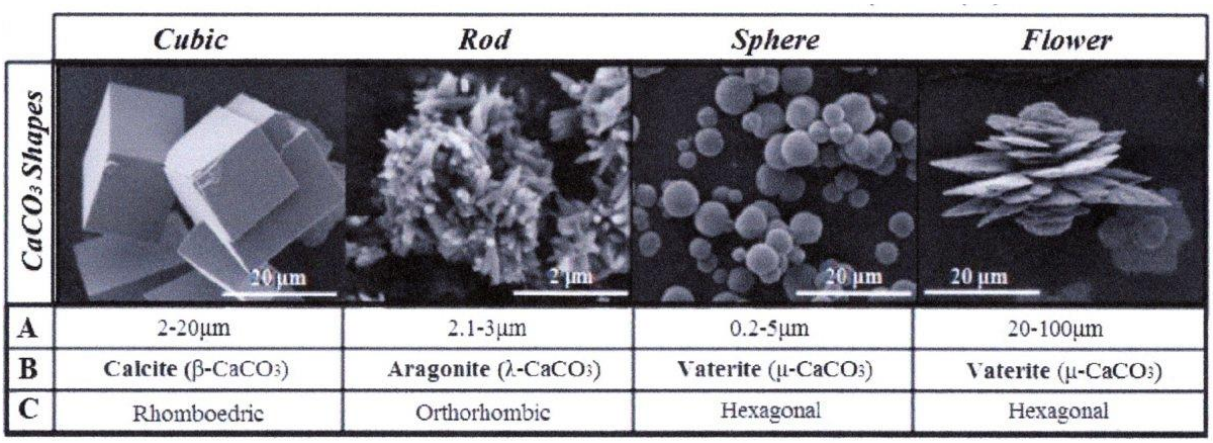

A	2-20µm	2.1-3µm	0.2-5µm	20-100µm
B	Calcite (β-$CaCO_3$)	Aragonite (λ-$CaCO_3$)	Vaterite (µ-$CaCO_3$)	Vaterite (µ-$CaCO_3$)
C	Rhomboedric	Orthorhombic	Hexagonal	Hexagonal

Figure 1.31 Typical morphology of $CaCO_3$ particles (Reproduced from [47])

In the absence of additives spherical microparticles are formed, which are homogeneous and highly porous, *c.f.* the rhombohedral crystals typical of calcite. Consequently, additives are used to direct synthesis, a process often referred to as templating. The additives have a significant influence on the morphology, crystal structure and particle size of the calcium carbonated formed.

Attempts to control the crystallisation process and phase transformation, have adopted facile synthetic methods, for preparation of both solid and hollow particulate calcium carbonate. Most fall into four main categories (spontaneous precipitation, carbon

dioxide bubbling, slow carbonation, reverse (W/O) emulsion), as depicted in **Figure 1.32.**

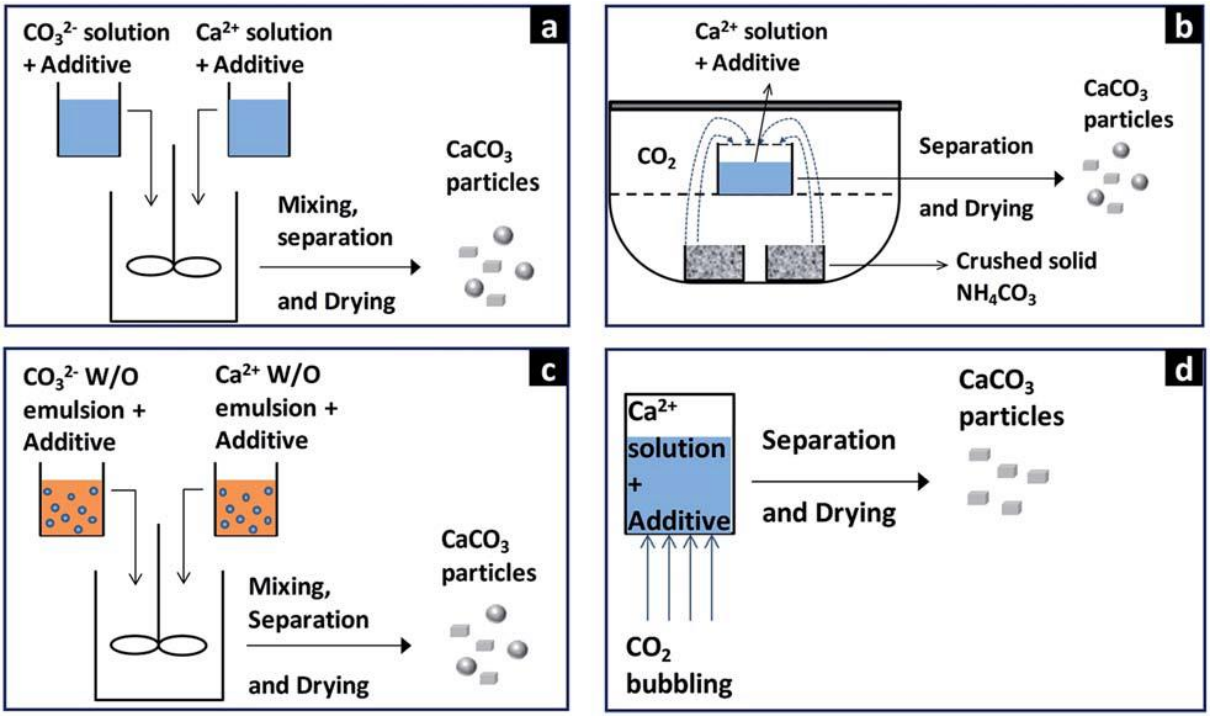

Figure 1.32 Key methods for the synthesis of $CaCO_3$: (a) the spontaneous precipitation method, (b) the slow carbonation method, (c) the reverse (W/O) emulsion method, and (d) the CO_2 bubbling method. (Reproduced from [48])

1.6.1.1 Spontaneous precipitation

Spontaneous precipitation is usefully illustrated by natural processes, where calcium carbonate formation is facilitated by protein-based templates. In biomineralization, ACC is stabilised by acid-rich glycoproteins serving as the precursor for a regulated transformation into the crystalline forms seen in nature, e.g., mollusc shells [49].

In the laboratory, hollow calcium carbonate spheres have been most successfully produced by spontaneous precipitation when using combinations of polymer and surfactant templates (additives). Across the published studies **(36-32)**, polymer concentrations range from 0.2-10 g L^{-1} and surfactant concentrations from 1-20 mM. with pH 10, where reported, and temperatures in the range 20-30^{o}C, with reaction

times from 1 to 24 hours. **Table 1.8** gives examples of polymer-surfactant combinations and the resultant polymorphs and particle size formed for the hollow spheres.

Table 1.8 The influence of additive type on morphology, crystal structure and particle size of hollow shell calcium carbonate

Additives	Morphology	Polymorph	Size (μm)	Ref
Pluronic F127, SDS	Hollow spheres	Calcite	3-4	[50]
PEO-*b*-PMMA	Hollow spheres	Calcite	3.4	[51]
PEG, SDS	Hollow spheres	Calcite, Vaterite	3-6	[52]
PVP, SDS	Hollow spheres	Calcite	2-3	[53]
PSMA, CTAB	Hollow spheres	Calcite (96%), Vaterite (4%)	2-3	[54]

1.6.1.2 Slow carbonation precipitation

For precipitation by slow carbonation studies in the literature show that the Ca^{2+} concentration ranges from 10-20 mM, with the CO_2 source being $(NH_4)_2CO_3$. Temperatures are around 25°C and pH 8-9 and reaction times vary from 10 hours (PAA) to 120 hours (phytic acid) (**Table 1.9**).

Table 1.9 The influence of additive type on morphology, crystal structure and particle size of hollow shell calcium carbonate

Additives	Morphology	Polymorph	Size (μm)	Ref
PAA (20 ppm)	Hollow spheres	Vaterite	1	[55]
Phytic acid	Hollow spheres	ACC	1-3	[56]

If the temperature is increased to 80°C, particle diameters are increased to 4-7 μm. In one study [57], sodium carbonate and calcium nitrate were reacted in the presence of PAA (molecular weight 8000 g mol^{-1}) and SDS. Here the authors proposed an alternative formation mechanism for the hollow shell calcium carbonate formed (**Figure 1.33**). It was considered that according to Fick's first law and Ostwald ripening the ACC formed diffuses to the outer surface, with spheres initially formed by electrostatic interactions between the PAA and SDS with Ca^{2+} ions [58].

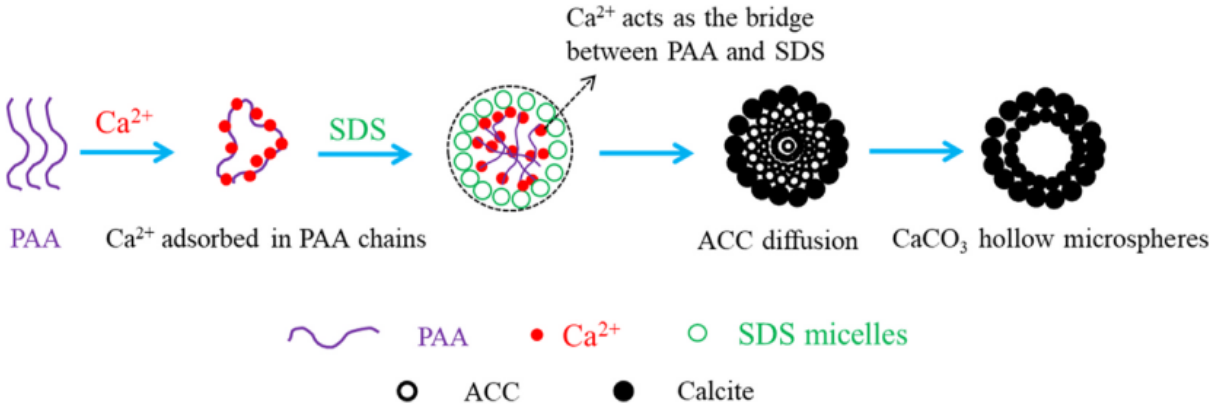

Figure 1.33 Schematic diagram to represent the formation of hollow shell calcium carbonate. (Reproduced from [59])

1.6.1.3 Reverse (W/O) emulsion

Thermodynamic dispersions of water and oil, stabilised by interfacial layers of surfactants, are named reverse W/O emulsions. The addition of Ca^{2+} and CO_3^{2-} forms micelles, which allow a more controlled precipitation to form micro and nano-sized particles that have various shapes and morphologies, but with narrow particle size distribution. Kojima and co-workers identified hollow $CaCO_3$ by adsorption of $CaCO_3$ onto an octane droplet surface dispersed in $CaCl_2$ solution [60].

1.6.1.4 Carbon dioxide bubbling

In contrast to the slow carbonation method which uses carbonate salts as an indirect source of CO_2, the main process used by industry to produce calcium carbonate is to use CO_2 gas by direct bubbling into $Ca(OH)_2$ [slaked lime] at high pH. This produces aggregates of nanosized calcite of cubic or rhombohedral morphology which can be

used as fillers for polymers. However, particles produced using this method though they have porosity are not hollow shells. To produce the latter CO_2 is bubbled into a solution of $CaCl_2$ at high pH (e.g., in the presence of ammonia, pH 10) at 27°C [61], [62]. This process tends to produce the vaterite phase. Here the CO_2 bubble

acts as a template with primary particles (vaterite) attaching to form a continuous solid shell with hollow interior. The fraction of vaterite reaches a maximum at pH ≥ 10. **Figure 1.34** and **Figure 1.35** depict respectively the process and micrograph of the spheres formed.

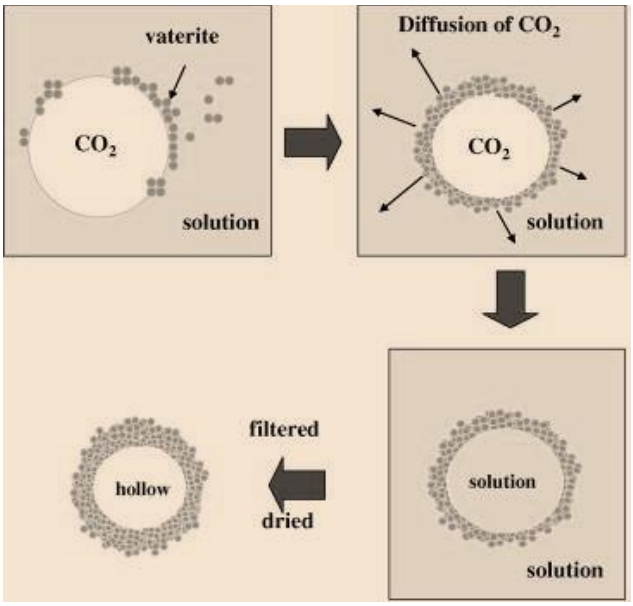

Figure 1.34 Schematic diagram to represent CO_2 bubble acting as a template in the production of hollow shell vaterite. (Reproduced from [63])

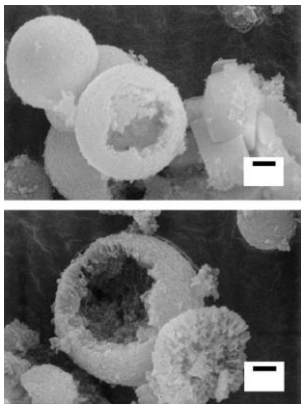

Figure 1.35 SEM micrograph of hollow shell calcium carbonate at pH 9.8 showing mainly spherical particles with some rhombohedral crystals (**-** = 1μm). (Reproduced from [64])

1.6.2 Chemical-Physical Factor influencing form and size of $CaCO_3$

1.6.2.1 Role of $[Ca^{2+}]$:$[CO_3^{2-}]$

If the $[Ca^{2+}] > [CO_3^{2-}]$ (pH 7-8) more positively charged sites attract negatively charged groups on the additives by electrostatic interaction at the particle surface, which controls (reduces) crystal growth, resulting in smaller particles [65]. For solutions with $[CO_3^{2-}] > [Ca^{2+}]$ (pH 9.5-10.5) nucleation, due to supersaturation, is promoted. If the $[Ca^{2+}]$ is relatively low (*c.f.* $[CO_3^{2-}]$) the calcite polymorph is formed in greater abundance than vaterite (in the temperature range 15-30^{o}C) [66].

1.6.2.2 Role of additive type and concentration

If no additives are used spheres (4-6 μm) of calcite are formed, which is the most thermodynamically stable form. The crystallisation process and phase transformation are not as simple as initial consideration implies. In all cases additives play an important role in determining the final morphology of the $CaCO_3$ formed, by provision of sites for nucleation of $CaCO_3$ from Ca^{2+} ions. An example of this is illustrated in **Figure 1.36** and **Figure 1.37**, where the additive Na-PAA directs phase transformation.

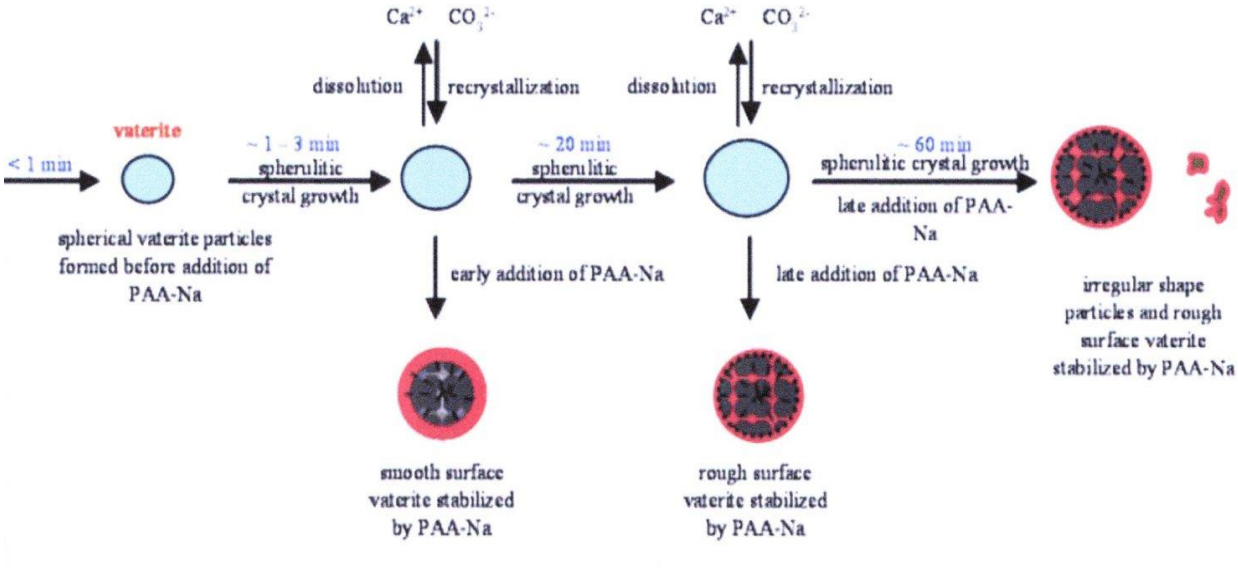

Figure 1.36 Schematic diagram to represent the formation of calcium carbonate spherulites and amorphous phase transformation to Vaterite, from the delayed addition of PAA-Na to supersaturated Ca^{2+}/CO_3^{2-} amorphous precursors. (Adapted from [67])

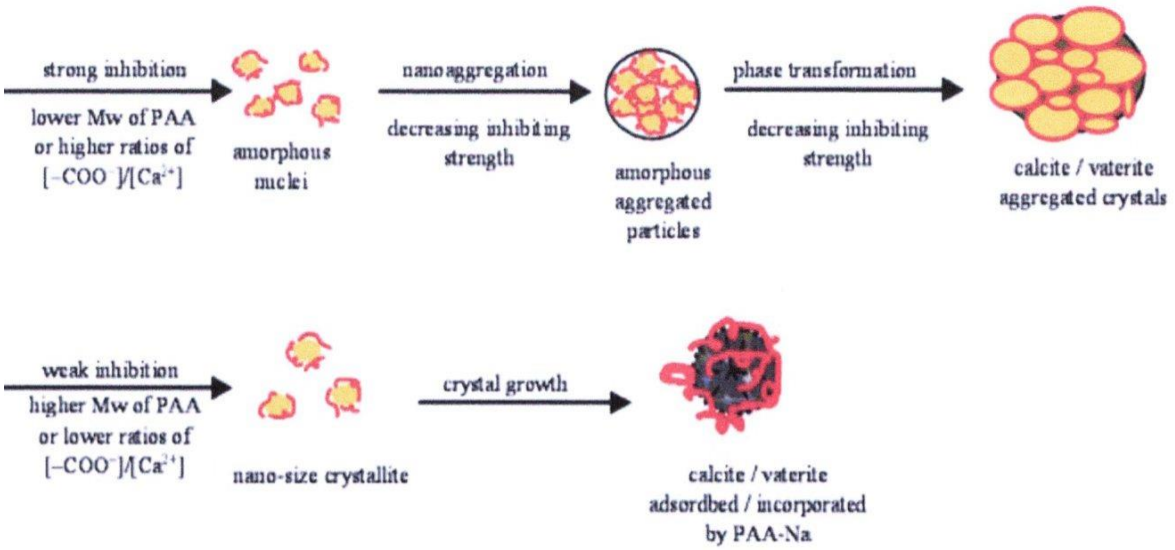

Figure 1.37 Schematic diagram to represent the formation of calcium carbonate spherulites and amorphous phase transformation to Vaterite and Calcite, from the instantaneous addition of PAA-Na to supersaturated Ca^{2+}/CO_3^{2-} amorphous precursors. (Adapted from [68])

1.6.2.3 Role of reaction (mixing) time and order of mixing

During the reaction time there are changes in polymorphs formed, morphology and size of crystallites. In one study during the precipitation reaction in the presence of an additive (PSSS) at high pH (pH = 10) in the first 30 minutes loose ACC aggregates (20-40 nm) formed instantly on precipitation [69]. Aggregation continued up to 90 minutes and after 2 hours spherical particles formed (2-5 μm). After 3 hours these particles became monodispersed (8 μm) and increased in number. This process continued up to 12 hours when no further changes were seen. In another study

In most studies, agglomeration, and crystallisation of ACC (nano) particles leads to the more stable calcite or vaterite phases (**Figure 1.38**), unless high temperatures are used when aragonite is formed (see **Figure 1.39**).

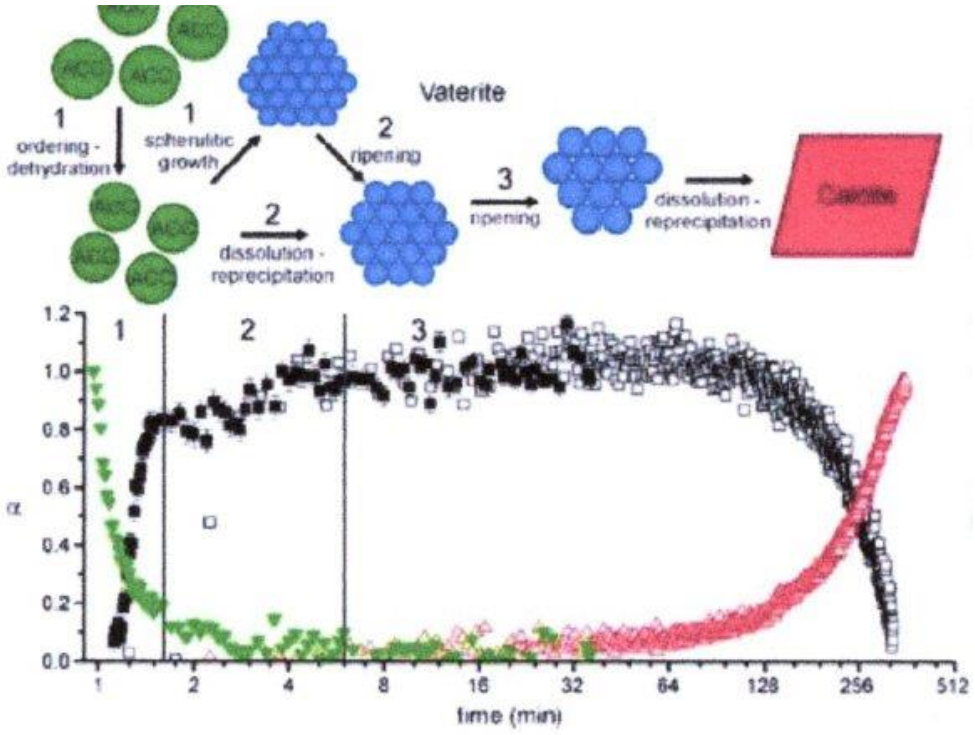

Figure 1.38 Schematic diagram to represent the pathway for ACC-vaterite-calcite crystallisation. (Reproduced from [70])

In the absence of additives increasing reaction time increases particle size (diameter) by a factor of 3 (4-6 mm to 15-20 mm).

The order of addition of Ca^{2+} and CO_3^{2-} is also important. When CO_3^{2-} is added to Ca^{2+}, particle size is often smaller and the distribution of particle sizes narrower. Vice-versa the opposite addition leads to irregular size and larger particles.

1.6.2.4 Role of pH

Although varying pH, for most of the methods reported by the literature, does not affect polymorphism, it does influence morphology and particle size. This is not surprising, since crystal growth depends on interaction between negatively charged groups on the additive and calcium ions in solution. Essentially, a greater number of groups on the additive will be ionised to produce negative charges to 'mop-up' Ca^{2+} ions blocking growth in three dimensions. In conjunction with increasing ionization of groups at high pH, supersaturation increases (i.e., hydrocarbonate/carbonate buffer effect) which reduces nucleation rate. The net effect of this is that a balance in pH is required (pH 9-11 to effectively control particle size (crystal growth)). However, if nucleation rate is too low the phase transition of vaterite (metastable) to calcite is inhibited. One interesting observation in the literature is the use of phytic acid as an additive at pH 3 at longer reaction time (2 hours) resulting in hollow spheres of ACC **(Table 1.9)**

1.6.2.5 Role of temperature

Crystal growth (size), in the presence of additives, is often accompanied by aggregation, which increases at higher temperatures. Although, where core dissolution and recrystallisation at the particle surface is possible this can take place even at high temperatures to give particles < 2 μm.

Temperature also influences the polymorph formed. Higher temperatures favour aragonite by phase transformation of calcite and vaterite (**Figure 1.39**). Around room temperature (15-30^{o}C) the particle size of the precipitate if affected, with an increase as temperature is increased regardless of concentration of Ca^{2+} and CO_3^{2-}. However, for slow carbonation precipitation (in the presence of surfactant) the opposite trend is seen. Also, solubility plays a role if no additives are used: at higher temperatures in the range smaller calcite crystals are formed.

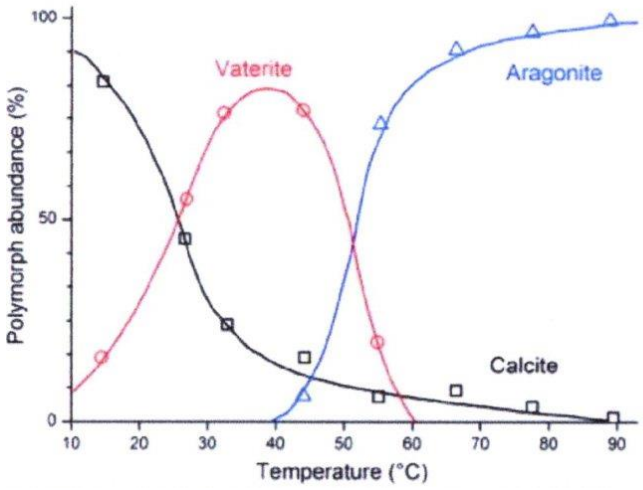

Figure 1.39 Dependence of (initial) $CaCO_3$ polymorph formation on temperature. (Reproduced from [71])

1.7 Aims and Objectives

In this context, the main aim of the present study is to assess the performance of hollow calcium carbonate as an alternative filler to hollow glass microspheres in PVC. This will be achieved by the following objectives:

- Synthesis and characterisation of hollow calcium carbonate
- Incorporation of hollow calcium carbonate (and hollow glass microspheres) in PVC formulations typical of those used in boat-decking
- Evaluation of the performance (density, mechanical and thermal properties) of the resultant PVC-hollow filler composites

2.0 Experimental:

Synthesis of Hollow Calcium Carbonate and Testing in PVC

2.1 Materials

Poly(diallyldimethylammonium chloride) solution (PDADMAC or PDDA) 20wt.% in water (Sigma Aldrich) of high molecular weight (M_w 400,000-500,000) was used to prepare a 0.5 wt.% stock solution (15g of 20 wt.% in 600g H_2O). The structure of PDDA is given in **Figure 2.1**.

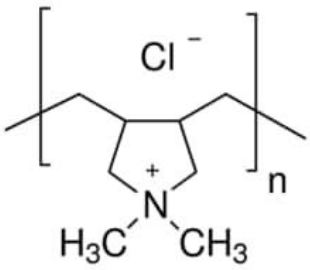

Figure 2.1 Structure of Poly(diallyldimethylammonium Chloride) (PDDA)

Calcium chloride (reagent grade, ≥ 98%, anhydrous, Sigma Aldrich) and Sodium Carbonate (reagent grade, ≥ 99.5%, anhydrous, Sigma Aldrich) were used to prepare aqueous solutions in the range 0.1-1.0 M. milliQ distilled water was used for preparation of all solutions.

Ammonium Hydroxide solution (2.0 M, Sigma Aldrich) was used to adjust the pH of solutions (pH = 10).

PVC resin (K70), plasticiser, one-pack stabiliser and Hollow Glass Spheres (3M™) were supplied by Flexiteek.

2.2 Synthesis of hollow calcium carbonate

A simple experimental design was adopted to prepare hollow calcium carbonate by varying the concentrations of Ca^{2+}, CO_3^{2-} and PDDA, as well as varying mixing time.

This is summarised in **Table 2.1** and described in detail thereafter.

Table 2.1 Variation in the concentrations of Ca^{2+}, CO_3^{2-} and PDDA, and mixing time for the synthesis of hollow calcium carbonate

Sample	$CaCl_2$/PDDA in water			Na_2CO_3/PDDA in water			Stirring Time (mins)
	$[Ca^{2+}]$ (M)	PDDA wt.%	volume (mL)	$[CO_3^{2-}]$ (M)	PDDA wt.%	volume (mL)	
MP1	0.1	0.5	10.0	0.1	water	10.0	60
MP2	0.1	Chitin 0.5	10.0	0.1	water	10.0	60
MP3	0.01	0.5	10.0	0.1	water	10.0	60
MP4	1.0	0.5	10.0	1.0	0.5	10.0	15
MP5	1.0	1.0	10.0	1.0	1.0	10.0	15
MP6	0.1	0.5	100.0	0.1	0.5	100.0	60
MP7	0.5	0.5	10.0	0.5	0.5	10.0	60
MP8	*	*	*	*	*	*	*
MP9	0.1	0.5	300.0	0.1	0.5	300.0	15
MP10	*	*	*	*	*	*	*
MP11	1.0	water	10.0	1.0	water	10.0	15
MP12**	*	*	*	*	*	*	*
MP13**	*	*	*	*	*	*	*
MP14	1.0	0.5	300.0	1.0	0.5	300.0	60
MP15	1.0	0.5	300.0	1.0	0.5	300.0	60
MP16	1.0	0.5	300.0	1.0	0.5	300.0	120
MP17	1.0	0.5	300.0	1.0	0.5	300.0	1440
MP18	1.0	0.5	300.0	1.0	0.5	300.0	1440
MP19	1.0	0.5	300.0	1.0	0.5	300.0	120
MP20	1.0	0.5	300.0	1.0	0.5	300.0	120

** refer to detailed methodology*

*** SEM images of samples MP12 and MP13 are given in the Appendix but are not discussed in this report since the objective for their preparation was to effect comparison/ confirmation of similar particle sizes.*

Synthesis of MP1, MP2, MP3

$CaCl_2$ (aq.,0.1 M) was prepared by dissolving 0.11g in PDDA stock (0.5 wt.%, 10.0 g). Na_2CO_3 (aq., 0.1M, 10.0g) was added dropwise and the resultant solution was mixed for 60 minutes (**MP1**). The same procedure (MP1) was adopted but replacing PDDA with chitin (**MP2**). Finally, the same procedure (MP1), was followed but the concentration of $CaCl_2$ was reduced to (0.01 M) (**MP3**). In each case, solutions (**MP1, MP2, MP3**) were stirred for 60 minutes, filtered and the filtrate oven dried (80^{o}C).

Synthesis of MP4, MP5, MP6, MP7 MP8

$CaCl_2$ (aq.,0.1 M) was prepared by dissolving 1.1 g in PDDA stock (0.5 wt.%, 10.0 g). A solution of Na_2CO_3 (aq.,0.1 M) was also prepared by dissolving 1.1 g in PDDA stock (0.5 wt.%, 10.0 g). The solutions were then mixed and stirred for 15 minutes (**MP4**). This procedure was then repeated but using 1.0 wt.% PDDA (**MP5**). In each case, solutions (**MP4, MP5**) were stirred for 15 minutes, filtered and oven dried (80^{o}C). Sample **MP8** was prepared by addition of water (10 ml) to sample **MP4** (0.2 g), followed by ultrasonication (1 hour), filtration and drying (80^{o}C). Samples **MP6** and **MP7** were prepared using the same method as **MP4**, except that for **MP7** the concentrations of CaCl2 aq. and Na_2CO_3 aq., were 0.5 M and, for **MP6** the concentrations were 0.1 M in PDDA (0.5 wt.%, 100.0 g).

Synthesis of MP9, MP10, MP12, MP13

Sample (**MP9**) was prepared by the same method as **MP6** but 300g of PDDA (0.5 wt.%) used. Sample **MP10** was prepared by addition of water (300 ml) to sample **MP9,** followed by ultrasonication (1 hour), filtration and drying (80^{o}C). Sample **MP10** was mixed with water (1:10 ratio) and ultrasonicated (1 hour) to give sample **MP12**. The filtrate (cloudy) was collected to recover sample **MP13**.

Synthesis of MP11

$CaCl_2$ (1.0 M) in water (10.0 g) was adjusted to pH 10 (NH_4OH dropwise addition). This process was then repeated for Na_2CO_3. The solutions were then stirred for 15 minutes, filtered and oven dried (80^oC).

Synthesis of MP14, MP15

$CaCl_2$ (1.0 M) in PDDA stock (0.5%, 300.0 g) was mixed with Na_2CO_3 (1.0 M) in PDDA stock (0.5%, 300.0 g). The solution was then stirred for 60 minutes, filtered and oven dried (80^oC) (**MP14**). This procedure was then repeated to produce a second batch for comparison (**MP15**)

Synthesis of MP16, MP17, MP18, MP19, MP20

Samples **MP16, MP19** and **MP20** were batches produced by the same method as sample **MP14,** except that the stirring time was 120 minutes (2 hours). Samples **MP17** and **MP18** were batches produced by the same method as sample **MP14,** except that the stirring time was 1440 minutes (24 hours).

2.3 Preparation of PVC Test Plaques/Bars

Test plaques/bars were prepared from the formulations given in **Table 2.2**. The hollow filler was either hollow glass spheres (3M) or hollow calcium carbonate (**MP21**, **MP22**, **MP23**).

Table 2.2 PVC Formulations used to prepare test plaques/bars

Formulation Components	phr*			weight (g)		
	Low	Mid	High	Low	Mid	High
PVC (K70)	100	100	100	31.88	26.89	25.17
Plasticiser	44	62	62	14.03	16.67	15.61
Hollow Filler	26	40	54	8.29	10.76	13.59
One-Pack Stabiliser	2.5	2.5	2.5	0.8	0.67	0.63

* percent hundred ratio (see glossary for extended definition)

The 'One-Pack' stabiliser is a package of additives that are a combination of substances such as antioxidants, process aids etc. The 'One-Pack' used here is non-toxic based on calcium and zinc antioxidants blended with other co-stabilisers.

Separate batches of hollow calcium carbonate (**MP21, MP22, MP23**) were then prepared according to the method for MP16. The samples were heated for 4 hours at 80^{o}C to remove water and then calcined at 550^{o}C for 4 hours. Samples **MP21** and **MP23** were incorporated into PVC in the range 15-24 wt.% (typical in commercial formulations) according to **Table 2.2**.

Dry blends of the formulations were mixed in a Rheometer. Normally, the rheological properties of the material at processing temperatures are measured. Here torque is used to reflect the viscosity and elasticity of the material (K-value of PVC is a measure of viscosity, while die swell is a measure of elasticity). The relationship between torque, time and temperature gives information on fusion behaviour, safe processing window (time and onset of degradation).

In this study the conditions of mixing were informed by previous commercial work, so the rheometer was used only for mixing of formulations to prepare test plaques/bars. **Figure 2.2** depicts the mixed formulation.

Figure 2.2 PVC formulation containing hollow calcium carbonate filler (19 wt.%) after rheometric mixing

Samples were prepared using a Thermo Scientific HAAKE™ Polydrive Rheomix 600. The following test conditions were applied: Mixer temperature: 150 °C; Rotor speed: 100 rpm; Sample weight: 55 g; 5 bar pressure pneumatic ram; Mixing time 5 minutes.

Samples were then size reduced (grinding), and compression moulded into plaques using a hydraulic press (Bradley and Turton Ltd., capacity 50 tonne) between two aluminium plates (platens). Heated platens should be at the temperature which is at least 50 °C above the melting points of the polymer in the case of semi-crystalline polymers, but this is not necessary for amorphous polymers like PVC. Care should be taken that the platen temperature is not too high to prevent degradation of the polymer.

Ground PVC chips (100 g) were pressed into plaques in a two-stage moulding cycle. First the polymer was held in contact with the heated plate at a low temperature for 10 minutes to allow uniform heating and melting. Subsequently, the applied pressure was increase to 35 psi/ton for 10 minutes at 170^{o}C. The sample was then quench cooled by immersion in a bath of cold running water for 10 minutes.

Tensile tests were conducted on dumbbell specimens (see **Section 2.4.4**).

2.4 Characterisation

2.4.1 X-ray diffraction (XRD)

X-ray diffraction data were collected on a PANalytical X'pert Powder X-ray diffractometer using Cu Kα radiation (λ=0.51054Å) with generator settings of 45kV, 40mA. Automatic divergence and antiscatter slits were used on the incident and diffracted beam paths with data collected using a PIXCel 1-D detector operating in scanning line mode with an active length of 3.347 °2θ. The incident beam was passed through a 10mm beam mask with the automatic divergence slits on the source set to maintain a constant irradiated length of 5mm throughout the scan. The automatic antiscatter slits on the detector were also set to maintain constant 5mm aperture. Data were collected in the range 10 -140° 2θ with a step size of 0.013° 2θ and a measuring time of 89s/step. The samples were rotated at 60 rpm during the data collection. Data was truncated to the range 15 -70° 2θ, converted to fixed divergence slit and the $k\alpha_2$ component was removed. Phases were identified using the search-match function in HighScore Plus against the Crystallography Open Database for any mineral phases with unit cell and crystallite size parameters determined using Pawley refinement. A characteristic XRD for the different phases of calcium carbonate from the literature is given in **Figure 2.3**

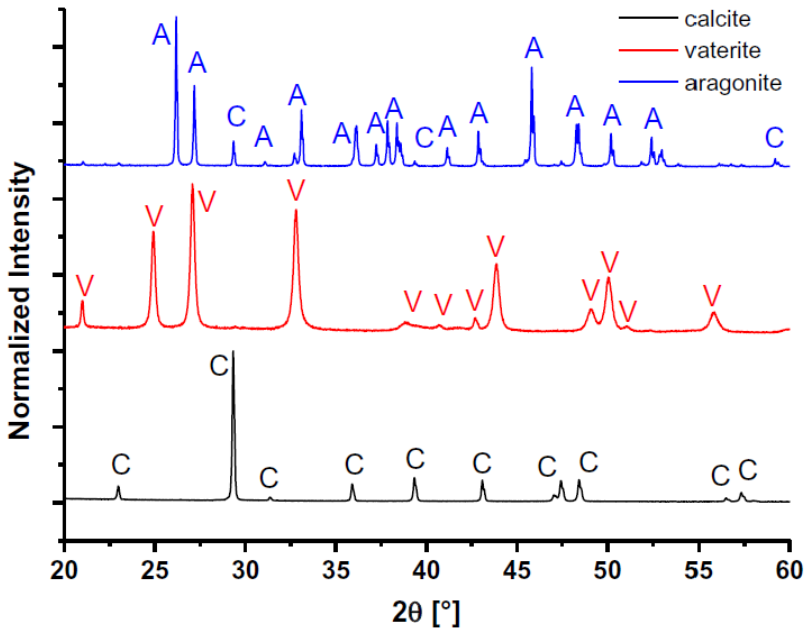

Figure 2.3 XRD spectra of calcium carbonate polymorphs (from [72])

2.4.2 Scanning electron microscopy (SEM)

The morphology of samples was determined by scanning electron microscopy Calcium carbonate samples (MP1-MP23, synthesised by methods in **Section 2.2**) were applied using SEM adhesive. The surface of the samples was examined with a high-resolution scanning electron microscope (SEM) Quanta 450 FEG (FEI) using a secondary electron detector. Analyses were performed at accelerating voltage between 5 and 20 kV.

Samples used for dilatometry were dispersed as powders on carbon tape. All the samples were gold coated with a 5-nm thick layer. The sputter coater was a Polaron SEM coating system (Coating time 30s, voltage 800 V, current 5 mA). SEM (Carl Zeiss Ltd., Supra 40VP, **Figure 2.4**) was used to verify morphology, particle size and evidence of porosity. Data was processed using SmartSEM™ software. Five areas of each sample were analysed at 5K magnification.

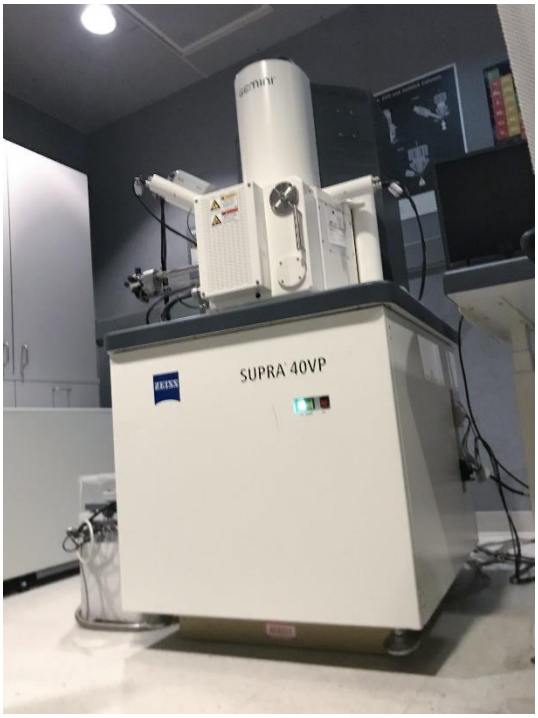

Figure 2.4 Carl Zeiss Ltd., Supra 40VP scanning electron microscope

2.4.3 Density

Polymer density was calculated by gravimetric water displacement [73]. To obtain an accurate reading of weight, water ($50cm^3$, volumetric flask) was shaken then ultrasonicated (2 minutes) to remove air bubbles and weighed on a four-figure balance. The process was then repeated with samples of PVC granulate (**Section 2.3**) in water ($50cm^3$, volumetric flask) shaken and ultrasonicated (2 minutes) to remove air bubbles and weighed on a four-figure balance. All measurements were performed in triplicate. Although this method was used to determine filled polymer density, modified methods can be used to verify sample porosity [74].

2.4.4 Mechanical Properties

Five 'dumbell' test bars were cut from the plaques prepared (described in Section 2.2.3). The shape of the dumbbell (**Figure 2.5**) cut is determined by the rigidity and thickness of a PVC plaque (in this case 6mm). Hence each dumbbell specimen was cut to thickness, 6mm, width 27 mm, length 117 mm, gauge length 45 mm

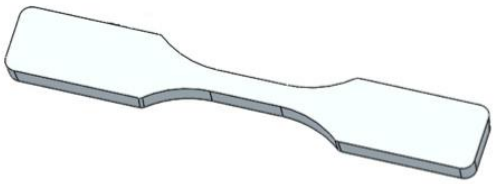

Figure 2.5 Tensile test bar (middle section) gauge length 45 mm.

Test bars were loaded into tensile grips and attached to the extensometer of the tensile test instrument.

Stress-strain curves were obtained using a Tinius Olsen H10KS (**Figure 2.6**) tensiometer fitted with an extensometer, and data was processed using Horizon software. Modulus values were determined using Horizon software program for ASTM D638 with a crosshead speed of 50 mm min^{-1} until rupture of the sample. This standard

test method is one of the most common plastic strength specifications and covers the tensile properties of unfilled and filled polymers.

Figure 2.6 Tinius Olsen H10KS tensiometer.

2.4.5 Thermal Properties

Thermogravimetric analysis (TGA) was carried out using an SDT 650 thermal analysis instrument (TA Instruments) in N_2 atmosphere (50 mL/min). Standard TGA was undertaken at a heating rate of 10 ◦C/min and a temperature ramp of 25 to 300 ◦C. Isothermal TGA was undertaken by ramping to 180^{o}C at 100^{o}C/min and then held at this temperature for 90 min under N_2.

Thermal conductivity was predicted using theoretical equations (**Equations 5.2** and **5.3**) and compared with data supplied for the commercial sample.

3.0 Results and Discussion

3.1 Rationale for synthetic procedure adopted

A range of molecular templates to direct crystallisation by controlled nucleation of Ca^{2+} and CO_3^{2-} to produce hollow calcium carbonate has been described in the introduction (**Sections 1.4.1.1 and 1.4.1.2**). Polyelectrolytes are commonly used as templates for self-assembly, especially when stable, homogeneous films are required. The most prevalent are commercially available polymers that are grouped as cationic (e.g., poly(ethyleneimine), poly(allylamine), poly(allylamine hydrochloride poly(diallyldimethylammonium chloride), diazo-resin) and anionic (poly(styrene sulfonate), poly(vinylsulfate) and poly(acrylic acid) [75-78]. The literature reports that the colloidal template may be used as a sacrificial core. Following multilayer assembly by sequential adsorption the core is removed by either chemical methods or calcination. This process allows a higher degree of control over particle size, shape, and wall thickness.

Here rationale for the selection of a cationic electrolyte with high charge density, namely Poly(diallyldimethylammonium chloride) (PDADMAC or PDDA), as a colloidal template to produce hollow calcium carbonate is presented. PDDA has been used as a template in production of both hollow silica and titania [79]. Akhondi and Jamalizadeh have prepared cubic and spherical hollow silica (**Figure 3.1**) using a hard templating method with polystyrene-PDADMAC and polystyrene-polyethyleneimine [80]. Other workers have shown that an understanding of amine-silicate interactions enables the formation of both hollow and non-porous silicates to be controlled and undertaken under milder conditions (i.e., room temperature in aqueous systems around neutral pH) [81].

An alternative approach that is simple and economical is known as the “self-template” method. It has been used to produce porous silica by alkaline treatment of PDDA. The PDDA deposited on silica spheres is attacked by hydroxyl ions that permeate the template layer and attack the silica sphere to generate dissolved silicate oligomers in the presence of ammonia. The oligomers are negatively charged and deposit on the

positively charged PDDA forming a silica-PDDA shell. Sodium hydroxide is then used to etch the interior of the silica spheres [82].

The influence of ammonia and selected amines on the characteristics of calcium carbonate precipitated from calcium chloride solutions via carbonation has been reported in the literature [83]. Although the latter work does not encompass the preparation of hollow calcium carbonate, it does add confidence to an approach based on colloidal self-templating using PDDA to allow a high degree of control over particle size, shape, and wall thickness. Furthermore, such a tactic is attractive from a commercial perspective because the raw materials are low cost, readily available and reaction times are short. Hence this approach has been adopted in this study. To establish how the presence of PDDA, PDDA concentration, mixing time, ultrasonication and calcination affect the morphology and structure of calcium carbonate a simple experimental design was used, by varying components.

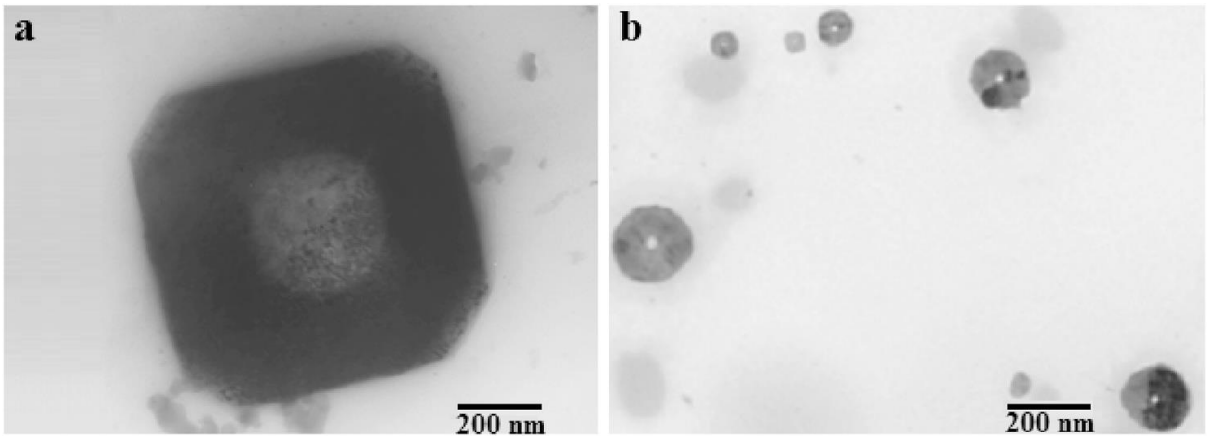

Figure 3.1 TEM images of hollow silica prepared using a PDADMAC template: Hollow cubic morphology (a) and hollow spherical morphology (b) (Reproduced from [80])

3.2 Synthesis and Structure of Hollow Shell Calcium Carbonate

3.2.1 Comparison of absence and presence of a molecular template (additive)

Previous studies have shown that the chemical composition of ACC (amorphous calcium carbonate) is nominally hydrated calcium carbonate ($CaCO_3.H_2O$), with a calcium-rich nanoscale framework with pores containing water and carbonate ions [84]. However, as stated in the introduction, ACC is thermodynamically unstable and crystallises at room temperature from aqueous solution (in minutes to hours) leading to calcite and/or vaterite depending on conditions (**Figure 3.2** and **Figure 3.3**).

The highly porous spherical particles of calcite and/or vaterite produced by rapid mixing, in the absence of a molecular template, can be seen in the SEM image in **Figure 3.1** (**MP11**: [Ca^{2+}] 10 mL of 1.0 M, aq. + [CO_3^{2-}], 10 mL of 1.0 M, aq., combined stir time 15 mins). The presence of both calcite (40%) and vaterite (60%), rather than ACC, is confirmed by XRD in **Figure 3.3**. The SEM (**Figure 3.2**) also shows the relatively small size of the spherical particles produced (<2 μm), which is expected due to the shorter mixing time of 15 minutes.

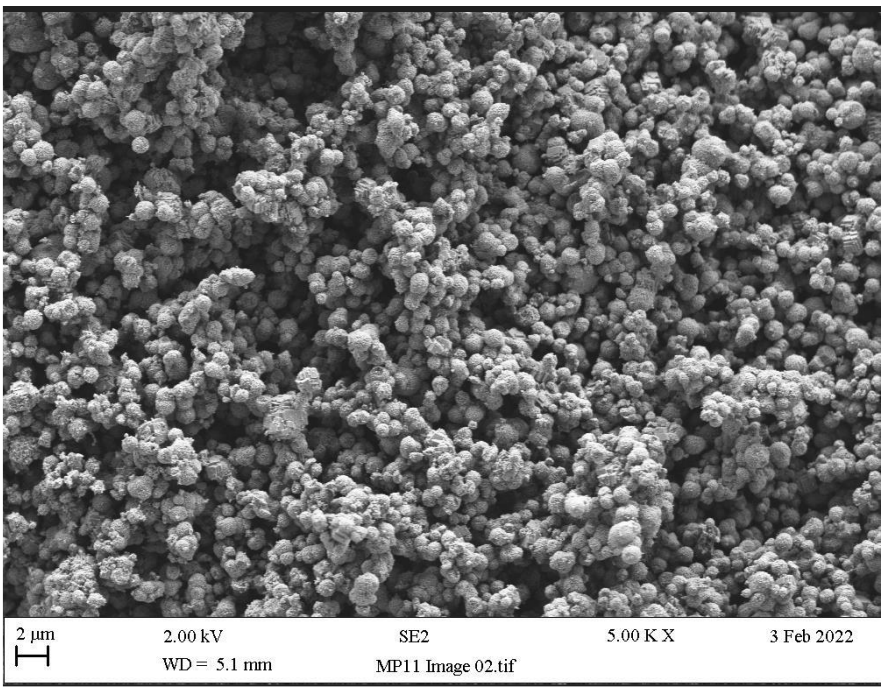

Figure 3.2 SEM image of calcium carbonate synthesised by precipitation in the absence of PDDA additive (**MP11**)

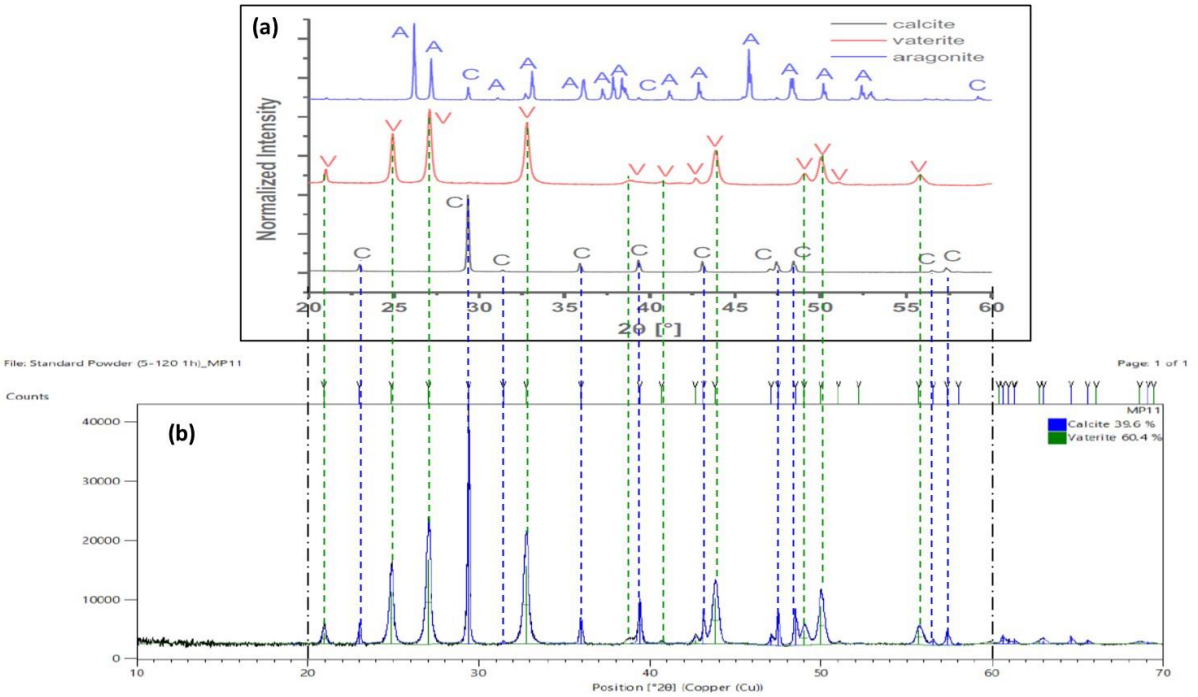

Figure 3.3 Selected region of XRD spectra of (a) individual calcium carbonate polymorphs synthesised by precipitation with no additive (Reproduced from [72]) and (b) calcium carbonate synthesised by precipitation in the absence of PDDA additive (**MP11**)

Figure 3.5 illustrates the effect of addition of chitin as a molecular template to the solution of Ca^{2+} ions (**MP2**: [Ca^{2+}] 0.1 M in 10 mL aq. Chitin 0.5 wt% + [CO_3^{2-}], 10 mL of 1.0 M, aq., combined stir time 60 mins), while the CO_3^{2-} ions remain as an aqueous solution with no additive present. After mixing and stirring for 60 minutes the SEM of the calcium carbonate formed suggests that rhombohedral calcite crystals are formed. This is likely driven by precipitation of the calcite polymorph on chitin, facilitated by interaction with its carbonyl and amide groups (**Figure 3.4** (1) and (2)**)** [85]. Despite the longer mixing time (60 minutes) there is evidence that ACC diffusion is incomplete.

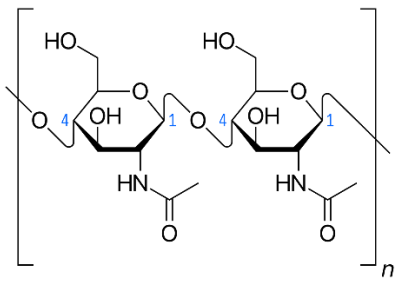

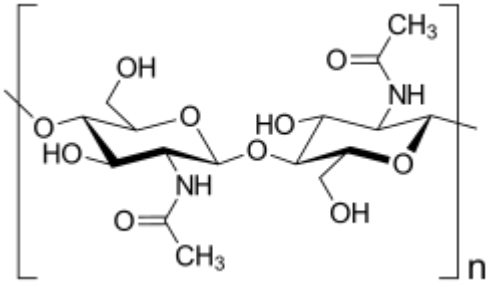

Figure 3.4 Structure of chitin (1) Structure of chitin (2)

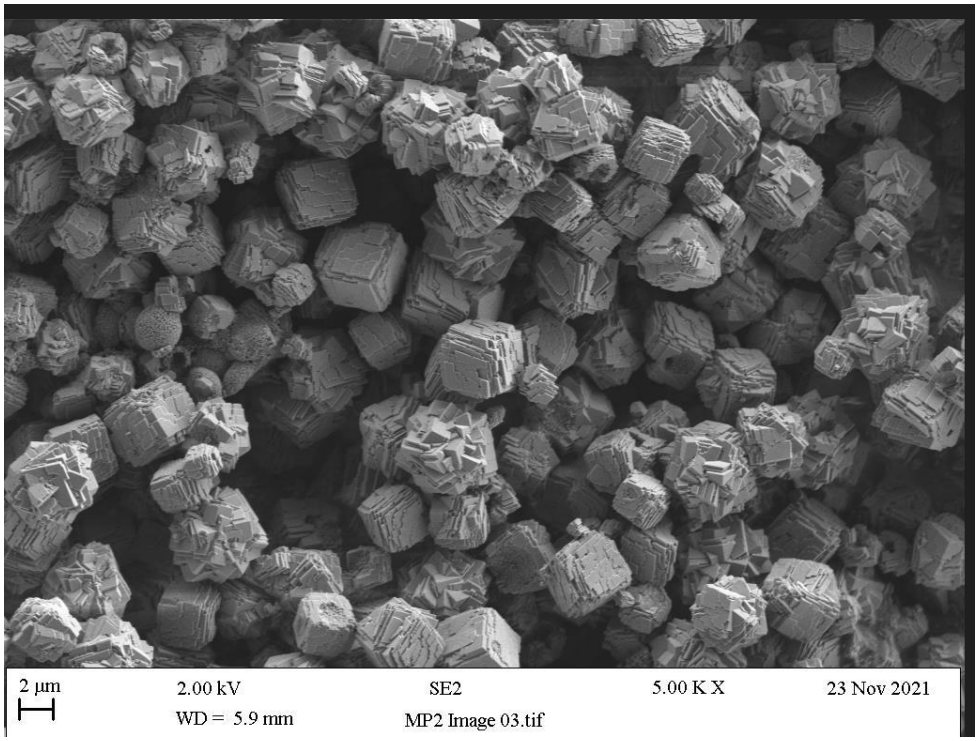

Figure 3.5 SEM image of calcium carbonate synthesised by precipitation from Ca^{+} (aq, 0.1M) in the presence of chitin as a molecular template (0.5 wt.%) (**MP2**)

Figure 3.6 shows the effect of replacing chitin with PDDA as a molecular template to the solution of Ca^{2+} ions (**MP1**: [Ca^{2+}] 0.1 M in 10 mL aq. PDDA 0.5 wt% + [CO_3^{2-}], 10 mL of 1.0 M, aq., combined stir time 60 mins), with CO_3^{2-} in water. It might be expected that as a cationic electrolyte with high charge density (**Figure 2.2**, **Section 2.2.1**) it could direct crystallisation and nucleation. Unfortunately, there is little evidence of 'controlled' precipitation when PDDA is added only to the Ca^{2+} solution. Instead, calcite crystals (rhombohedral) attached to vaterite (spherical), with the development of growth steps on the calcite surface is seen. However, there is some evidence that the calcite formed is hollow (highlighted by yellow circles, **Figure 3.6)** [86]**.** Reducing the concentration of Ca^{2+} did drive the reaction towards the formation of calcite, though crystal formation is still transitional (i.e., ACC diffusion is still not complete, **Figure 3.7**, **MP3**: [Ca^{2+}] 0.01 M in 10 mL aq. PDDA 0.5 wt% + [CO_3^{2-}], 10 mL of 1.0 M, aq., combined stir time 60 mins**)**. Samples **M1**, **MP2** and **MP3** have been stirred for 60 minutes rather than 15 minutes (**MP11**) to allow longer time for the phase transition to take place.

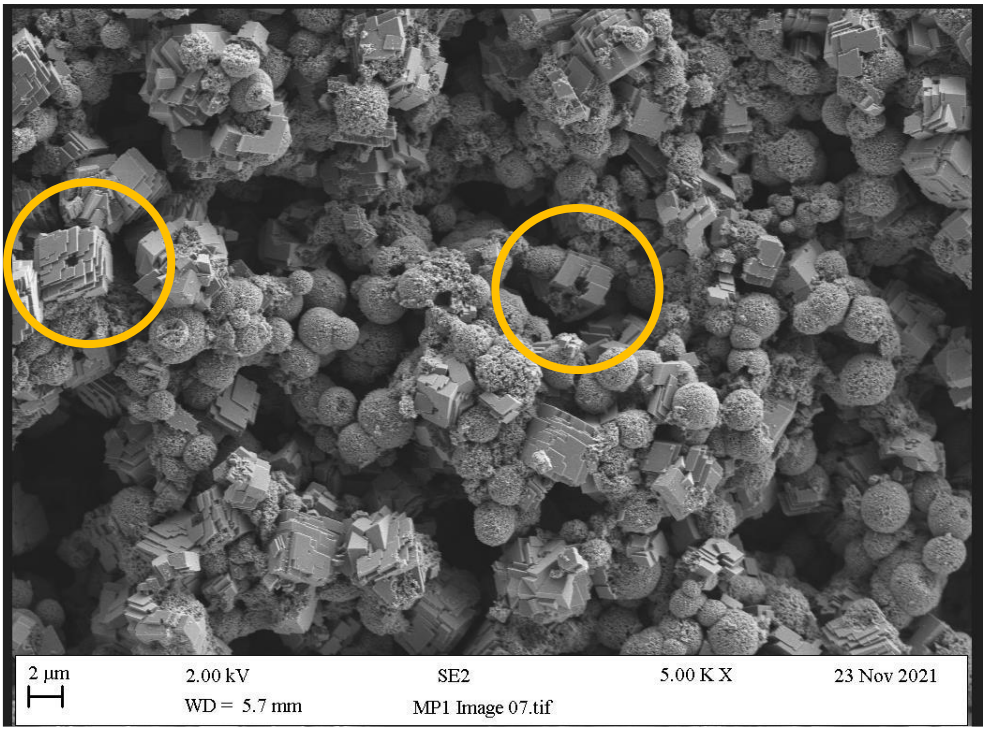

Figure 3.6 SEM image of calcium carbonate synthesised by precipitation from Ca^{+} (aq, 0.1M) in the presence of PDDA as a molecular template (0.5 wt.%) (**MP1**). Areas circled yellow highlight evidence for hollow particles

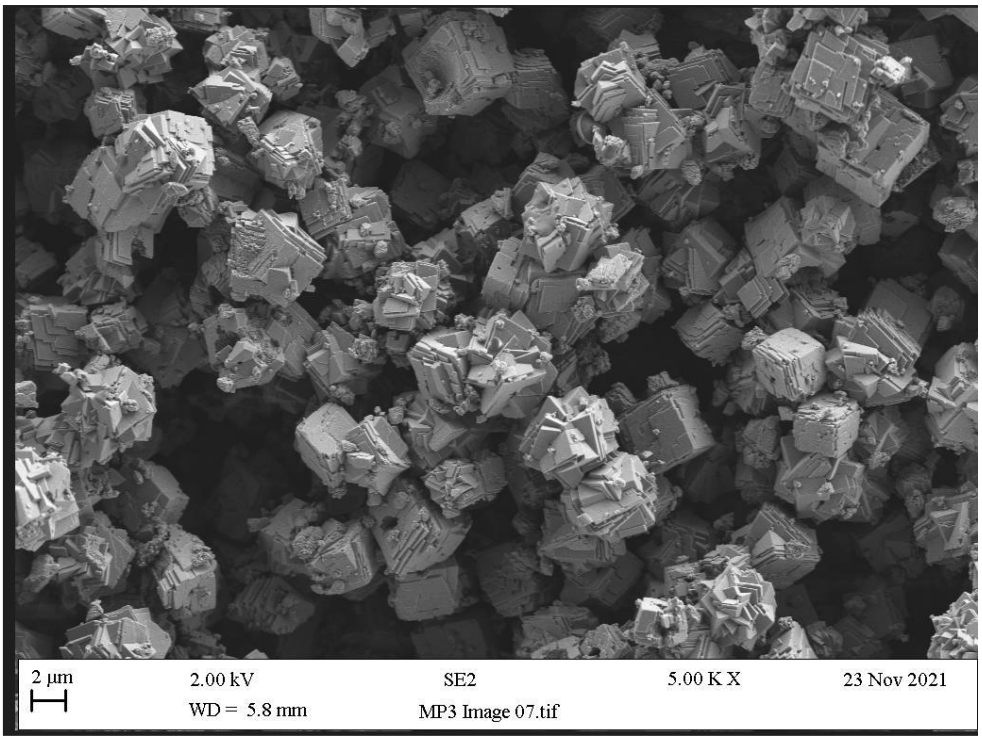

Figure 3.7 SEM image of calcium carbonate synthesised by precipitation from Ca^{+} (aq, 0.01M) in the presence of PDDA as a molecular template (0.5 wt.%) (**MP3**)

3.2.2 Effect of addition of PDDA to solutions of Ca^{2+} and CO_3^{2-} before mixing

From the SEM image of **MP4** ([Ca^{2+}] 1.0 M in 10 mL aq. PDDA 0.5 wt% + [CO_3^{2-}], 1.0 M in 10 mL aq. PDDA 0.5 wt%, combined stir time 15 mins) in **Figure 3.8**, it was seen that keeping the concentration of PDDA constant but doubling the concentration of Ca^{2+} and CO_3^{2-}, resulted in the formation of spherical crystals. These were confirmed as calcite and vaterite by XRD (**Figure 3.9**).

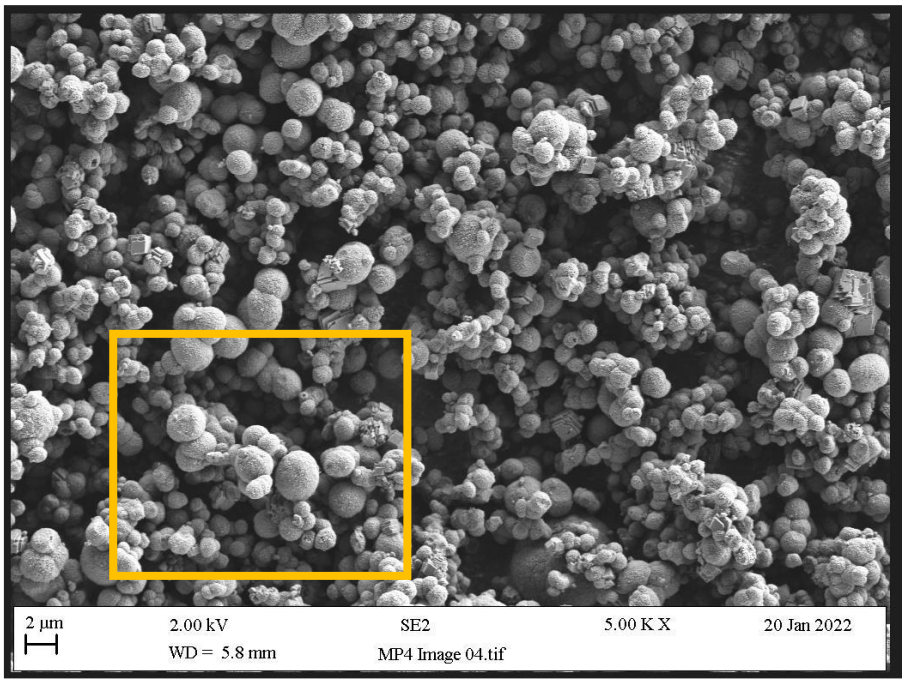

Figure 3.8 SEM image of calcium carbonate precipitated after mixing solutions of Ca^{+} (1.0 M, 10 mL) in PDDA (aq., 0.5 wt.%) and CO_3^{2-} (1.0 M, 10 mL) in PDDA (aq.,0.5 wt.%) followed by stirring for 15 minutes (**MP4**).

In sample **MP5** ([Ca^{2+}] 1.0 M in 10 mL aq. PDDA 1.0 wt% + [CO_3^{2-}], 1.0 M in 10 mL aq. PDDA 1.0 wt%, combined stir time 15 mins, **Figure 3.10**) the concentrations of Ca^{+} and CO_3^{2-} solutions were each kept at 1.0 M, but the concentration of PDDA was doubled, while the stirring time after mixing remained at 15 minutes. Again, spherical particles are formed (probably of vaterite and calcite) but at this shorter timeframe transition to rhomboidal calcite is not evident.

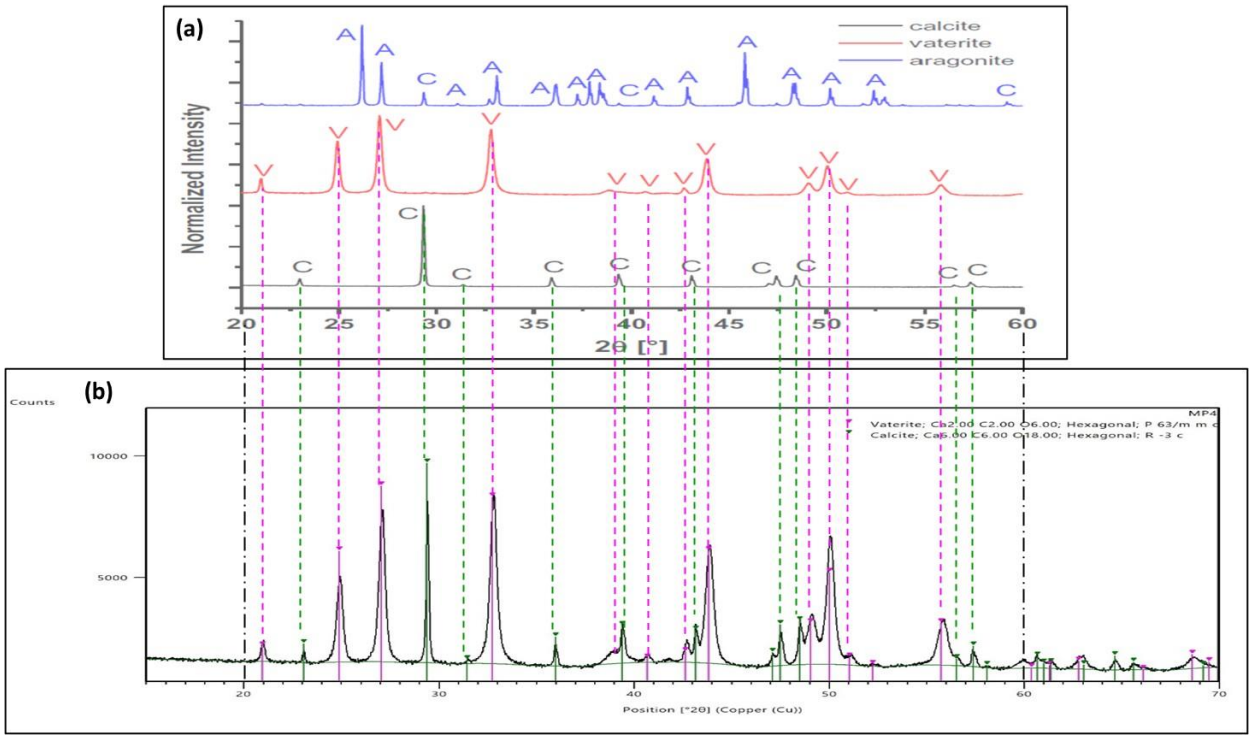

Figure 3.9 Selected region of XRD spectra of (a) individual calcium carbonate polymorphs synthesised by precipitation with no additive (Reproduced from [72]) and (b) calcium carbonate synthesised by precipitation in the presence of PDDA additive (**MP4**)

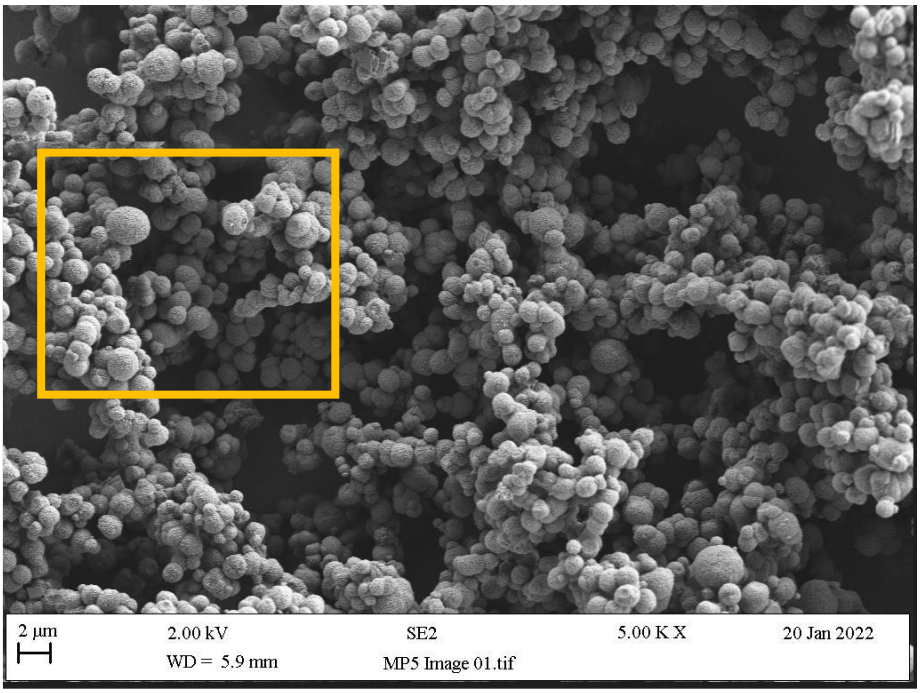

Figure 3.10 SEM image of calcium carbonate precipitated after mixing solutions of Ca^{+} (1.0 M, 10 mL) in PDDA (aq., 1.0 wt.%) and CO_3^{2-} (1.0 M, 10 mL) in PDDA (aq.,1.0 wt.%) followed by stirring for 15 minutes (**MP5**).

Figure 3.11 shows the expanded areas of the SEM images of $CaCO_3$ precipitates of **MP4** and **MP5** for the different PDDA concentrations. As the PDDA concentration is increased the morphologies change to more uniform spherical structures. It is expected that lower PDDA concentration reduces its ability to bridge nanoscale particles [87]. However, the spheres in **MP5** appear to be more solid than those in **MP4** (see area circled). This could be caused by long chains of the PDDA surrounding microspheres preventing $CaCO_3$ particles in the interior diffusing out, so increasing the nucleation density.

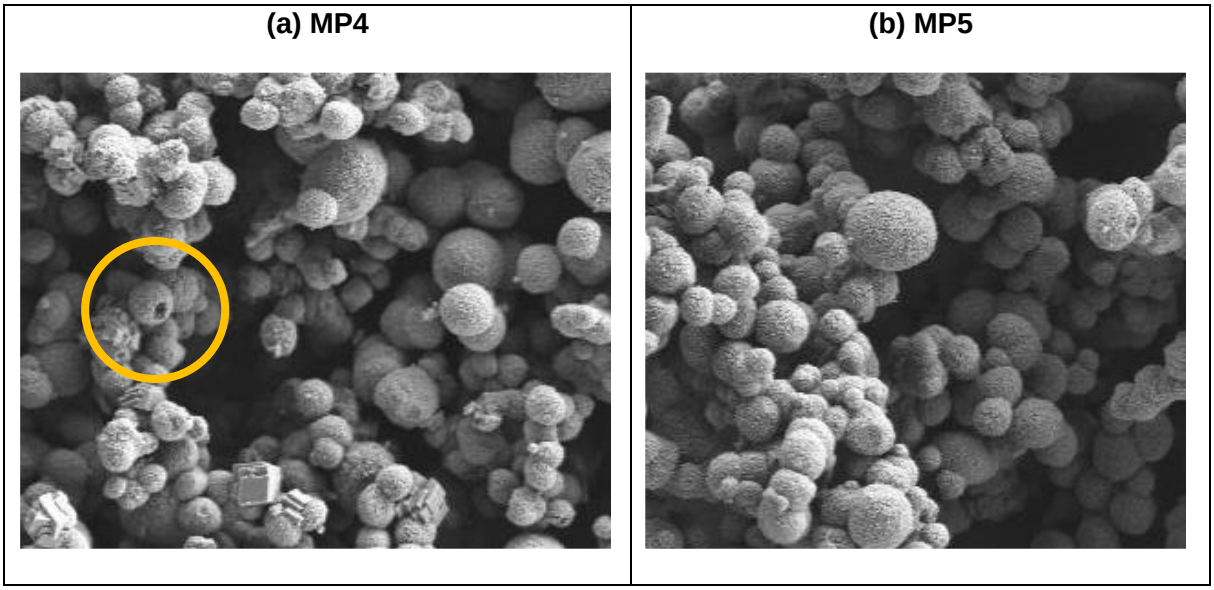

Figure 3.11 Expanded SEM image of calcium carbonate for samples **MP4** (taken from **Figure 3.9**) and **MP5** (taken from **Figure 3.10**). Areas circled yellow highlight evidence for hollow particles

For sample **MP7** ([Ca^{2+}] 0.5 M in 10 mL aq. PDDA 0.5 wt% + [CO_3^{2-}], 0.5 M in 10 mL aq. PDDA 0.5 wt%, combined stir time 60 mins) PDDA was present at the same concentration as sample **MP4**, but the combined solutions were stirred for a longer time of 60 minutes. Furthermore, the concentrations of Ca^{2+} (0.5 M) and CO_3^{2-} (0.5 M) were reduced in comparison to **MP4.** This effectively increased the relative amount of PDDA in **MP7**. Evidence of greater solidity in samples when stirred for longer times, with higher concentrations of molecular template, is supported by the SEM image for

MP7 in **Figure 3.12**. Again, it is seen that the longer time has promoted the formation of (solid) rhombohedral calcite.

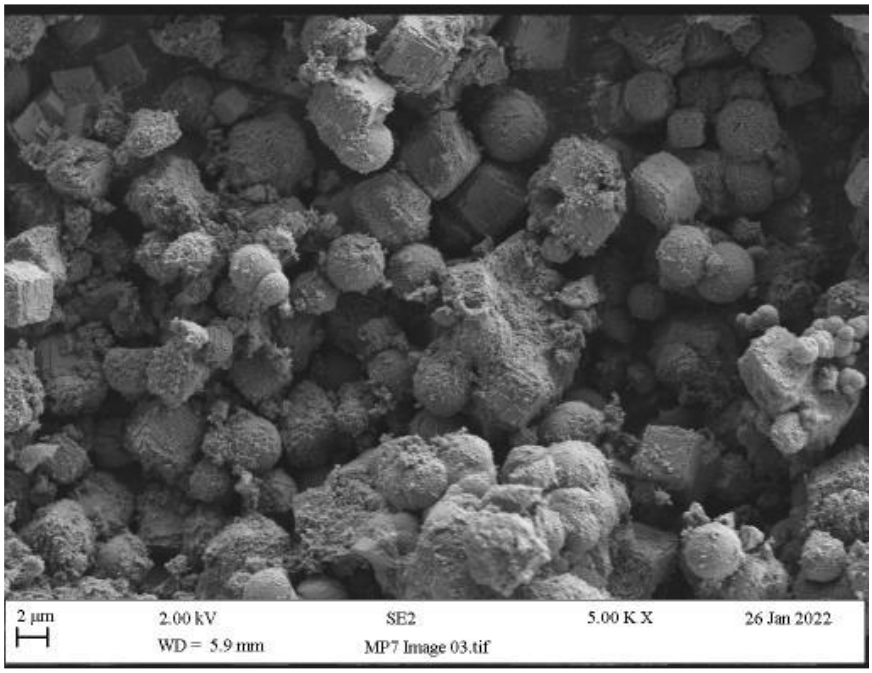

Figure 3.12 SEM image of calcium carbonate precipitated after mixing solutions of Ca^{+} (0.5 M, 10 mL) in PDDA (aq., 0.5 wt.%) and CO_3^{2-} (0.5 M, 10 mL) in PDDA (aq.,0.5 wt.%) (**MP7**).

3.2.3 Effect of dilution of solutions of Ca^{2+} in PDDA and CO_3^{2-} in PDDA before mixing

Compared to sample **MP7,** sample **MP6** ([Ca^{2+}] 0.1 M in 100 mL aq. PDDA 0.5 wt% + [CO_3^{2-}], 0.1 M in 100 mL aq. PDDA 0.5 wt%, combined stir time 60 mins) further reduces the concentration of Ca^{2+} (0.1 M) and CO_3^{2-} (0.1 M). Overall dilution and longer stirring time (60 minutes) further supports the arguments in the previous section. The SEM image (**Figure 3.13**) shows porosity in the spherical particles, along with evidence of rhombohedral calcite.

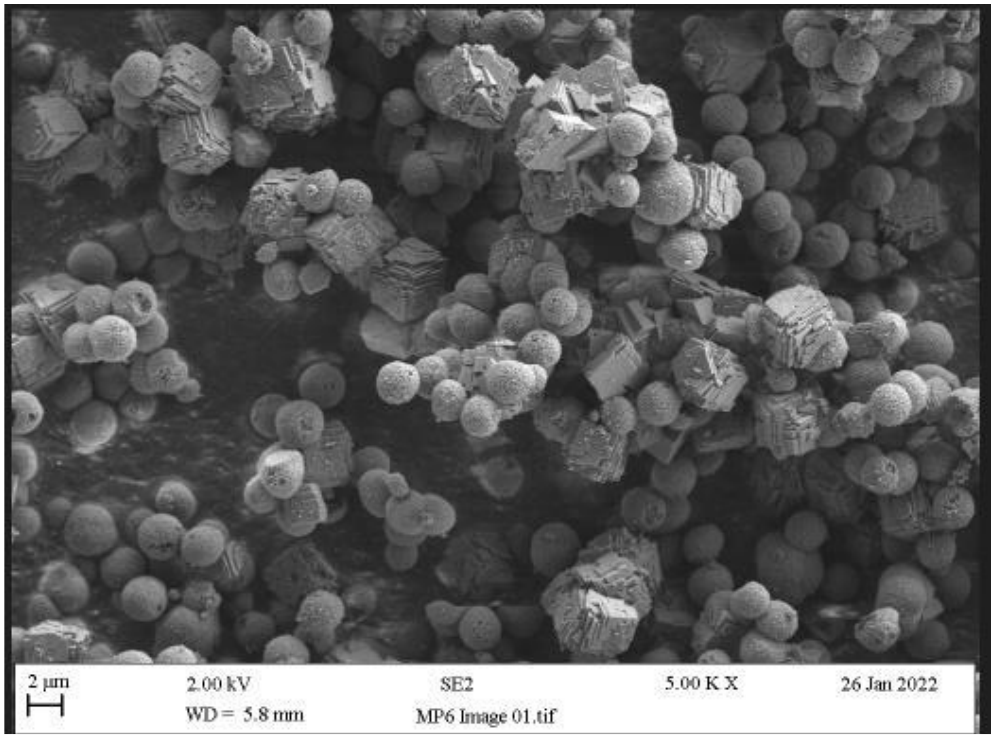

Figure 3.13 SEM image of calcium carbonate precipitated after mixing solutions of Ca^{+} (1.0 M, 100 mL) in PDDA (aq., 0.5 wt.%) and CO_3^{2-} (1.0 M, 100 mL) in PDDA (aq.,0.5 wt.%) (**MP6**).

Similarly, sample **MP15** ([Ca^{2+}] 1.0 M in 300 mL aq. PDDA 0.5 wt% + [CO_3^{2-}], 1.0 M in 300 mL aq. PDDA 0.5 wt%, combined stir time 60 mins) is of identical concentrations to sample **MP4** but scaled-up in volume (300 mL *c.f.* 10 mL). Because samples **MP14** ([Ca^{2+}] 1.0 M in 300 mL aq. PDDA 0.5 wt% + [CO_3^{2-}], 1.0 M in 300 mL aq. PDDA 0.5 wt%, combined stir time 60 mins) and **MP15** were made by identical methods, the SEM for sample **MP15** is given here as being representative. The SEM image (**Figure 3.14**) clearly shows the porous nature of the particle.

Sample **MP15** can also be compared with sample **MP9** (**Figure 3.15**), but in the latter case the stirring time is reduced to 15 minutes. The contrast between the two samples is obvious with significantly less porosity in the sample stirred for only 15 minutes *c.f.* 60 minutes. This suggests that Ostwald ripening is an important factor in particle growth and phase transitions [88].

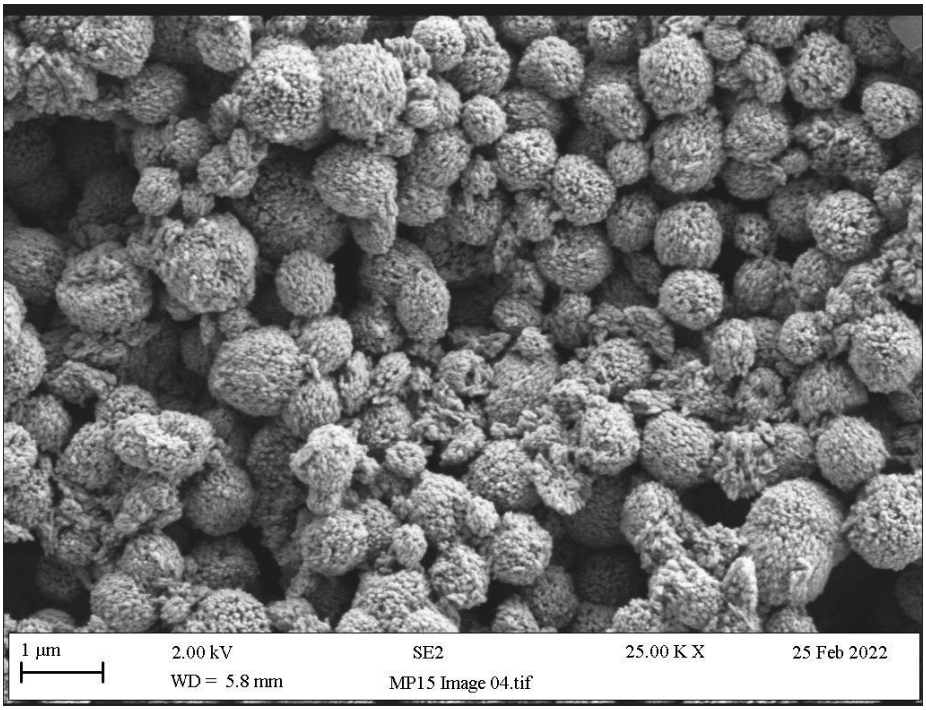

Figure 3.14 SEM image of calcium carbonate precipitated after mixing solutions of Ca^{+} (1.0 M, 300 mL) in PDDA (aq., 0.5 wt.%) and CO_3^{2-} (1.0 M, 300 mL) in PDDA (aq.,0.5 wt.%) and stirring for 60 minutes (1 hour) (**MP15**).

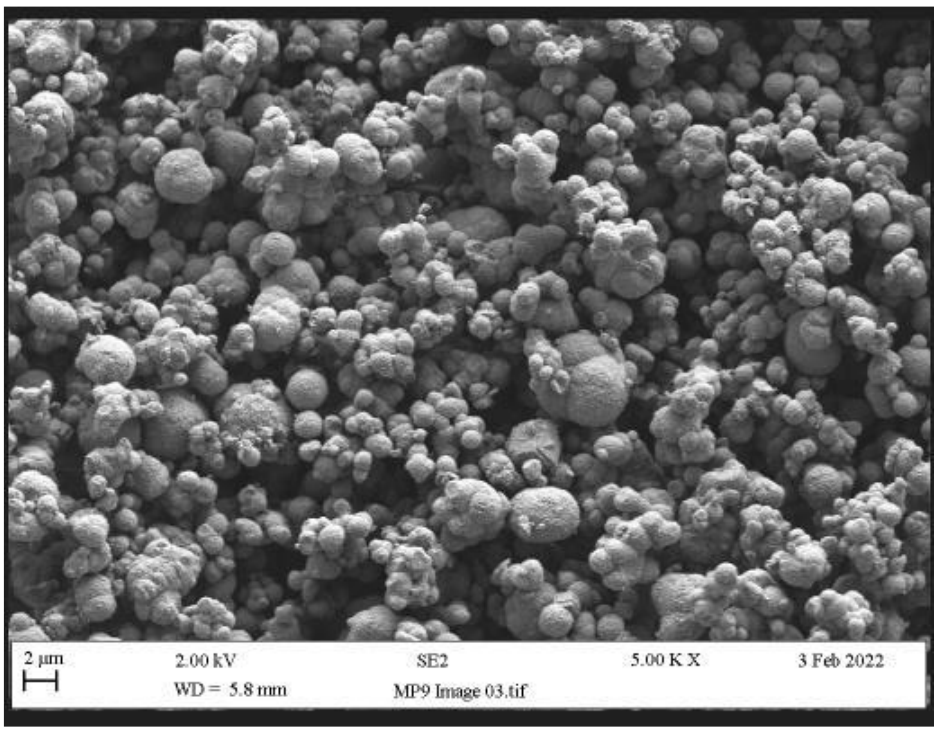

Figure 3.15 SEM image of calcium carbonate precipitated after mixing solutions of Ca^{+} (0.1 M, 300 mL) in PDDA (aq., 0.5 wt.%) and CO_3^{2-} (1.0 M, 300 mL) in PDDA (aq.,0.5 wt.%) (**MP9**).

3.2.4 Effect of extended mixing time

The influence of mixing time on morphology is further emphasised by comparing the SEM images in **Figure 3.16 (MP15**: [Ca^{2+}] 1.0 M in 300 mL aq. PDDA 0.5 wt% + [CO_3^{2-}], 1.0 M in 300 mL aq. PDDA 0.5 wt%, combined stir time 60 mins**), Figure 3.17 (MP16**: [Ca^{2+}] 1.0 M in 300 mL aq. PDDA 0.5 wt% + [CO_3^{2-}], 1.0 M in 300 mL aq. PDDA 0.5 wt%, combined stir time 120 mins**)** and **Figure 3.18 (MP18**: [Ca^{2+}] 1.0 M in 300 mL aq. PDDA 0.5 wt% + [CO_3^{2-}], 1.0 M in 300 mL aq. PDDA 0.5 wt%, combined stir time 1440 mins**)**, where stirring time is increased (1, 2 and 24 hours).

The process of spherulitic growth, dissolution and reprecipitation usually take place during the first 15 minutes of stirring (reaction). With ACC being converted to spherical porous vaterite (and calcite) (**Figure 1.38,** reproduced here for ease of comparison from **Section 1.4.2.3**). The SEM for **MP15** (**Figure 3.16**) shows that the transition to highly porous vaterite has taken place after 60 minutes. By 120 minutes, diffusion of ACC from the pore interior to the outer surface has resulted in smoother, spherical particles to give a vaterite/calcite mixture (**Figure 3.17**, **MP16**). After 1440 minutes (24 hours), the transition to calcite crystals with some vaterite casts is seen [89]. The hollow nature of the rhombohedral calcite is implied by the area highlighted in the SEM (yellow circle, **Figure 3.18**).

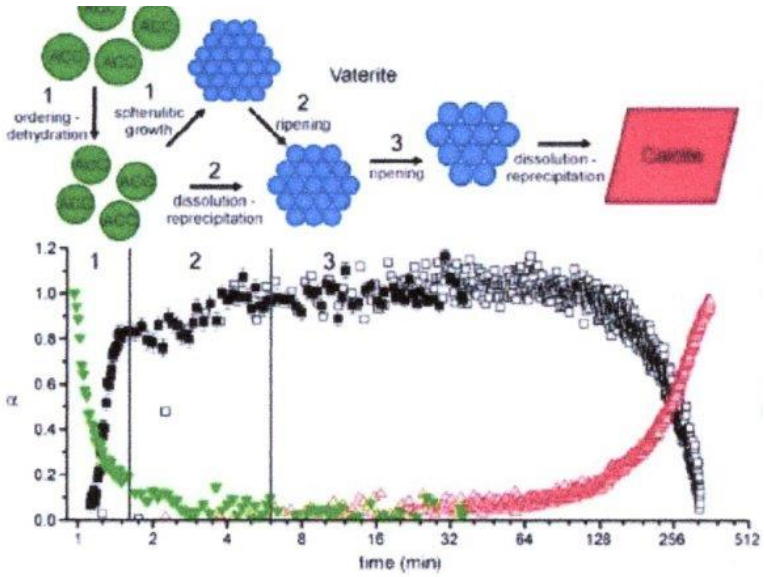

Figure 1.38 Schematic diagram to represent the pathway for ACC-vaterite-calcite crystallisation. (Reproduced from [70])

In the absence of additives increasing reaction time increases particle size (diameter) by a factor of 3 (4-6 mm to 15-20 mm).

The order of addition of Ca^{2+} and CO_3^{2-} is also important. When CO_3^{2-} is added to Ca^{2+}, particle size is often smaller and the distribution of particle sizes narrower. Vice-versa the opposite addition leads to irregular size and larger particles.

1.6.2.4 Role of pH

Although varying pH, for most of the methods reported by the literature, does not affect polymorphism, it does influence morphology and particle size. This is not surprising, since crystal growth depends on interaction between negatively charged groups on the additive and calcium ions in solution. Essentially, a greater number of groups on the additive will be ionised to produce negative charges to 'mop-up' Ca^{2+} ions blocking growth in three dimensions. In conjunction with increasing ionization of groups at high pH, supersaturation increases (i.e., hydrocarbonate/carbonate buffer effect) which reduces nucleation rate. The net effect of this is that a balance in pH is required (pH 9-11 to effectively control particle size (crystal growth)). However, if nucleation rate is too low the phase transition of vaterite (metastable) to calcite is inhibited. One interesting observation in the literature is the use of phytic acid as an additive at pH 3 at longer reaction time (2 hours) resulting in hollow spheres of ACC **(Table 1.9)**

1.6.2.5 Role of temperature

Crystal growth (size), in the presence of additives, is often accompanied by aggregation, which increases at higher temperatures. Although, where core dissolution and recrystallisation at the particle surface is possible this can take place even at high temperatures to give particles < 2 μm.

Temperature also influences the polymorph formed. Higher temperatures favour aragonite by phase transformation of calcite and vaterite (**Figure 1.39**). Around room temperature (15-30^{o}C) the particle size of the precipitate if affected, with an increase as temperature is increased regardless of concentration of Ca^{2+} and CO_3^{2-}. However, for slow carbonation precipitation (in the presence of surfactant) the opposite trend is

seen. Also, solubility plays a role if no additives are used: at higher temperatures in the range smaller calcite crystals are formed.

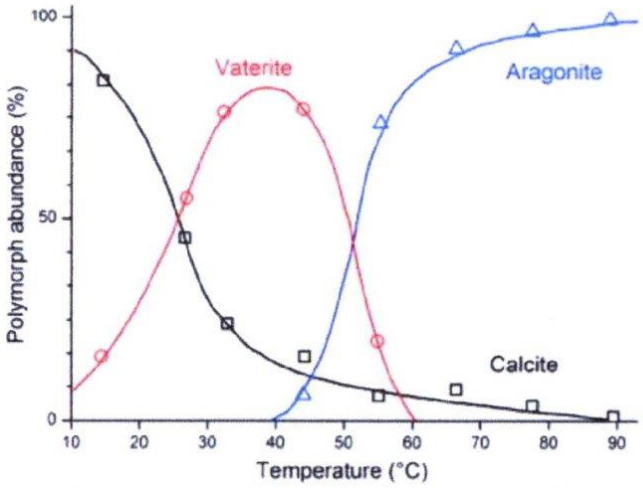

Figure 1.39 Dependence of (initial) $CaCO_3$ polymorph formation on temperature. (Reproduced from [71])

1.7 Aims and Objectives

In this context, the main aim of the present study is to assess the performance of hollow calcium carbonate as an alternative filler to hollow glass microspheres in PVC. This will be achieved by the following objectives:

- Synthesis and characterisation of hollow calcium carbonate
- Incorporation of hollow calcium carbonate (and hollow glass microspheres) in PVC formulations typical of those used in boat-decking
- Evaluation of the performance (density, mechanical and thermal properties) of the resultant PVC-hollow filler composites

2.0 Experimental:

Synthesis of Hollow Calcium Carbonate and Testing in PVC

2.1 Materials

Poly(diallyldimethylammonium chloride) solution (PDADMAC or PDDA) 20wt.% in water (Sigma Aldrich) of high molecular weight (M_w 400,000-500,000) was used to prepare a 0.5 wt.% stock solution (15g of 20 wt.% in 600g H_2O). The structure of PDDA is given in **Figure 2.1**.

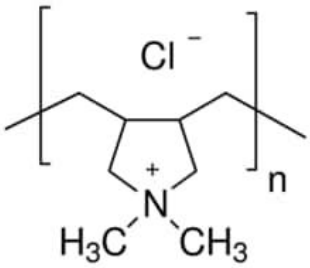

Figure 2.1 Structure of Poly(diallyldimethylammonium Chloride) (PDDA)

Calcium chloride (reagent grade, ≥ 98%, anhydrous, Sigma Aldrich) and Sodium Carbonate (reagent grade, ≥ 99.5%, anhydrous, Sigma Aldrich) were used to prepare aqueous solutions in the range 0.1-1.0 M. milliQ distilled water was used for preparation of all solutions.

Ammonium Hydroxide solution (2.0 M, Sigma Aldrich) was used to adjust the pH of solutions (pH = 10).

PVC resin (K70), plasticiser, one-pack stabiliser and Hollow Glass Spheres (3M™) were supplied by Flexiteek.

2.2 Synthesis of hollow calcium carbonate

A simple experimental design was adopted to prepare hollow calcium carbonate by varying the concentrations of Ca^{2+}, CO_3^{2-} and PDDA, as well as varying mixing time.

This is summarised in **Table 2.1** and described in detail thereafter.

Table 2.1 Variation in the concentrations of Ca^{2+}, CO_3^{2-} and PDDA, and mixing time for the synthesis of hollow calcium carbonate

Sample	$CaCl_2$/PDDA in water			Na_2CO_3/PDDA in water			Stirring Time (mins)
	$[Ca^{2+}]$ (M)	PDDA wt.%	volume (mL)	$[CO_3^{2-}]$ (M)	PDDA wt.%	volume (mL)	
MP1	0.1	0.5	10.0	0.1	water	10.0	60
MP2	0.1	Chitin 0.5	10.0	0.1	water	10.0	60
MP3	0.01	0.5	10.0	0.1	water	10.0	60
MP4	1.0	0.5	10.0	1.0	0.5	10.0	15
MP5	1.0	1.0	10.0	1.0	1.0	10.0	15
MP6	0.1	0.5	100.0	0.1	0.5	100.0	60
MP7	0.5	0.5	10.0	0.5	0.5	10.0	60
MP8	*	*	*	*	*	*	*
MP9	0.1	0.5	300.0	0.1	0.5	300.0	15
MP10	*	*	*	*	*	*	*
MP11	1.0	water	10.0	1.0	water	10.0	15
MP12**	*	*	*	*	*	*	*
MP13**	*	*	*	*	*	*	*
MP14	1.0	0.5	300.0	1.0	0.5	300.0	60
MP15	1.0	0.5	300.0	1.0	0.5	300.0	60
MP16	1.0	0.5	300.0	1.0	0.5	300.0	120
MP17	1.0	0.5	300.0	1.0	0.5	300.0	1440
MP18	1.0	0.5	300.0	1.0	0.5	300.0	1440
MP19	1.0	0.5	300.0	1.0	0.5	300.0	120
MP20	1.0	0.5	300.0	1.0	0.5	300.0	120

** refer to detailed methodology*

*** SEM images of samples MP12 and MP13 are given in the Appendix but are not discussed in this report since the objective for their preparation was to effect comparison/ confirmation of similar particle sizes.*

Synthesis of MP1, MP2, MP3

$CaCl_2$ (aq.,0.1 M) was prepared by dissolving 0.11g in PDDA stock (0.5 wt.%, 10.0 g). Na_2CO_3 (aq., 0.1M, 10.0g) was added dropwise and the resultant solution was mixed for 60 minutes (**MP1**). The same procedure (MP1) was adopted but replacing PDDA with chitin (**MP2**). Finally, the same procedure (MP1), was followed but the concentration of $CaCl_2$ was reduced to (0.01 M) (**MP3**). In each case, solutions (**MP1, MP2, MP3**) were stirred for 60 minutes, filtered and the filtrate oven dried (80^oC).

Synthesis of MP4, MP5, MP6, MP7 MP8

$CaCl_2$ (aq.,0.1 M) was prepared by dissolving 1.1 g in PDDA stock (0.5 wt.%, 10.0 g). A solution of Na_2CO_3 (aq.,0.1 M) was also prepared by dissolving 1.1 g in PDDA stock (0.5 wt.%, 10.0 g). The solutions were then mixed and stirred for 15 minutes (**MP4**). This procedure was then repeated but using 1.0 wt.% PDDA (**MP5**). In each case, solutions (**MP4, MP5**) were stirred for 15 minutes, filtered and oven dried (80^oC). Sample **MP8** was prepared by addition of water (10 ml) to sample **MP4** (0.2 g), followed by ultrasonication (1 hour), filtration and drying (80^oC). Samples **MP6** and **MP7** were prepared using the same method as **MP4**, except that for **MP7** the concentrations of CaCl2 aq. and Na_2CO_3 aq., were 0.5 M and, for **MP6** the concentrations were 0.1 M in PDDA (0.5 wt.%, 100.0 g).

Synthesis of MP9, MP10, MP12, MP13

Sample (**MP9**) was prepared by the same method as **MP6** but 300g of PDDA (0.5 wt.%) used. Sample **MP10** was prepared by addition of water (300 ml) to sample **MP9,** followed by ultrasonication (1 hour), filtration and drying (80^oC). Sample **MP10** was mixed with water (1:10 ratio) and ultrasonicated (1 hour) to give sample **MP12**. The filtrate (cloudy) was collected to recover sample **MP13**.

Synthesis of MP11

$CaCl_2$ (1.0 M) in water (10.0 g) was adjusted to pH 10 (NH_4OH dropwise addition). This process was then repeated for Na_2CO_3. The solutions were then stirred for 15 minutes, filtered and oven dried (80^oC).

Synthesis of MP14, MP15

$CaCl_2$ (1.0 M) in PDDA stock (0.5%, 300.0 g) was mixed with Na_2CO_3 (1.0 M) in PDDA stock (0.5%, 300.0 g). The solution was then stirred for 60 minutes, filtered and oven dried (80^oC) (**MP14**). This procedure was then repeated to produce a second batch for comparison (**MP15**)

Synthesis of MP16, MP17, MP18, MP19, MP20

Samples **MP16, MP19** and **MP20** were batches produced by the same method as sample **MP14,** except that the stirring time was 120 minutes (2 hours). Samples **MP17** and **MP18** were batches produced by the same method as sample **MP14,** except that the stirring time was 1440 minutes (24 hours).

2.3 Preparation of PVC Test Plaques/Bars

Test plaques/bars were prepared from the formulations given in **Table 2.2**. The hollow filler was either hollow glass spheres (3M) or hollow calcium carbonate (**MP21**, **MP22**, **MP23**).

Table 2.2 PVC Formulations used to prepare test plaques/bars

Formulation Components	phr*			weight (g)		
	Low	Mid	High	Low	Mid	High
PVC (K70)	100	100	100	31.88	26.89	25.17
Plasticiser	44	62	62	14.03	16.67	15.61
Hollow Filler	26	40	54	8.29	10.76	13.59
One-Pack Stabiliser	2.5	2.5	2.5	0.8	0.67	0.63

* percent hundred ratio (see glossary for extended definition)

The 'One-Pack' stabiliser is a package of additives that are a combination of substances such as antioxidants, process aids etc. The 'One-Pack' used here is non-toxic based on calcium and zinc antioxidants blended with other co-stabilisers.

Separate batches of hollow calcium carbonate (**MP21, MP22, MP23**) were then prepared according to the method for MP16. The samples were heated for 4 hours at 80^{o}C to remove water and then calcined at 550^{o}C for 4 hours. Samples **MP21** and **MP23** were incorporated into PVC in the range 15-24 wt.% (typical in commercial formulations) according to **Table 2.2**.

Dry blends of the formulations were mixed in a Rheometer. Normally, the rheological properties of the material at processing temperatures are measured. Here torque is used to reflect the viscosity and elasticity of the material (K-value of PVC is a measure of viscosity, while die swell is a measure of elasticity). The relationship between torque, time and temperature gives information on fusion behaviour, safe processing window (time and onset of degradation).

In this study the conditions of mixing were informed by previous commercial work, so the rheometer was used only for mixing of formulations to prepare test plaques/bars. **Figure 2.2** depicts the mixed formulation.

Figure 2.2 PVC formulation containing hollow calcium carbonate filler (19 wt.%) after rheometric mixing

Samples were prepared using a Thermo Scientific HAAKE™ Polydrive Rheomix 600. The following test conditions were applied: Mixer temperature: 150 °C; Rotor speed: 100 rpm; Sample weight: 55 g; 5 bar pressure pneumatic ram; Mixing time 5 minutes.

Samples were then size reduced (grinding), and compression moulded into plaques using a hydraulic press (Bradley and Turton Ltd., capacity 50 tonne) between two aluminium plates (platens). Heated platens should be at the temperature which is at least 50 °C above the melting points of the polymer in the case of semi-crystalline polymers, but this is not necessary for amorphous polymers like PVC. Care should be taken that the platen temperature is not too high to prevent degradation of the polymer.

Ground PVC chips (100 g) were pressed into plaques in a two-stage moulding cycle. First the polymer was held in contact with the heated plate at a low temperature for 10 minutes to allow uniform heating and melting. Subsequently, the applied pressure was increase to 35 psi/ton for 10 minutes at 170^{o}C. The sample was then quench cooled by immersion in a bath of cold running water for 10 minutes.

Tensile tests were conducted on dumbbell specimens (see **Section 2.4.4**).

2.4 Characterisation

2.4.1 X-ray diffraction (XRD)

X-ray diffraction data were collected on a PANalytical X'pert Powder X-ray diffractometer using Cu Kα radiation (λ=0.51054Å) with generator settings of 45kV, 40mA. Automatic divergence and antiscatter slits were used on the incident and diffracted beam paths with data collected using a PIXCel 1-D detector operating in scanning line mode with an active length of 3.347 °2θ. The incident beam was passed through a 10mm beam mask with the automatic divergence slits on the source set to maintain a constant irradiated length of 5mm throughout the scan. The automatic antiscatter slits on the detector were also set to maintain constant 5mm aperture. Data were collected in the range 10 -140° 2θ with a step size of 0.013° 2θ and a measuring time of 89s/step. The samples were rotated at 60 rpm during the data collection. Data was truncated to the range 15 -70° 2θ, converted to fixed divergence slit and the $k\alpha_2$ component was removed. Phases were identified using the search-match function in HighScore Plus against the Crystallography Open Database for any mineral phases with unit cell and crystallite size parameters determined using Pawley refinement. A characteristic XRD for the different phases of calcium carbonate from the literature is given in **Figure 2.3**

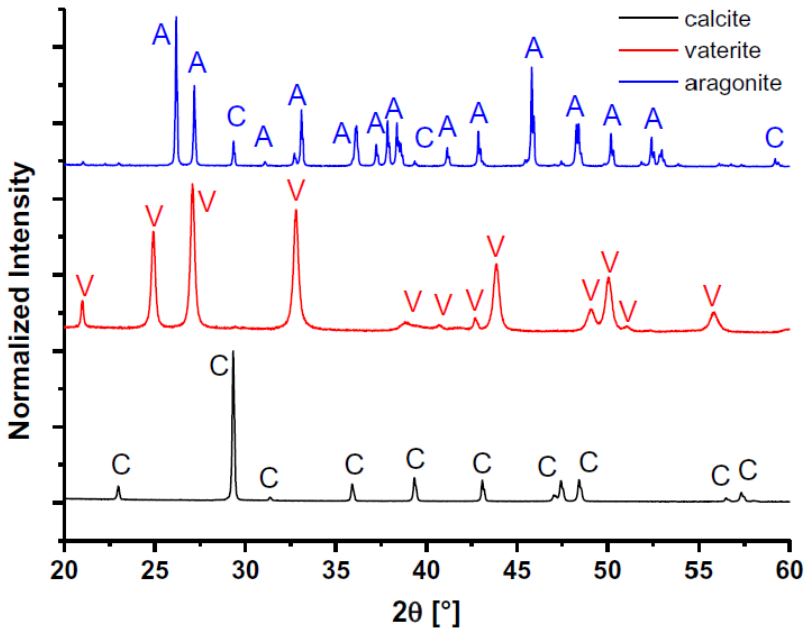

Figure 2.3 XRD spectra of calcium carbonate polymorphs (from [72])

2.4.2 Scanning electron microscopy (SEM)

The morphology of samples was determined by scanning electron microscopy Calcium carbonate samples (MP1-MP23, synthesised by methods in **Section 2.2**) were applied using SEM adhesive. The surface of the samples was examined with a high-resolution scanning electron microscope (SEM) Quanta 450 FEG (FEI) using a secondary electron detector. Analyses were performed at accelerating voltage between 5 and 20 kV.

Samples used for dilatometry were dispersed as powders on carbon tape. All the samples were gold coated with a 5-nm thick layer. The sputter coater was a Polaron SEM coating system (Coating time 30s, voltage 800 V, current 5 mA). SEM (Carl Zeiss Ltd., Supra 40VP, **Figure 2.4**) was used to verify morphology, particle size and evidence of porosity. Data was processed using SmartSEM™ software. Five areas of each sample were analysed at 5K magnification.

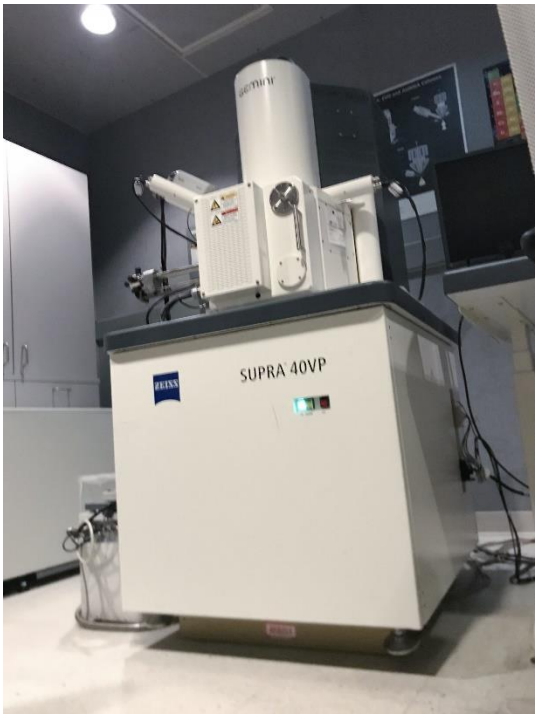

Figure 2.4 Carl Zeiss Ltd., Supra 40VP scanning electron microscope

2.4.3 Density

Polymer density was calculated by gravimetric water displacement [73]. To obtain an accurate reading of weight, water ($50cm^3$, volumetric flask) was shaken then ultrasonicated (2 minutes) to remove air bubbles and weighed on a four-figure balance. The process was then repeated with samples of PVC granulate (**Section 2.3**) in water ($50cm^3$, volumetric flask) shaken and ultrasonicated (2 minutes) to remove air bubbles and weighed on a four-figure balance. All measurements were performed in triplicate. Although this method was used to determine filled polymer density, modified methods can be used to verify sample porosity [74].

2.4.4 Mechanical Properties

Five 'dumbell' test bars were cut from the plaques prepared (described in Section 2.2.3). The shape of the dumbbell (**Figure 2.5**) cut is determined by the rigidity and thickness of a PVC plaque (in this case 6mm). Hence each dumbbell specimen was cut to thickness, 6mm, width 27 mm, length 117 mm, gauge length 45 mm

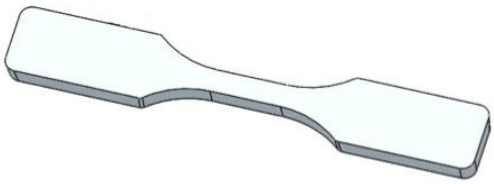

Figure 2.5 Tensile test bar (middle section) gauge length 45 mm.

Test bars were loaded into tensile grips and attached to the extensometer of the tensile test instrument.

Stress-strain curves were obtained using a Tinius Olsen H10KS (**Figure 2.6**) tensiometer fitted with an extensometer, and data was processed using Horizon software. Modulus values were determined using Horizon software program for ASTM D638 with a crosshead speed of 50 mm min^{-1} until rupture of the sample. This standard

test method is one of the most common plastic strength specifications and covers the tensile properties of unfilled and filled polymers.

Figure 2.6 Tinius Olsen H10KS tensiometer.

2.4.5 Thermal Properties

Thermogravimetric analysis (TGA) was carried out using an SDT 650 thermal analysis instrument (TA Instruments) in N_2 atmosphere (50 mL/min). Standard TGA was undertaken at a heating rate of 10 ◦C/min and a temperature ramp of 25 to 300 ◦C. Isothermal TGA was undertaken by ramping to 180^{o}C at 100^{o}C/min and then held at this temperature for 90 min under N_2.

Thermal conductivity was predicted using theoretical equations (**Equations 5.2** and **5.3**) and compared with data supplied for the commercial sample.

3.0 Results and Discussion

3.1 Rationale for synthetic procedure adopted

A range of molecular templates to direct crystallisation by controlled nucleation of Ca^{2+} and CO_3^{2-} to produce hollow calcium carbonate has been described in the introduction (**Sections 1.4.1.1 and 1.4.1.2**). Polyelectrolytes are commonly used as templates for self-assembly, especially when stable, homogeneous films are required. The most prevalent are commercially available polymers that are grouped as cationic (e.g., poly(ethyleneimine), poly(allylamine), poly(allylamine hydrochloride poly(diallyldimethylammonium chloride), diazo-resin) and anionic (poly(styrene sulfonate), poly(vinylsulfate) and poly(acrylic acid) [75-78]. The literature reports that the colloidal template may be used as a sacrificial core. Following multilayer assembly by sequential adsorption the core is removed by either chemical methods or calcination. This process allows a higher degree of control over particle size, shape, and wall thickness.

Here rationale for the selection of a cationic electrolyte with high charge density, namely Poly(diallyldimethylammonium chloride) (PDADMAC or PDDA), as a colloidal template to produce hollow calcium carbonate is presented. PDDA has been used as a template in production of both hollow silica and titania [79]. Akhondi and Jamalizadeh have prepared cubic and spherical hollow silica (**Figure 3.1**) using a hard templating method with polystyrene-PDADMAC and polystyrene-polyethyleneimine [80]. Other workers have shown that an understanding of amine-silicate interactions enables the formation of both hollow and non-porous silicates to be controlled and undertaken under milder conditions (i.e., room temperature in aqueous systems around neutral pH) [81].

An alternative approach that is simple and economical is known as the “self-template” method. It has been used to produce porous silica by alkaline treatment of PDDA. The PDDA deposited on silica spheres is attacked by hydroxyl ions that permeate the template layer and attack the silica sphere to generate dissolved silicate oligomers in the presence of ammonia. The oligomers are negatively charged and deposit on the

positively charged PDDA forming a silica-PDDA shell. Sodium hydroxide is then used to etch the interior of the silica spheres [82].

The influence of ammonia and selected amines on the characteristics of calcium carbonate precipitated from calcium chloride solutions via carbonation has been reported in the literature [83]. Although the latter work does not encompass the preparation of hollow calcium carbonate, it does add confidence to an approach based on colloidal self-templating using PDDA to allow a high degree of control over particle size, shape, and wall thickness. Furthermore, such a tactic is attractive from a commercial perspective because the raw materials are low cost, readily available and reaction times are short. Hence this approach has been adopted in this study. To establish how the presence of PDDA, PDDA concentration, mixing time, ultrasonication and calcination affect the morphology and structure of calcium carbonate a simple experimental design was used, by varying components.

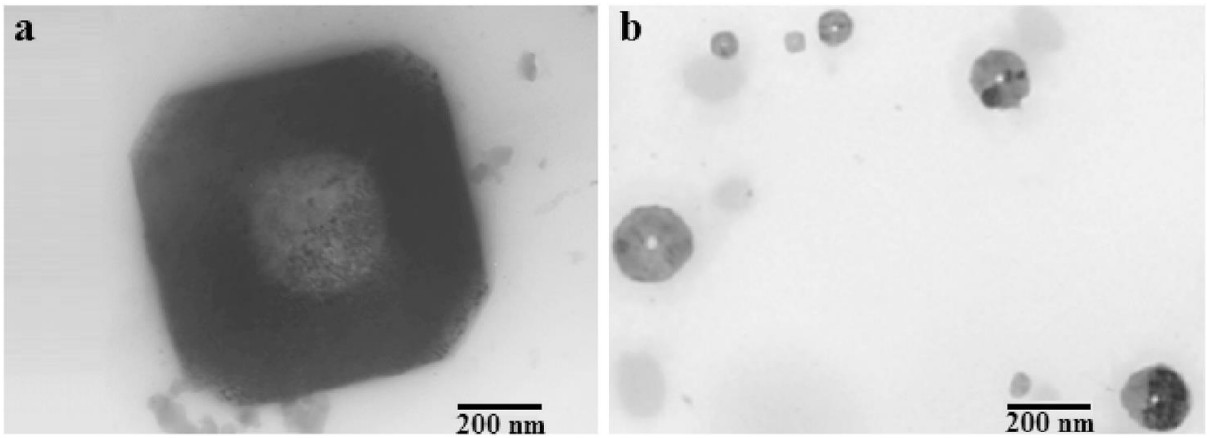

Figure 3.1 TEM images of hollow silica prepared using a PDADMAC template: Hollow cubic morphology (a) and hollow spherical morphology (b) (Reproduced from [80])

3.2 Synthesis and Structure of Hollow Shell Calcium Carbonate

3.2.1 Comparison of absence and presence of a molecular template (additive)

Previous studies have shown that the chemical composition of ACC (amorphous calcium carbonate) is nominally hydrated calcium carbonate ($CaCO_3.H_2O$), with a calcium-rich nanoscale framework with pores containing water and carbonate ions [84]. However, as stated in the introduction, ACC is thermodynamically unstable and crystallises at room temperature from aqueous solution (in minutes to hours) leading to calcite and/or vaterite depending on conditions (**Figure 3.2** and **Figure 3.3**).

The highly porous spherical particles of calcite and/or vaterite produced by rapid mixing, in the absence of a molecular template, can be seen in the SEM image in **Figure 3.1** (**MP11**: [Ca^{2+}] 10 mL of 1.0 M, aq. + [CO_3^{2-}], 10 mL of 1.0 M, aq., combined stir time 15 mins). The presence of both calcite (40%) and vaterite (60%), rather than ACC, is confirmed by XRD in **Figure 3.3**. The SEM (**Figure 3.2**) also shows the relatively small size of the spherical particles produced (<2 μm), which is expected due to the shorter mixing time of 15 minutes.

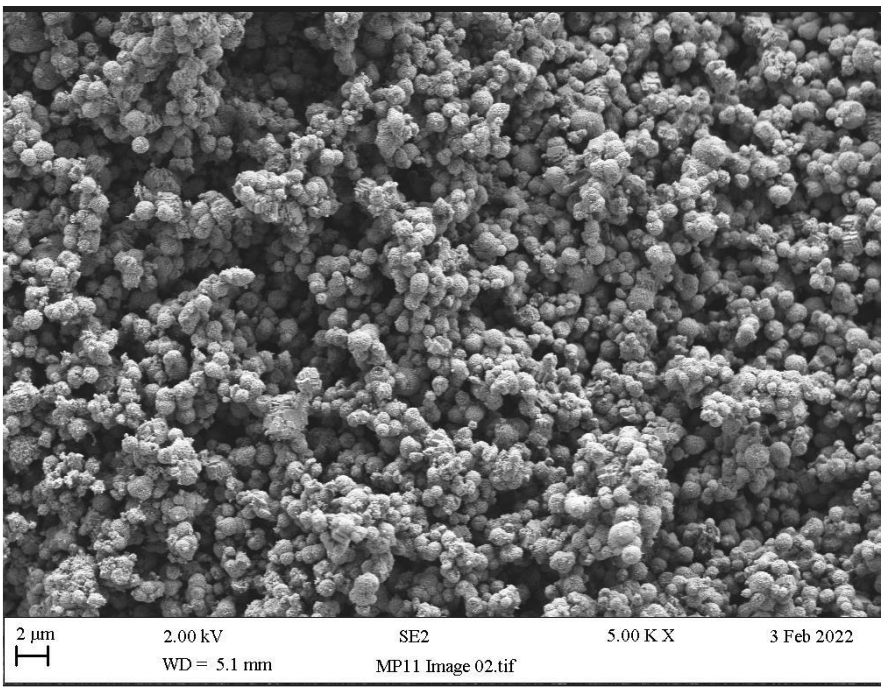

Figure 3.2 SEM image of calcium carbonate synthesised by precipitation in the absence of PDDA additive (**MP11**)

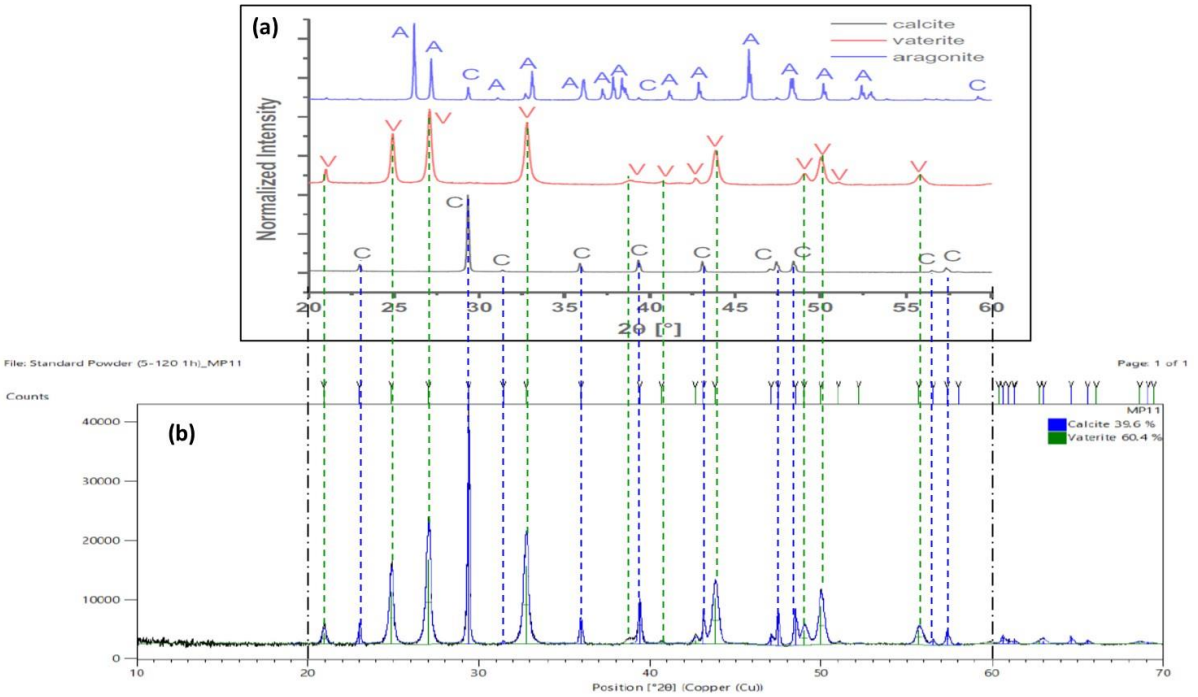

Figure 3.3 Selected region of XRD spectra of (a) individual calcium carbonate polymorphs synthesised by precipitation with no additive (Reproduced from [72]) and (b) calcium carbonate synthesised by precipitation in the absence of PDDA additive (**MP11**)

Figure 3.5 illustrates the effect of addition of chitin as a molecular template to the solution of Ca^{2+} ions (**MP2**: [Ca^{2+}] 0.1 M in 10 mL aq. Chitin 0.5 wt% + [CO_3^{2-}], 10 mL of 1.0 M, aq., combined stir time 60 mins), while the CO_3^{2-} ions remain as an aqueous solution with no additive present. After mixing and stirring for 60 minutes the SEM of the calcium carbonate formed suggests that rhombohedral calcite crystals are formed. This is likely driven by precipitation of the calcite polymorph on chitin, facilitated by interaction with its carbonyl and amide groups (**Figure 3.4** (1) and (2)**)** [85]. Despite the longer mixing time (60 minutes) there is evidence that ACC diffusion is incomplete.

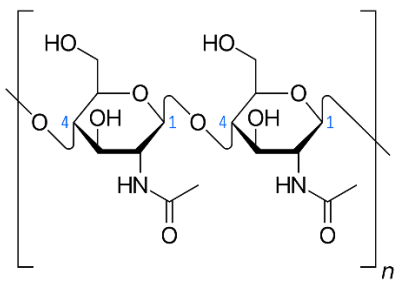

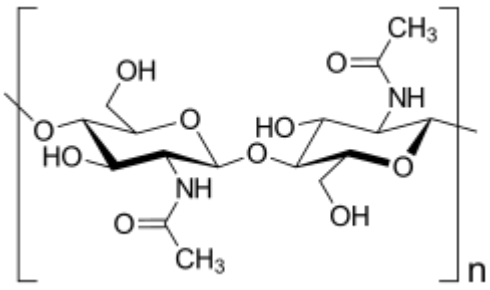

Figure 3.4 Structure of chitin (1) Structure of chitin (2)

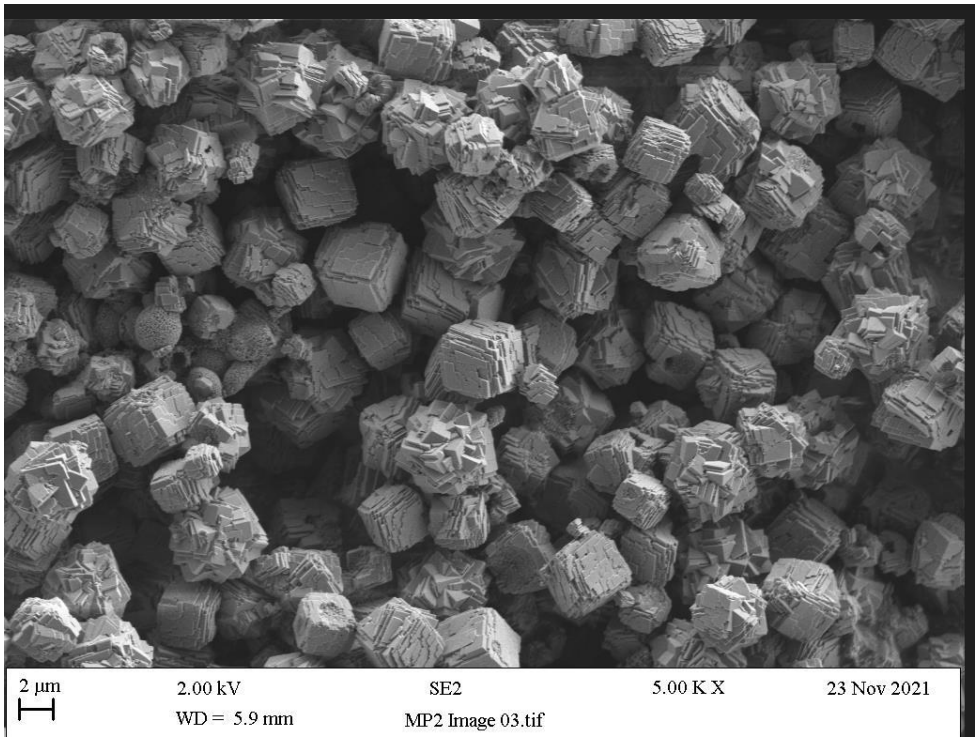

Figure 3.5 SEM image of calcium carbonate synthesised by precipitation from Ca^{+} (aq, 0.1M) in the presence of chitin as a molecular template (0.5 wt.%) (**MP2**)

Figure 3.6 shows the effect of replacing chitin with PDDA as a molecular template to the solution of Ca^{2+} ions (**MP1**: [Ca^{2+}] 0.1 M in 10 mL aq. PDDA 0.5 wt% + [CO_3^{2-}], 10 mL of 1.0 M, aq., combined stir time 60 mins), with CO_3^{2-} in water. It might be expected that as a cationic electrolyte with high charge density (**Figure 2.2**, **Section 2.2.1**) it could direct crystallisation and nucleation. Unfortunately, there is little evidence of 'controlled' precipitation when PDDA is added only to the Ca^{2+} solution. Instead, calcite crystals (rhombohedral) attached to vaterite (spherical), with the development of growth steps on the calcite surface is seen. However, there is some evidence that the calcite formed is hollow (highlighted by yellow circles, **Figure 3.6)** [86]**.** Reducing the concentration of Ca^{2+} did drive the reaction towards the formation of calcite, though crystal formation is still transitional (i.e., ACC diffusion is still not complete, **Figure 3.7**, **MP3**: [Ca^{2+}] 0.01 M in 10 mL aq. PDDA 0.5 wt% + [CO_3^{2-}], 10 mL of 1.0 M, aq., combined stir time 60 mins**)**. Samples **M1**, **MP2** and **MP3** have been stirred for 60 minutes rather than 15 minutes (**MP11**) to allow longer time for the phase transition to take place.

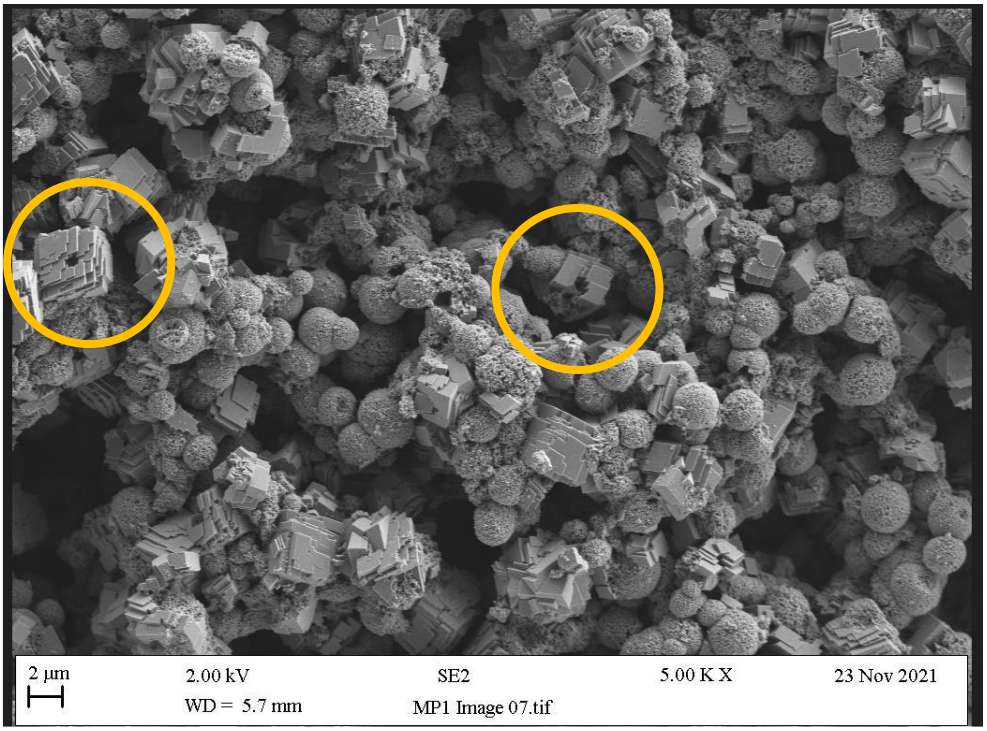

Figure 3.6 SEM image of calcium carbonate synthesised by precipitation from Ca^{+} (aq, 0.1M) in the presence of PDDA as a molecular template (0.5 wt.%) (**MP1**). Areas circled yellow highlight evidence for hollow particles

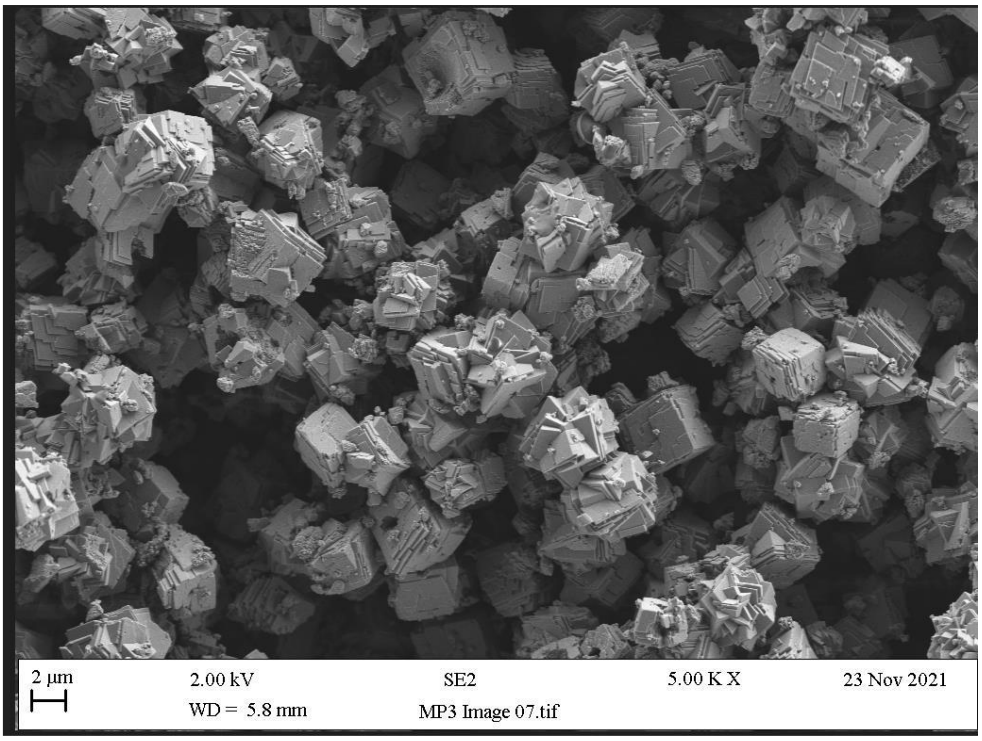

Figure 3.7 SEM image of calcium carbonate synthesised by precipitation from Ca^{+} (aq, 0.01M) in the presence of PDDA as a molecular template (0.5 wt.%) (**MP3**)

3.2.2 Effect of addition of PDDA to solutions of Ca^{2+} and CO_3^{2-} before mixing

From the SEM image of **MP4** ([Ca^{2+}] 1.0 M in 10 mL aq. PDDA 0.5 wt% + [CO_3^{2-}], 1.0 M in 10 mL aq. PDDA 0.5 wt%, combined stir time 15 mins) in **Figure 3.8**, it was seen that keeping the concentration of PDDA constant but doubling the concentration of Ca^{2+} and CO_3^{2-}, resulted in the formation of spherical crystals. These were confirmed as calcite and vaterite by XRD (**Figure 3.9**).

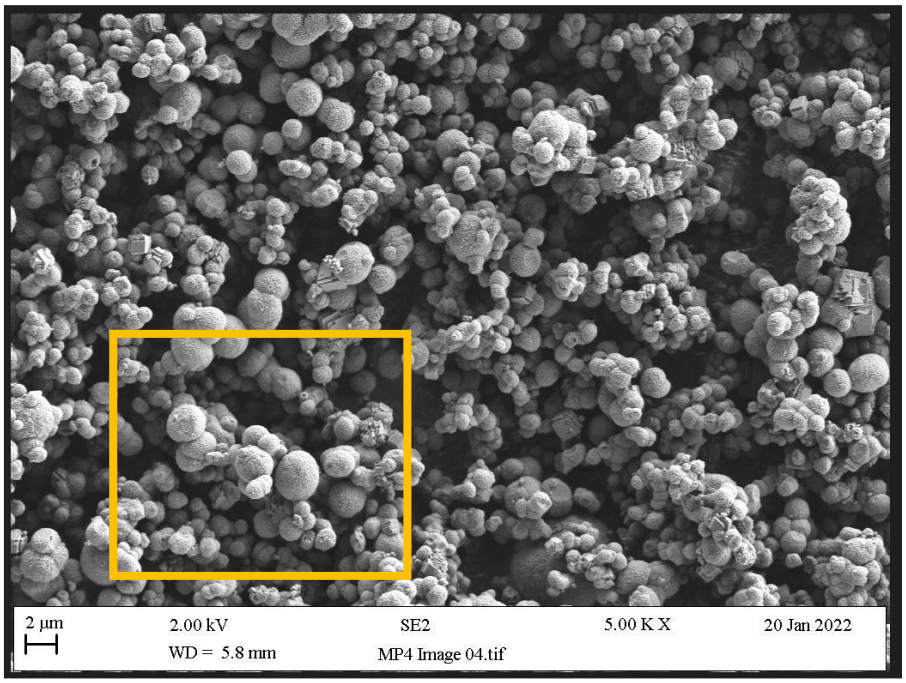

Figure 3.8 SEM image of calcium carbonate precipitated after mixing solutions of Ca^{+} (1.0 M, 10 mL) in PDDA (aq., 0.5 wt.%) and CO_3^{2-} (1.0 M, 10 mL) in PDDA (aq.,0.5 wt.%) followed by stirring for 15 minutes (**MP4**).

In sample **MP5** ([Ca^{2+}] 1.0 M in 10 mL aq. PDDA 1.0 wt% + [CO_3^{2-}], 1.0 M in 10 mL aq. PDDA 1.0 wt%, combined stir time 15 mins, **Figure 3.10**) the concentrations of Ca^{+} and CO_3^{2-} solutions were each kept at 1.0 M, but the concentration of PDDA was doubled, while the stirring time after mixing remained at 15 minutes. Again, spherical particles are formed (probably of vaterite and calcite) but at this shorter timeframe transition to rhomboidal calcite is not evident.

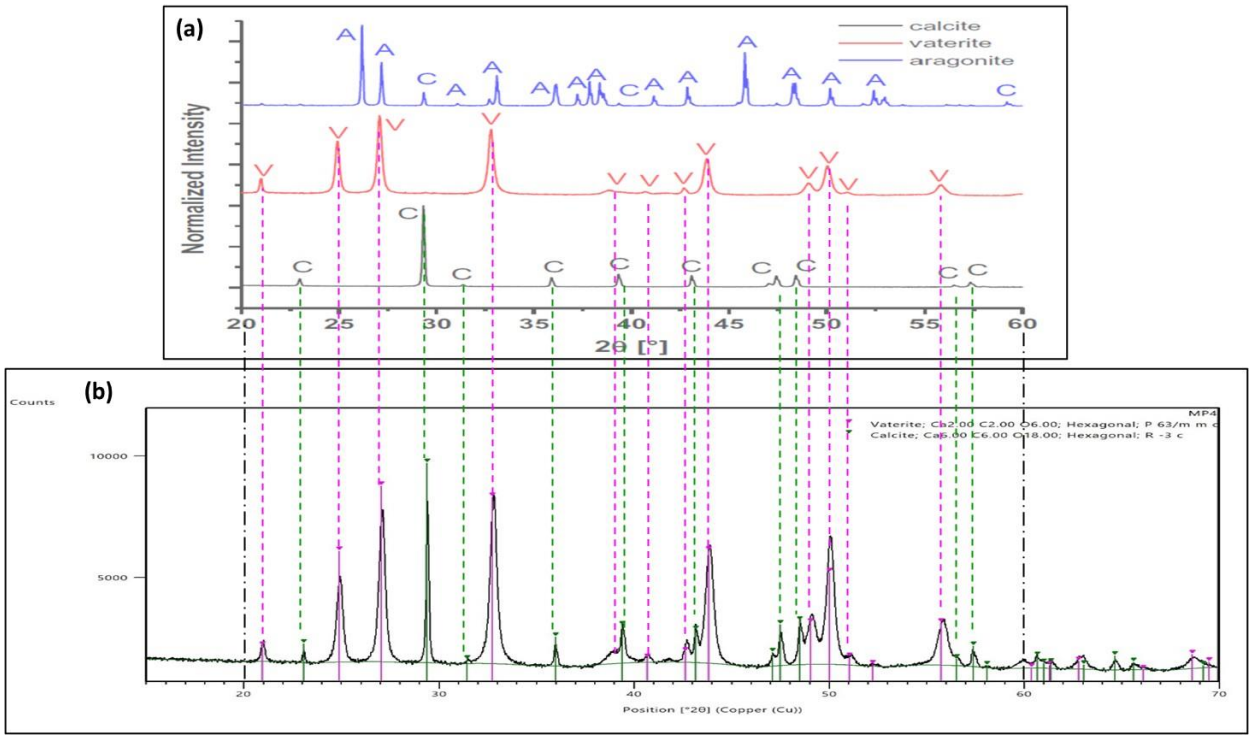

Figure 3.9 Selected region of XRD spectra of (a) individual calcium carbonate polymorphs synthesised by precipitation with no additive (Reproduced from [72]) and (b) calcium carbonate synthesised by precipitation in the presence of PDDA additive (**MP4**)

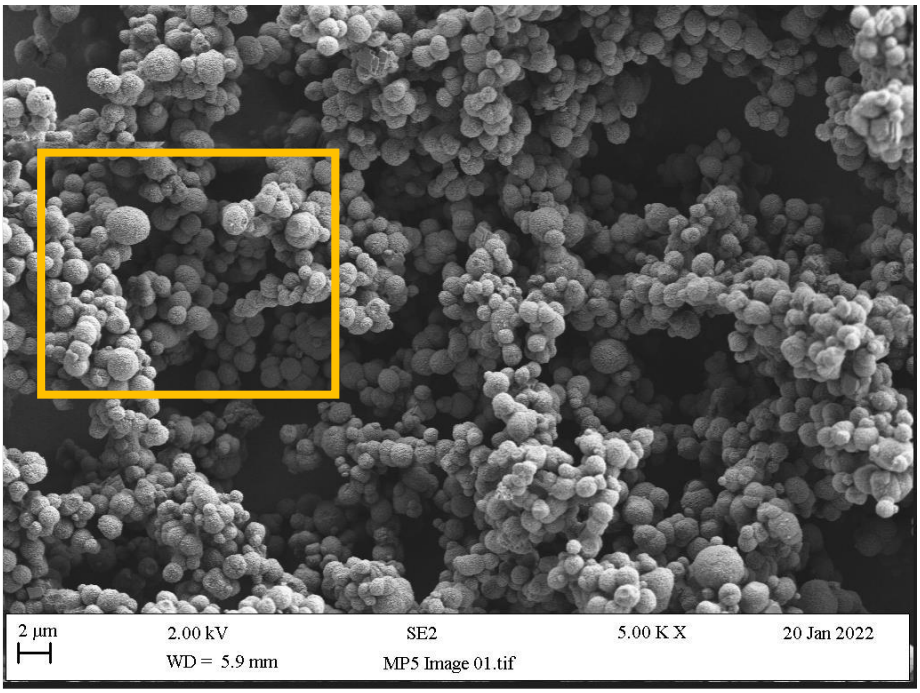

Figure 3.10 SEM image of calcium carbonate precipitated after mixing solutions of Ca^{+} (1.0 M, 10 mL) in PDDA (aq., 1.0 wt.%) and CO_3^{2-} (1.0 M, 10 mL) in PDDA (aq.,1.0 wt.%) followed by stirring for 15 minutes (**MP5**).

Figure 3.11 shows the expanded areas of the SEM images of $CaCO_3$ precipitates of **MP4** and **MP5** for the different PDDA concentrations. As the PDDA concentration is increased the morphologies change to more uniform spherical structures. It is expected that lower PDDA concentration reduces its ability to bridge nanoscale particles [87]. However, the spheres in **MP5** appear to be more solid than those in **MP4** (see area circled). This could be caused by long chains of the PDDA surrounding microspheres preventing $CaCO_3$ particles in the interior diffusing out, so increasing the nucleation density.

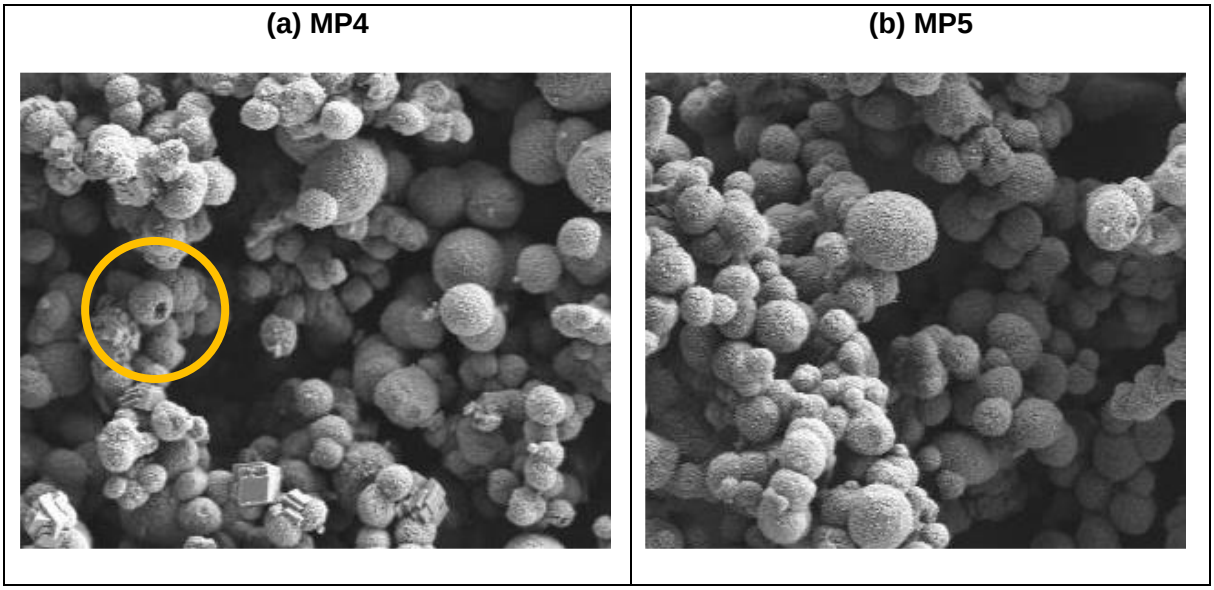

Figure 3.11 Expanded SEM image of calcium carbonate for samples **MP4** (taken from **Figure 3.9**) and **MP5** (taken from **Figure 3.10**). Areas circled yellow highlight evidence for hollow particles

For sample **MP7** ([Ca^{2+}] 0.5 M in 10 mL aq. PDDA 0.5 wt% + [CO_3^{2-}], 0.5 M in 10 mL aq. PDDA 0.5 wt%, combined stir time 60 mins) PDDA was present at the same concentration as sample **MP4**, but the combined solutions were stirred for a longer time of 60 minutes. Furthermore, the concentrations of Ca^{2+} (0.5 M) and CO_3^{2-} (0.5 M) were reduced in comparison to **MP4.** This effectively increased the relative amount of PDDA in **MP7**. Evidence of greater solidity in samples when stirred for longer times, with higher concentrations of molecular template, is supported by the SEM image for

MP7 in **Figure 3.12**. Again, it is seen that the longer time has promoted the formation of (solid) rhombohedral calcite.

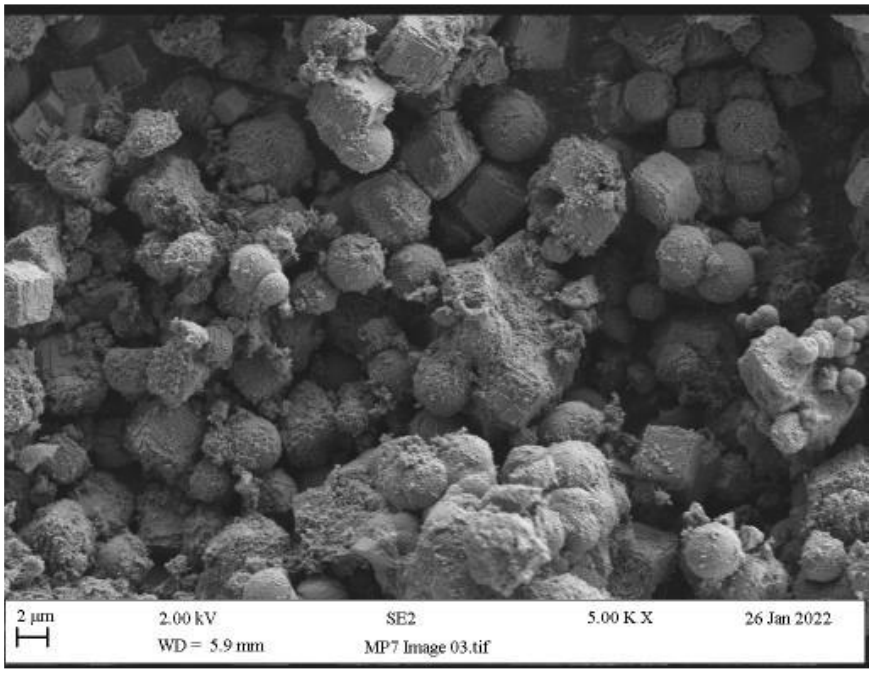

Figure 3.12 SEM image of calcium carbonate precipitated after mixing solutions of Ca^{+} (0.5 M, 10 mL) in PDDA (aq., 0.5 wt.%) and CO_3^{2-} (0.5 M, 10 mL) in PDDA (aq.,0.5 wt.%) (**MP7**).

3.2.3 Effect of dilution of solutions of Ca^{2+} in PDDA and CO_3^{2-} in PDDA before mixing

Compared to sample **MP7,** sample **MP6** ([Ca^{2+}] 0.1 M in 100 mL aq. PDDA 0.5 wt% + [CO_3^{2-}], 0.1 M in 100 mL aq. PDDA 0.5 wt%, combined stir time 60 mins) further reduces the concentration of Ca^{2+} (0.1 M) and CO_3^{2-} (0.1 M). Overall dilution and longer stirring time (60 minutes) further supports the arguments in the previous section. The SEM image (**Figure 3.13**) shows porosity in the spherical particles, along with evidence of rhombohedral calcite.

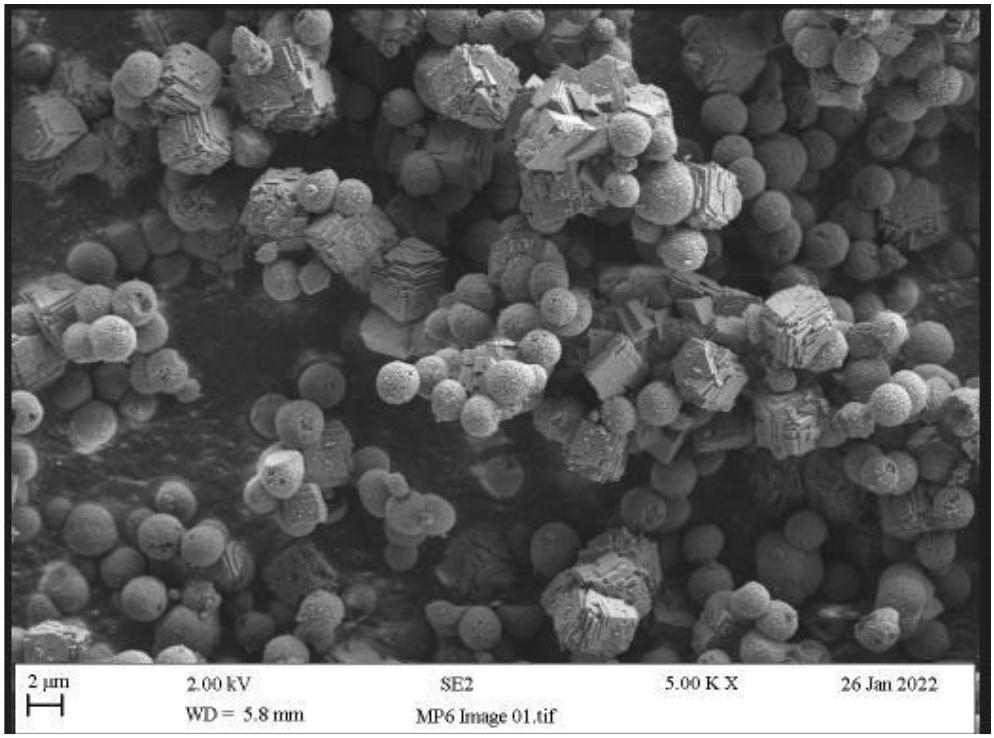

Figure 3.13 SEM image of calcium carbonate precipitated after mixing solutions of Ca^{+} (1.0 M, 100 mL) in PDDA (aq., 0.5 wt.%) and CO_3^{2-} (1.0 M, 100 mL) in PDDA (aq.,0.5 wt.%) (**MP6**).

Similarly, sample **MP15** ([Ca^{2+}] 1.0 M in 300 mL aq. PDDA 0.5 wt% + [CO_3^{2-}], 1.0 M in 300 mL aq. PDDA 0.5 wt%, combined stir time 60 mins) is of identical concentrations to sample **MP4** but scaled-up in volume (300 mL *c.f.* 10 mL). Because samples **MP14** ([Ca^{2+}] 1.0 M in 300 mL aq. PDDA 0.5 wt% + [CO_3^{2-}], 1.0 M in 300 mL aq. PDDA 0.5 wt%, combined stir time 60 mins) and **MP15** were made by identical methods, the SEM for sample **MP15** is given here as being representative. The SEM image (**Figure 3.14**) clearly shows the porous nature of the particle.

Sample **MP15** can also be compared with sample **MP9** (**Figure 3.15**), but in the latter case the stirring time is reduced to 15 minutes. The contrast between the two samples is obvious with significantly less porosity in the sample stirred for only 15 minutes *c.f.* 60 minutes. This suggests that Ostwald ripening is an important factor in particle growth and phase transitions [88].

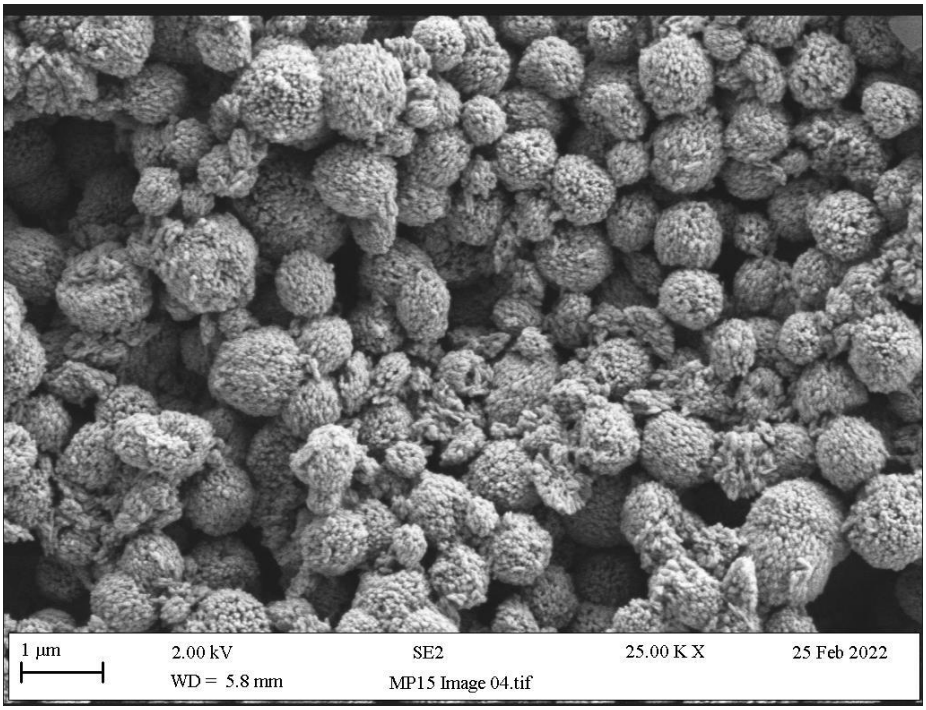

Figure 3.14 SEM image of calcium carbonate precipitated after mixing solutions of Ca^{+} (1.0 M, 300 mL) in PDDA (aq., 0.5 wt.%) and CO_3^{2-} (1.0 M, 300 mL) in PDDA (aq.,0.5 wt.%) and stirring for 60 minutes (1 hour) (**MP15**).

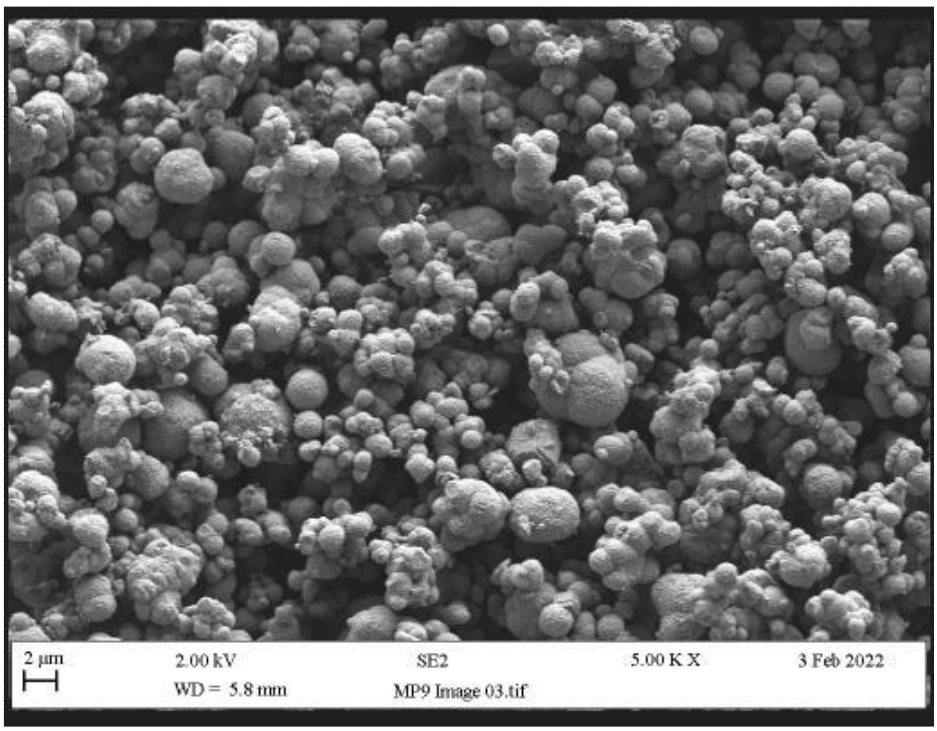

Figure 3.15 SEM image of calcium carbonate precipitated after mixing solutions of Ca^{+} (0.1 M, 300 mL) in PDDA (aq., 0.5 wt.%) and CO_3^{2-} (1.0 M, 300 mL) in PDDA (aq.,0.5 wt.%) (**MP9**).

3.2.4 Effect of extended mixing time

The influence of mixing time on morphology is further emphasised by comparing the SEM images in **Figure 3.16 (MP15**: [Ca^{2+}] 1.0 M in 300 mL aq. PDDA 0.5 wt% + [CO_3^{2-}], 1.0 M in 300 mL aq. PDDA 0.5 wt%, combined stir time 60 mins**), Figure 3.17 (MP16**: [Ca^{2+}] 1.0 M in 300 mL aq. PDDA 0.5 wt% + [CO_3^{2-}], 1.0 M in 300 mL aq. PDDA 0.5 wt%, combined stir time 120 mins**)** and **Figure 3.18 (MP18**: [Ca^{2+}] 1.0 M in 300 mL aq. PDDA 0.5 wt% + [CO_3^{2-}], 1.0 M in 300 mL aq. PDDA 0.5 wt%, combined stir time 1440 mins**)**, where stirring time is increased (1, 2 and 24 hours).

The process of spherulitic growth, dissolution and reprecipitation usually take place during the first 15 minutes of stirring (reaction). With ACC being converted to spherical porous vaterite (and calcite) (**Figure 1.38,** reproduced here for ease of comparison from **Section 1.4.2.3**). The SEM for **MP15** (**Figure 3.16**) shows that the transition to highly porous vaterite has taken place after 60 minutes. By 120 minutes, diffusion of ACC from the pore interior to the outer surface has resulted in smoother, spherical particles to give a vaterite/calcite mixture (**Figure 3.17**, **MP16**). After 1440 minutes (24 hours), the transition to calcite crystals with some vaterite casts is seen [89]. The hollow nature of the rhombohedral calcite is implied by the area highlighted in the SEM (yellow circle, **Figure 3.18**).

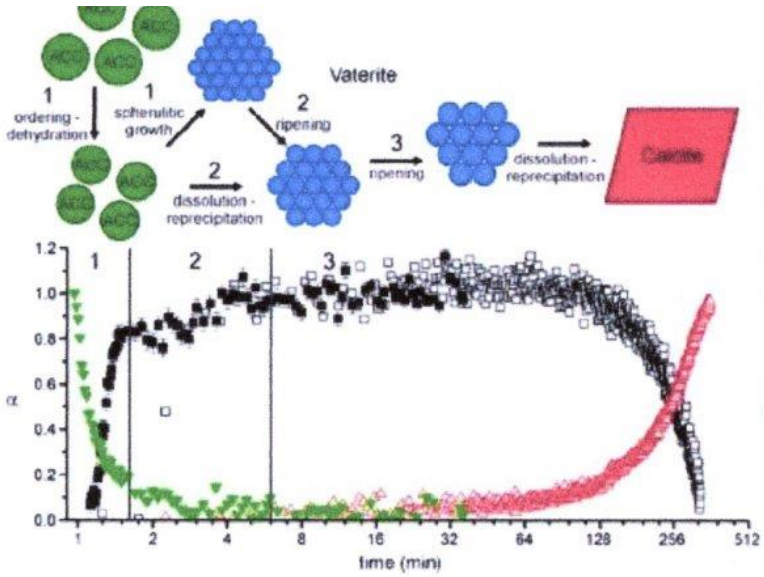

Figure 1.38 Schematic diagram to represent the pathway for ACC-vaterite-calcite crystallisation. (Reproduced from [70])

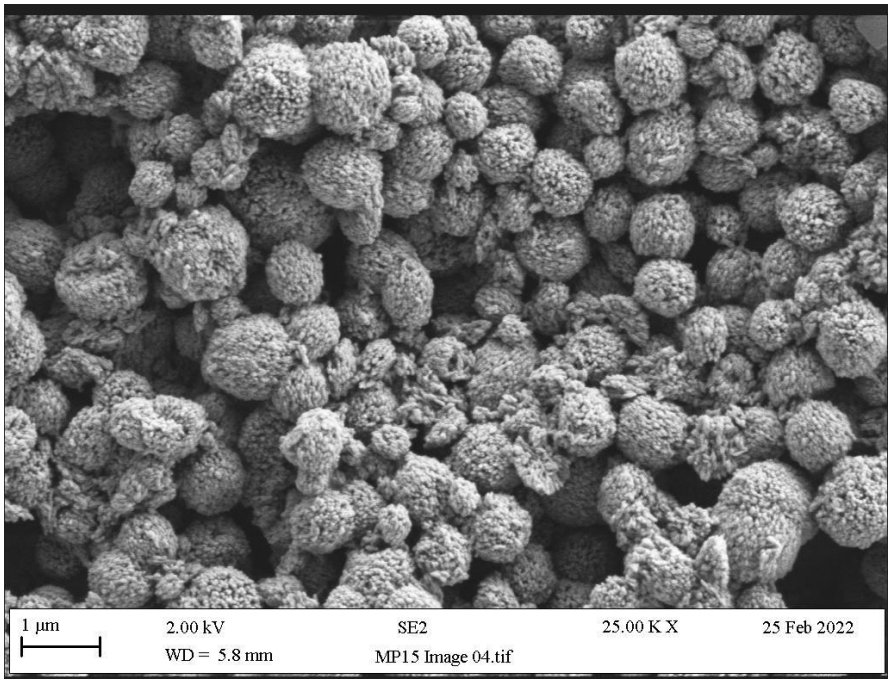

Figure 3.16 SEM image of calcium carbonate precipitated after mixing solutions of Ca^{+} (1.0 M, 300 mL) in PDDA (aq., 0.5 wt.%) and CO_3^{2-} (1.0 M, 300 mL) in PDDA (aq.,0.5 wt.%) and stirring for 60 minutes (1 hour) (**MP15**).

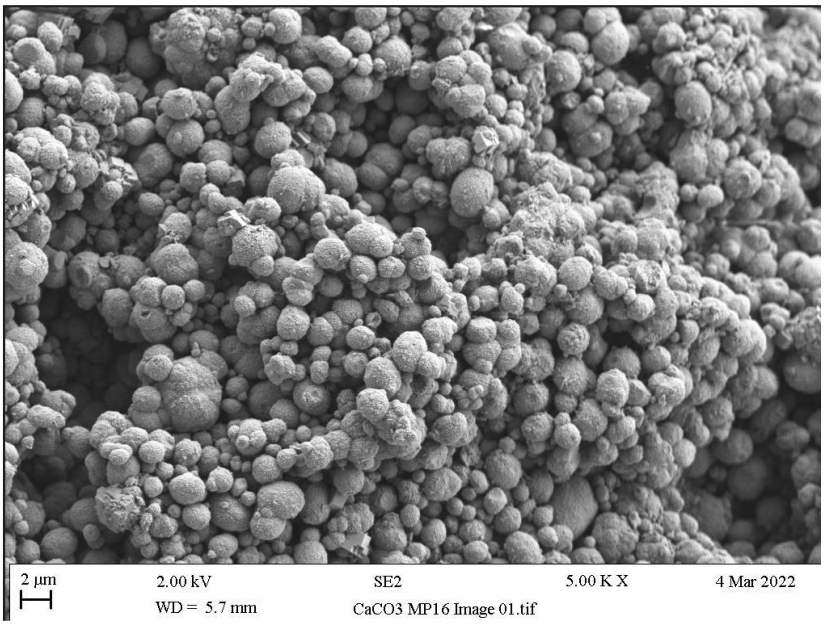

Figure 3.17 SEM image of calcium carbonate precipitated after mixing solutions of Ca^{+} (1.0 M, 300 mL) in PDDA (aq., 0.5 wt.%) and CO_3^{2-} (1.0 M, 300 mL) in PDDA (aq.,0.5 wt.%) and stirring for 120 minutes (2 hours) (**MP16**).

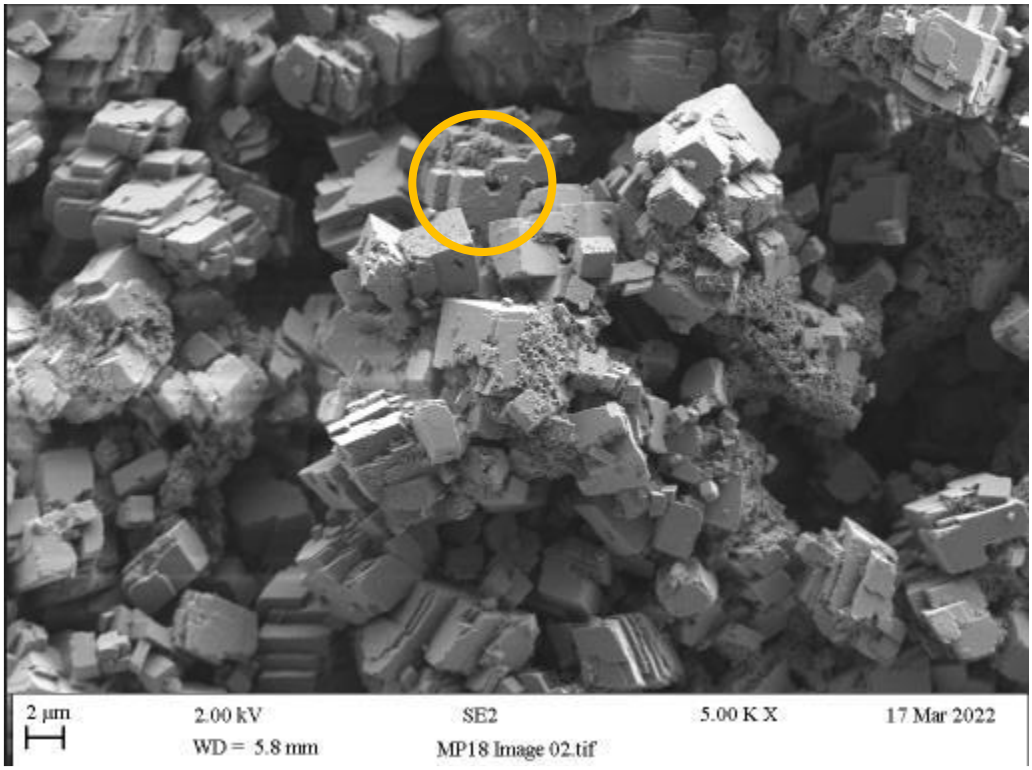

Figure 3.18 SEM image of calcium carbonate precipitated after mixing solutions of Ca^{+} (1.0 M, 300 mL) in PDDA (aq., 0.5 wt.%) and CO_3^{2-} (1.0 M, 300 mL) in PDDA (aq.,0.5 wt.%) and stirring for 1440 minutes (24 hours) (**MP18**).

3.2.5 Effect of ultrasonication

Figure 3.19 shows the SEM image of sample **MP8**, which was prepared by the addition of water (10 mL) to 0.2 g of **MP4** ([Ca^{2+}] 1.0 M in 10 mL aq. PDDA 0.5 wt% + [CO_3^{2-}], 1.0 M in 10 mL aq. PDDA 0.5 wt%, combined stir time 15 mins), followed by ultrasonication, centrifugation and drying. Here ultrasonication has produced particles that are slightly smaller in size *c.f.* **MP4**, but again resulted in hollow particles (*c.f.* with scaling up to 300 mL). Sample **MP10** (**Figure 3.30**) was prepared by addition of water (10 mL) to 0.2 g of **MP9** ([Ca^{2+}] 0.1 M in 300 mL aq. PDDA 0.5 wt% + [CO_3^{2-}], 0.1 M in 300 mL aq. PDDA 0.5 wt%, combined stir time 15 mins). In contrast to sample MP8, here the addition of water, followed by ultrasonication, centrifugation and drying, did not produce hollow spheres.

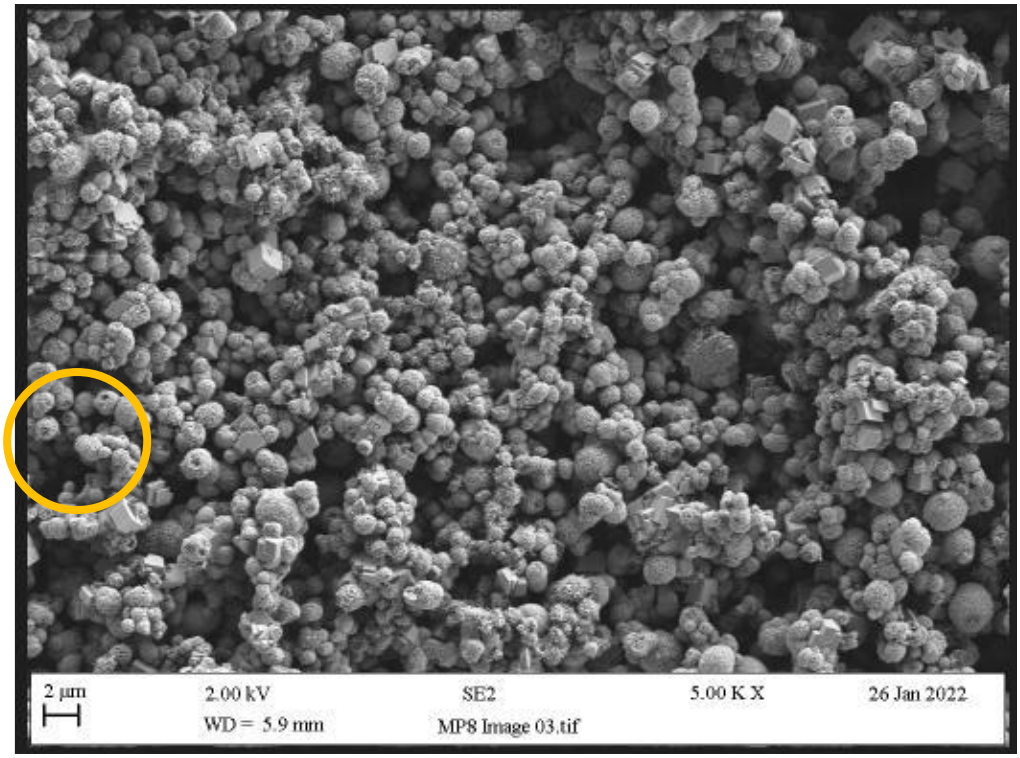

Figure 3.19 SEM image of calcium carbonate prepared from sample **MP4** (0.2 g), and addition of water (10 mL) followed by ultrasonication (1 hour), centrifugation and drying (**MP8**)

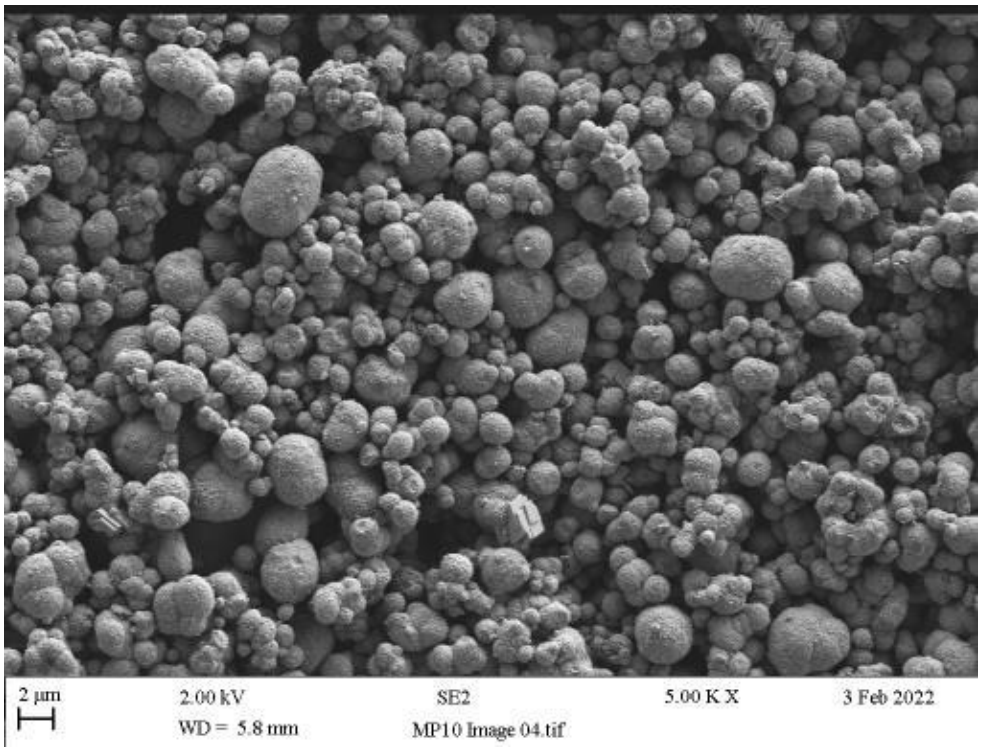

Figure 3.20 SEM image of calcium carbonate prepared from sample **MP9** (0.2 g), and addition of water (10 mL) followed by ultrasonication (1 hour), centrifugation and drying (**MP10**)

3.3 Properties of PVC formulations containing Hollow Fillers

3.3.1 SEM and XRD

Figure 3.21 depicts the SEM image of borosilicate glass microspheres, typical of a commercial PVC boat-decking formulation. The spheres have survived a compounding and extrusion process with little evidence of fracture, suggesting they have a high crush density. The spheres are approximately 10-20 μm in diameter, are well dispersed and, there is no adhesion to the PVC matrix, demonstrating that a coupling agent has not been used.

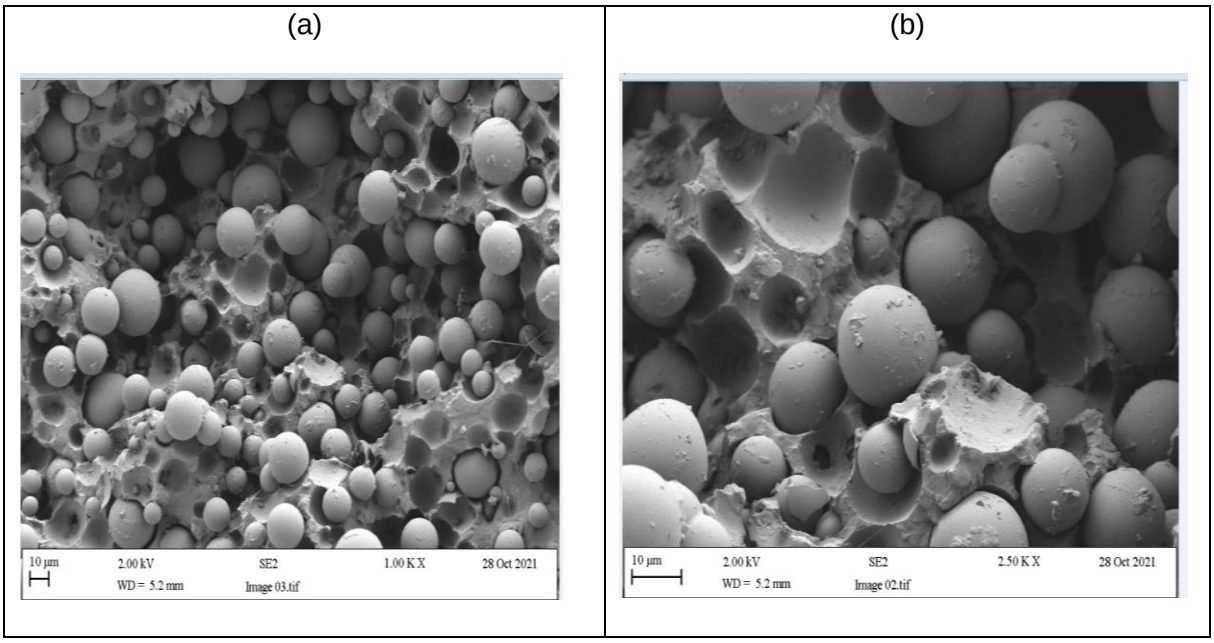

Figure 3.21 SEM image of hollow glass spheres in a commercial PVC formulation

The formulation containing hollow glass spheres prepared in this study is given in **Figure 3.22** for 15 wt.% and 24 wt.% iM16K. No coupling agent was used in these samples.

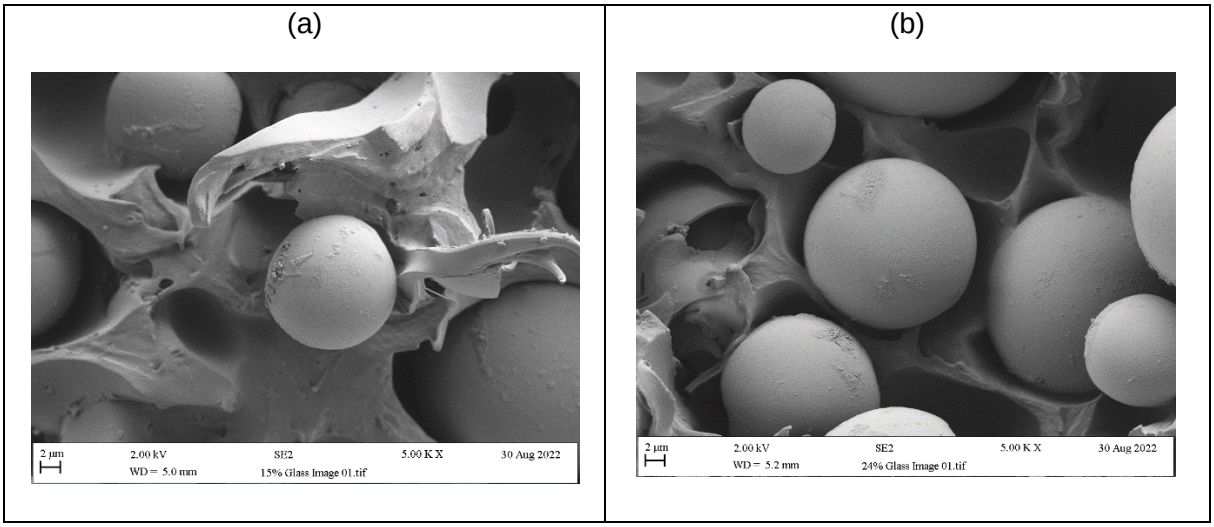

Figure 3.22 SEM image of hollow glass spheres 15 wt% (a) and 24 wt.% (b) for PVC formulations prepared according to **Table 2.2, Section 2.2.2.**

To affect a comparison with the hollow glass spheres, the calcium carbonate sample selected to incorporate in an identical PVC formulation was **MP16** ($[Ca^{2+}]$ 1.0 M in 300 mL aq. PDDA 0.5 wt% + $[CO_3^{2-}]$, 1.0 M in 300 mL aq. PDDA 0.5 wt%, combined stir time 120 mins). The SEM image in **Figure 3.23 (b)** illustrates this sample is highly porous, but the particle size is only 2-4 µm in diameter. The method for preparation for sample **MP16** was used to prepare 'identical' batches of samples **MP21, MP22 and MP23**. After preparation each of these samples were heated for four hours at 80°C to drive off bound water and then calcined at 550°C for four hours.

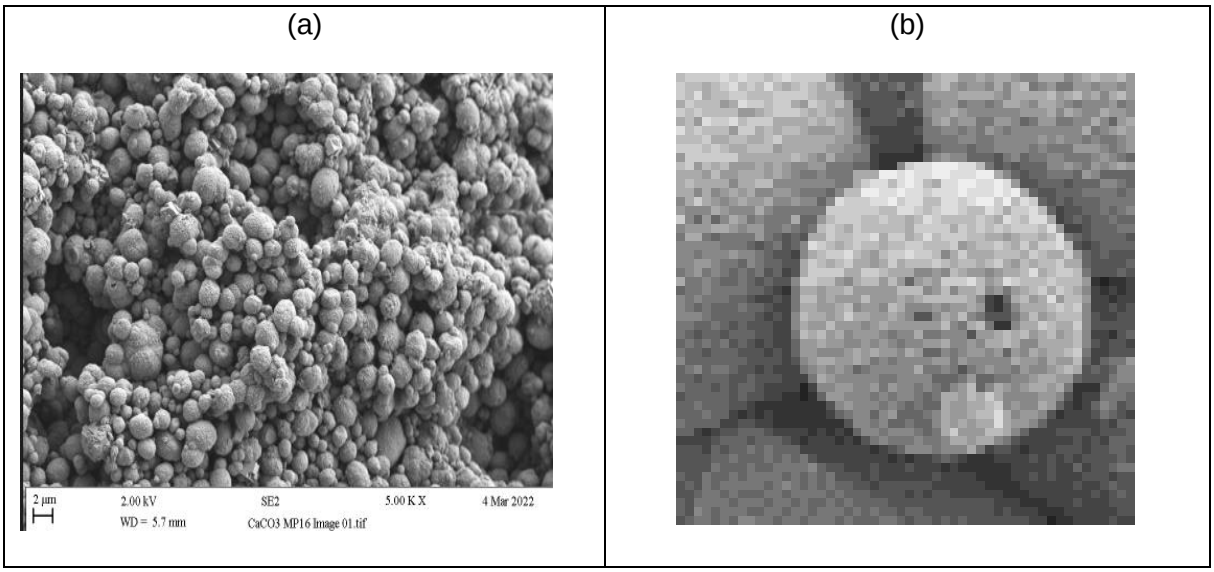

Figure 3.23 SEM image of calcium carbonate sample **MP16**.

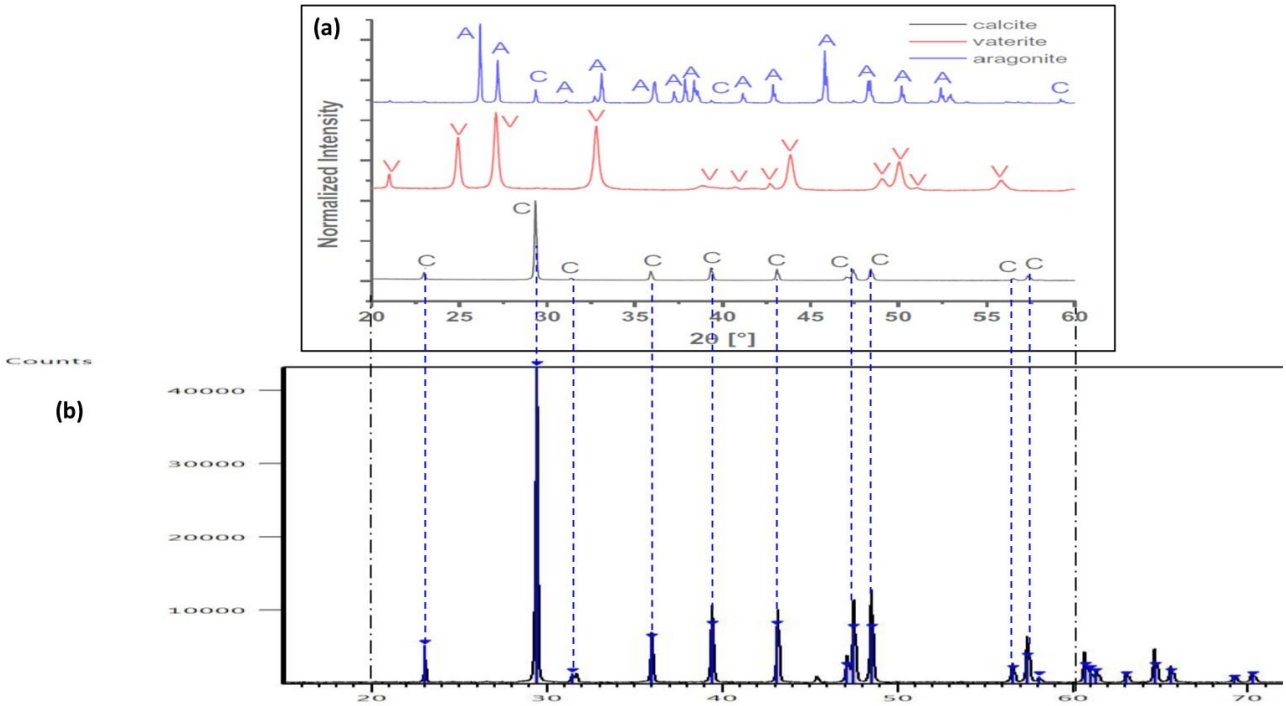

Figure 3.24 Selected region of XRD spectra of (a) individual calcium carbonate polymorphs synthesised by precipitation with no additive (Reproduced from [81]) and (b) calcium carbonate synthesised by precipitation in the presence of PDDA additive calcined at 550°C for 4 hours (**MP21**)

Heating vaterite in the presence of oxygen transforms it progressively to the calcite polymorph. Nassrallah-Aboukaïs and coworkers have shown that vaterite remains thermally stable up to a calcination temperature of 450°C. At 481°C, they found that a small amount of calcite was formed on the vaterite surface in a humid atmosphere. The transformation of the vaterite bulk continued at 491°C, with calcite being formed up to 500°C. The calcite phase then remained stable up to 700°C, but above this temperature CaO was formed [90].

Figure 3.24 shows the XRD for the first batch of calcium carbonate synthesised by the method for MP16 and then calcined at 550°C to give sample **MP21**. The vaterite polymorph has been converted to calcite, consistent with the literature. This is confirmed by the SEM image in **Figure 3.25**, which shows the characteristic rhombohedral crystals of calcite.

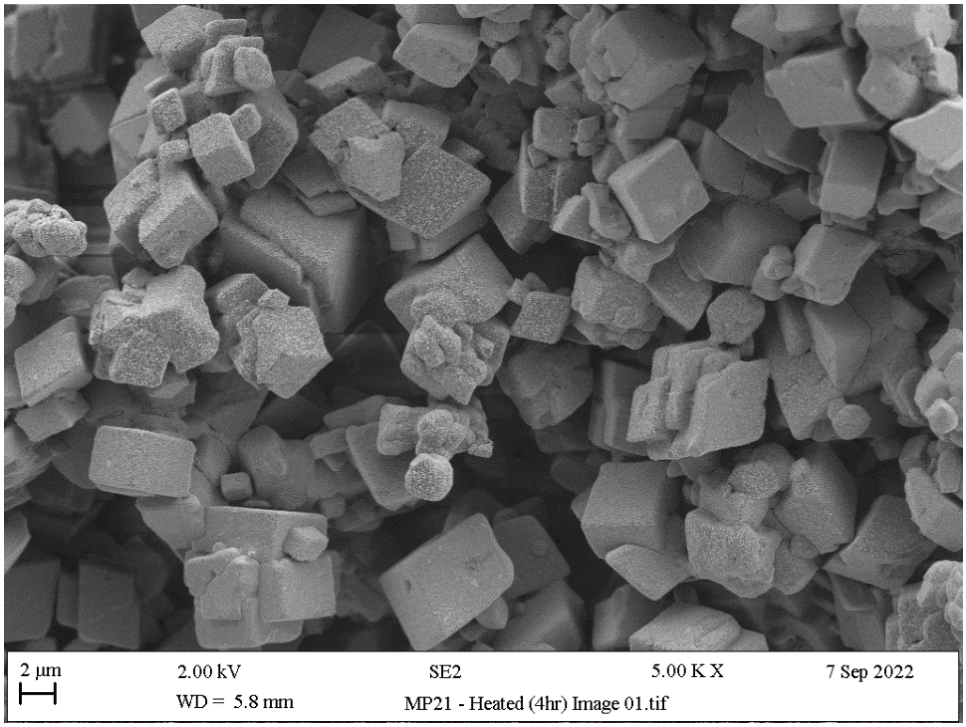

Figure 3.25 SEM image of calcium carbonate (**MP21**) produced by heating sample **MP16** for 4 hours, followed by calcination at 550^{o}C for 4 hours

The XRD for **MP23** (**Figure 3.26**) and SEM image of **MP23** (**Figure 3.27**) can be compared. Essentially, they should be identical to the respective SEM and XRD for **MP21**, since they were prepared by the same methodology. This is true for the XRD in **Figure 3.26**, where the calcite polymorph is confirmed. However, the SEM image suggest that the samples formed are at slightly different stages of transformation. It may be possible that for sample **MP21** in **Figure 3.25** there is a slight surface vaterite casting, though this should be confirmed by further analysis.

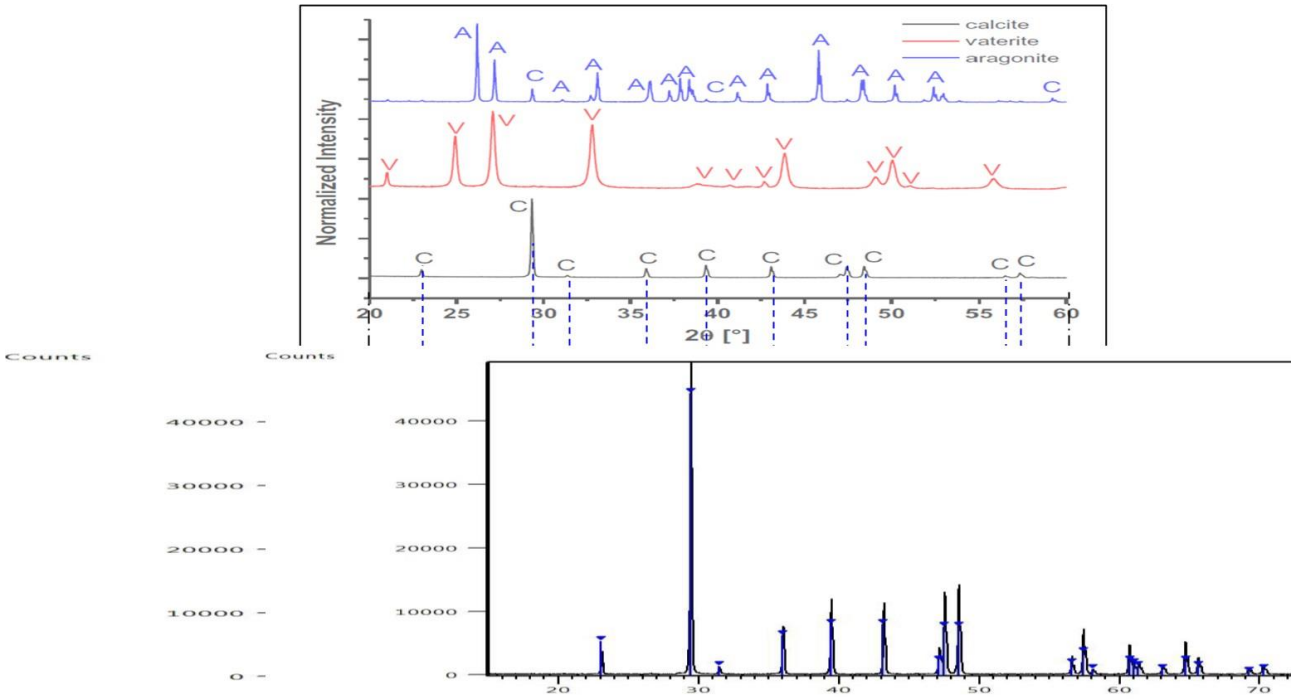

Figure 3.26 Selected region of XRD spectra of (a) individual calcium carbonate polymorphs synthesised by precipitation with no additive (Reproduced from [83]) and (b) calcium carbonate synthesised by precipitation in the presence of PDDA additive calcined at 550°C for 4 hours (**MP23**)

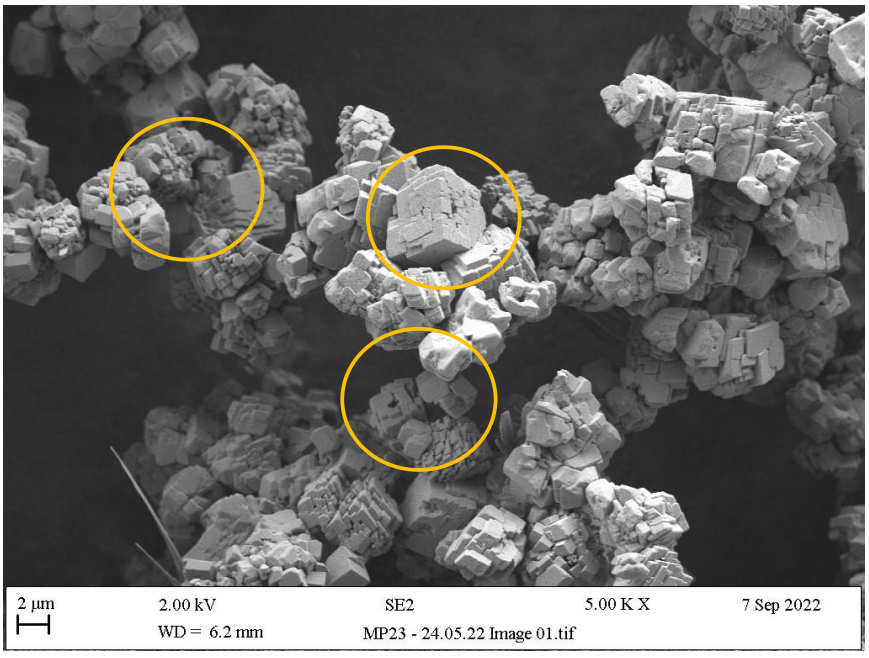

Figure 3.27 SEM image of calcium carbonate (**MP23**) produced by heating sample **MP16** for 4 hours, followed by calcination at 550°C for 4 hours. Areas circled yellow highlight evidence for hollow particles.

Samples **MP21** and **MP23** were then incorporated into PVC at 15 wt% (**Figure 3.28**) and 24 wt.% (**Figure 3.29**) respectively. The lack of adhesion to the PVC matrix, due to absence of a coupling agent, is seen as for hollow glass microspheres.

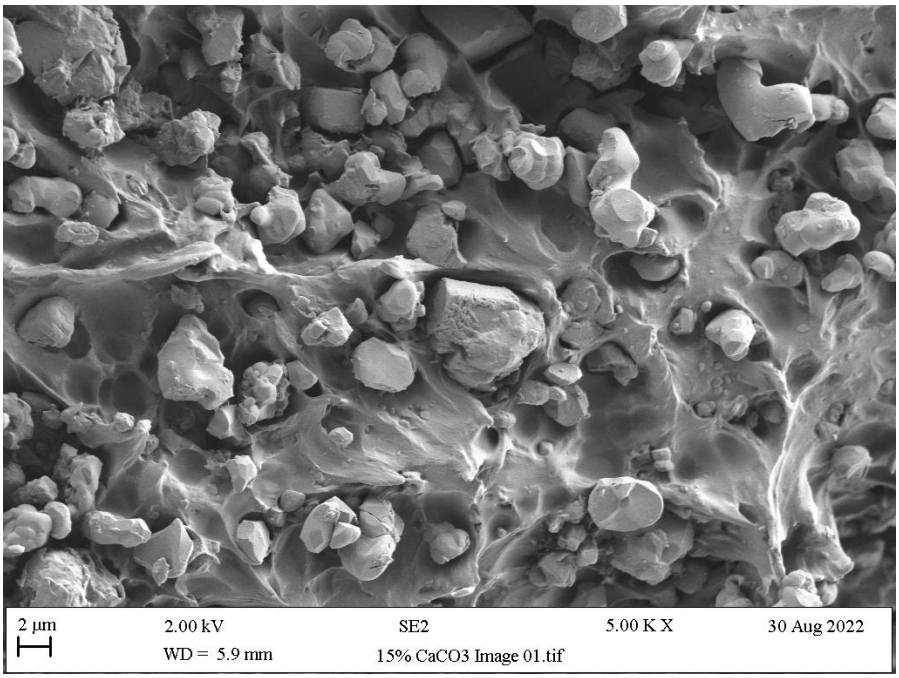

Figure 3.28 SEM image of calcium carbonate in a commercial PVC formulation

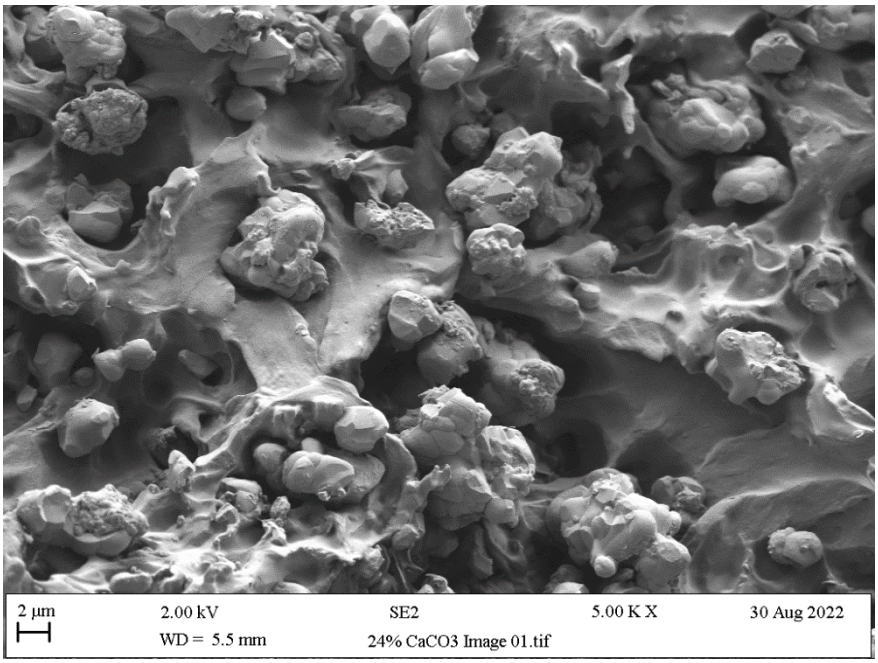

Figure 3.29 SEM image of hollow glass spheres in a commercial PVC formulation

3.3.2 Mechanical properties

Usually, fillers are added to thermoplastics to increase stiffness (modulus). However, for boat decking the main purposes of the (hollow) filler are light-weighting and thermal insulation. Despite this, the tensile and flexural moduli of the composite, which are rather similar, should meet an acceptable service-life value. The effect of addition of filler on the modulus of a thermoplastic is generally understood [91]. The simple 'rule of mixtures' provides a good estimation of the influence of filler level on mechanical properties at low strain levels, provided the filler distribution is isotropic [92]. For anisotropic fillers, which align in the direction of flow on processing, there are significant deviations from 'rule of mixtures' relationships.

As the volume percentage of filler is increased to *ca.* 20 volume percent, the relationship between filler amount and increase in mechanical properties is linear. It should be borne in mind that the method of preparation of test samples influences mechanical properties. For example, for injection moulded 'dog bone' shaped tests specimens there is often higher filler orientation than in normal processing, resulting in higher mechanical property values. Polymer-filler, filler-filler (e.g., in mica) and other interparticle interactions also influence the final mechanical properties [93-95]. A wide range of different fillers were examined by Pukansky [96]. Here the Young's modulus and the amount of filler bonded to the polymer (polypropylene) correlated with filler surface area and hence particle size and shape. The importance of the strength of interaction between the filler surface and polymer has also been demonstrated by Schreiber and Germain [97]. From these studies it is inferred that particle debonding, particle re-orientation and polymer orientation during processing and service life are also likely to play a part.

To validate data obtained in this study (and provide a benchmark for acceptable service-life properties) a comparison was made using a commercial compound designed for PVC-based boat decking. The stress-strain curves generated from the compound provided are given in **Figure 3.30**. The data obtained from an external laboratory on the same compound is compared with this data in **Table 3.1**. There is an acceptable correlation between the data from the two sources, but it should be noted that any variability may be due to specifics of test methodology and inclusion of additional process additives.

Table 3.1 Mechanical property data for commercial PVC compound containing hollow glass sphere filler.

	Commercial Sample* (Data from external Lab)	Commercial Sample** (Data from current study)
Tensile strength (MPa)	8.0	8.0
Yield strength (MPa)	-	4.3
Extension at break (%)	165	200
Modulus at 100% (MPa)	6.7	6.2
Modulus at 50% (MPa)	-	4.76

***BS2782 320A** ****D638**

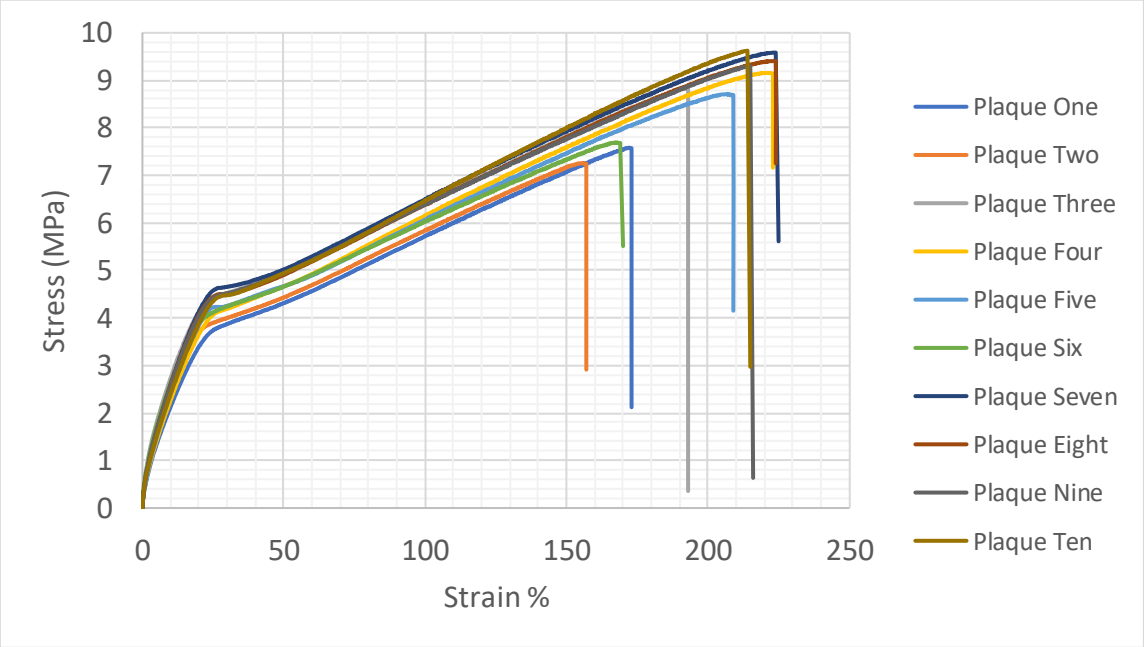

Figure 3.30 Stress-strain curves for test bars cut from plaques pressed from commercial PVC compound containing hollow glass filler.

Figure 3.31 and **Figure 3.32** depict the tensile test data for PVC formulations containing hollow glass sphere filler at 1 wt.% and 25 wt.% respectively. Specific mechanical property data is given in **Table 3.2**. According to standard method D638, five replicates of each sample were tested, and an average value of the mechanical property quoted in the table. Mechanical failure of filled plastics samples is influenced by not only by the polymer-filler, filler-filler and other interparticle interactions mentioned previously, but also the distribution of particles in the matrix and any agglomeration. Data may therefore produce apparent outliers from some test bars cut from replicates within a given plaque, though these are included in the data under the test method to account for this.

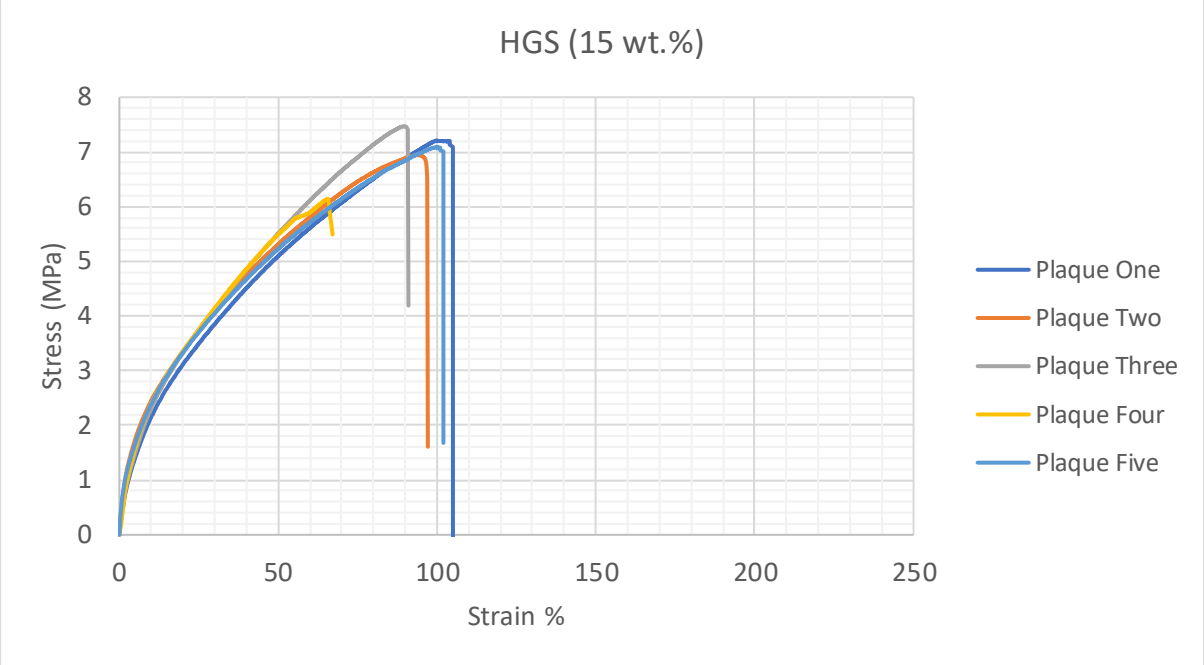

Figure 3.31 Stress-strain curves for PVC formulation (see **Table 2.2**) containing hollow glass filler (15 wt.%)

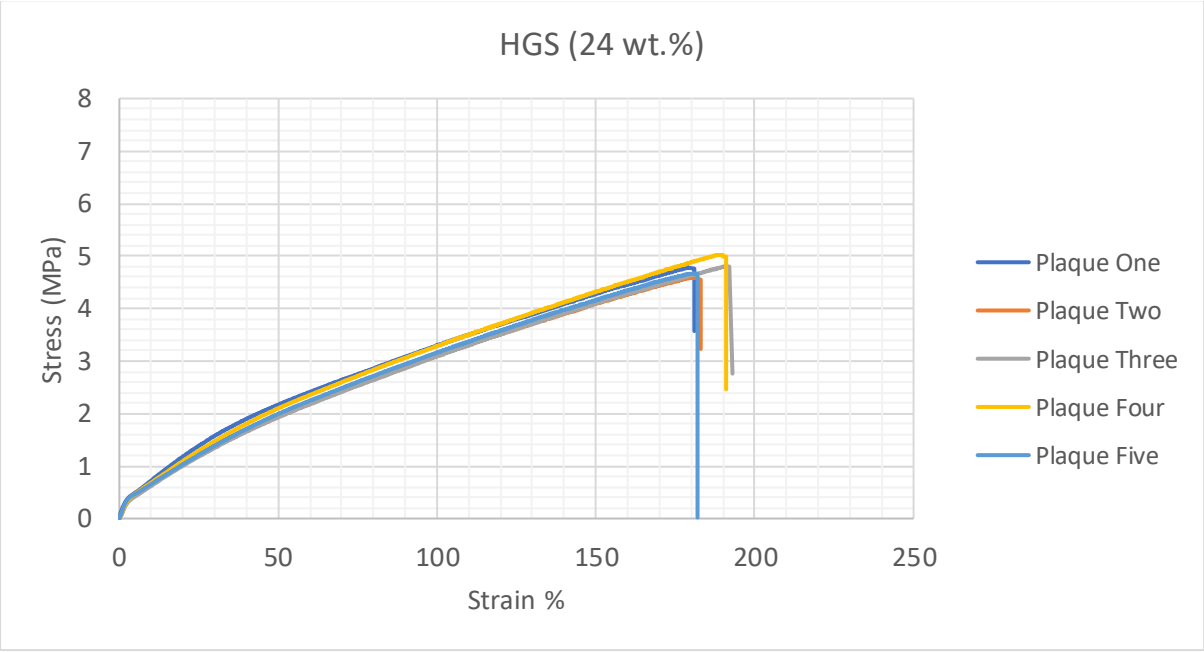

Figure 3.32 Stress-strain curves for PVC formulation (see **Table 2.2**) containing hollow glass filler (24 wt.%)

Table 3.2 Mechanical property data for PVC formulations (see **Table 2.2**) containing hollow glass sphere filler (at 15 wt.% and 25 wt.%)

	HGS (15 wt.%)	HGS (24 wt.%)
Tensile strength (MPa)	6.3	7.5
Extension at break (%)	93	186
Modulus at 100% (MPa)	6.9	3.2
Modulus at 50% (MPa)	4.9	2.0

The data is consistent with observations reported by other workers. Liang [98] has shown that for PVC filled with hollow glass beads tensile yield strength decreases gradually with increasing volume fraction of hollow glass spheres. In contrast, the tensile break strength (in the range 0-20 wt.% filler) was somewhat greater than that of unfilled PVC. The notched impact strength decreased significantly with increasing volume fraction of filler to a minimum and then increased slightly, with the influence of filler size being insignificant. Experimental values were in good agreement with calculated values from equations defined in [99].

Table 3.3 summarises the tensile test date in **Figure 3.33** and **Figure 3.34** for corresponding samples containing hollow calcium carbonate (rhombohedral) at 15 wt.% and 24 wt.% respectively. The mechanical properties are mostly consistent with those for the commercial samples and those containing hollow glass spheres. However, it should be recognised that the laboratory test samples were produced by compression (press) whilst the commercial samples were produced by extrusion. However, the correlation of improved tensile strength and extension at break at the higher filler loading (24 wt.%) is evident.

Whilst tensile stress-strain curves give a good, initial indication of the performance and integrity of the filled polymer, other mechanical properties are likely to be important for boat-decking applications. Here impact and puncture strength, along with abrasion resistance as a function of filler shape, addition level and crush strengthshould be assessed. Furthermore, the effect on mechanical properties of hollow particles crushed during recycling is required to quantify the amounts of recyclate that can be realistically incorporated into reprocessed composite.

Table 3.3 Mechanical property data for PVC formulations (see **Table 2.2**) containing hollow calcium carbonate filler (at 15 wt.% and 25 wt.%)

	Hollow $CaCO_3$ (15 wt.%)	Hollow $CaCO_3$ (24 wt.%)
Tensile strength (MPa)	6.5	7.8
Extension at break (%)	92	200
Modulus at 100% (MPa)	8.1	4.6
Modulus at 50% (MPa)	6.8	2.6

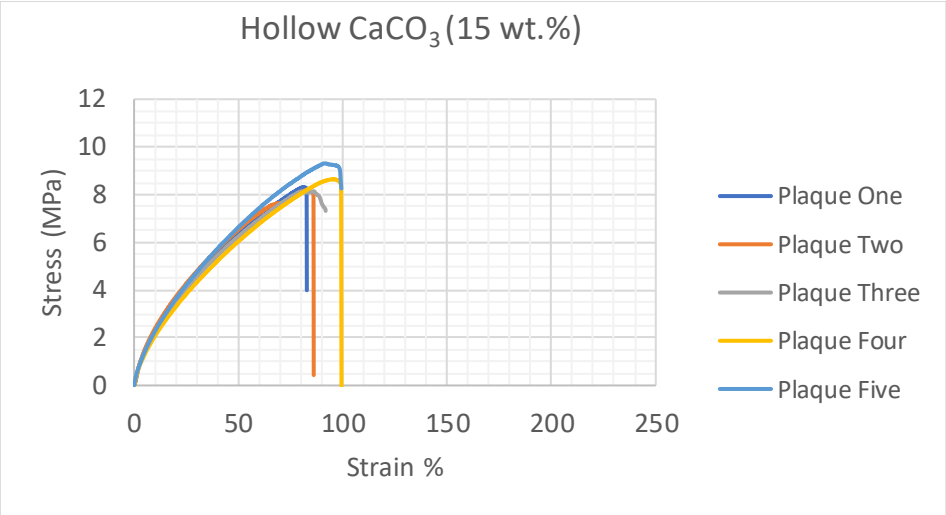

Figure 3.33 Stress-strain curves for PVC formulation (see **Table 2.2**) containing hollow calcium carbonate filler (15 wt.%)

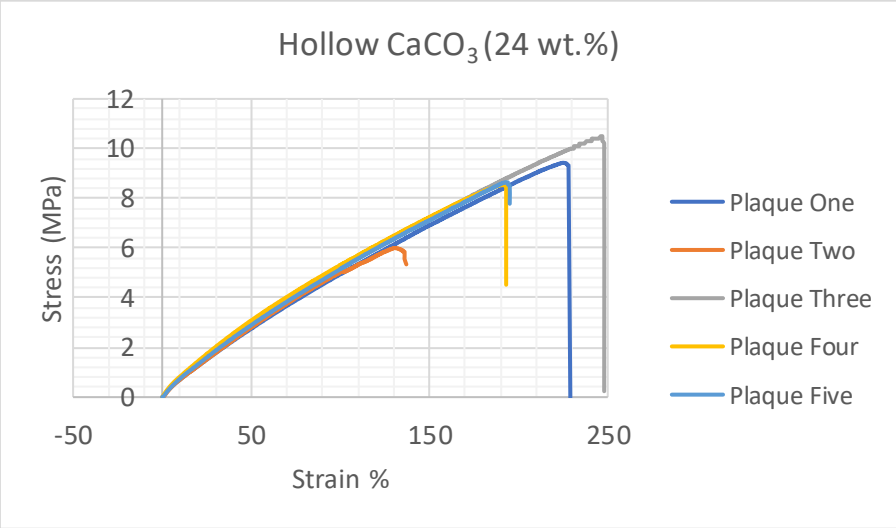

Figure 3.34 Stress-strain curves for PVC formulation (see **Table 2.2**) containing hollow calcium carbonate filler (24 wt.%)

3.3.3 Density

As stated previously, one of the main objectives when adding hollow filler is to reduce weight of the composite. **Figure 3.35** gives the predicted density for a range of fillers in PVC at the lower filler fraction of 0.15 and higher filler fraction of 0.24. Data has been calculated using 'rule of mixtures' equations (given in **Section 3.2.5**). The data has been calculated using the more reliable volume percentage in the equations, but the corresponding weight percent is given in the figures for ease of comparison. The densities of the fillers are given in **Figure 3.36**. The density of hollow rhombohedral calcium carbonate filler is relatively high *c.f.* other hollow fillers considered in this study. This suggests that hollow spherical calcium carbonate, having a significantly lower density, would be the better polymorph to use for lightweight applications. It was noted in the literature that hollow sphere, rather than hollow cubic or rhombohedral fillers tended to have thinner wall thickness, consistent with lower density. The lowest density fillers are expandable (Expancel™) microspheres, which have substantially lower densities than the commercially more widely used hollow glass spheres (IM16K and IM30K™). This is reflected in the composite densities given in **Figure 3.35**.

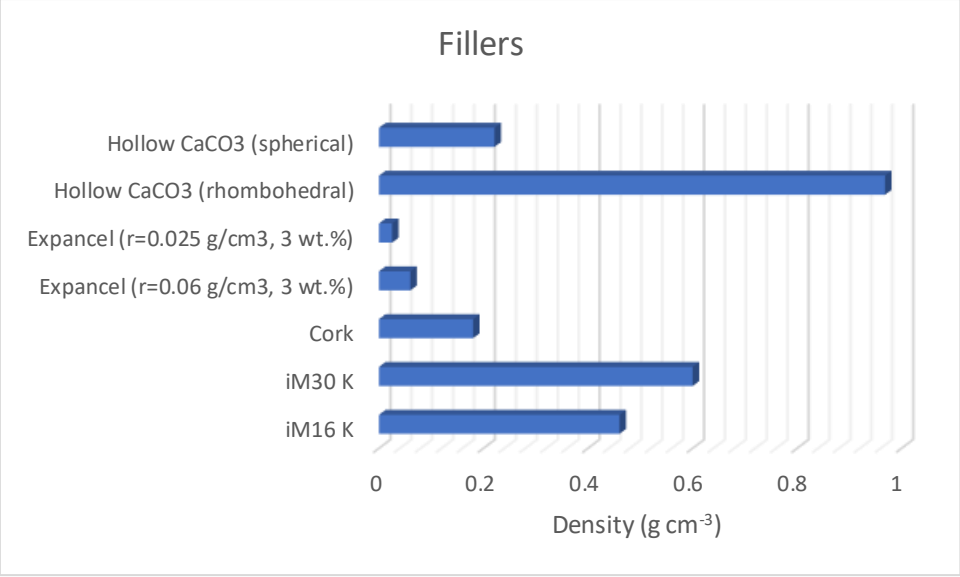

Figure 3.35 Density (g cm^{-3}) of fillers. Predicted data from a range of sources (commercial specification sheets, matmatch [100], matweb [101])

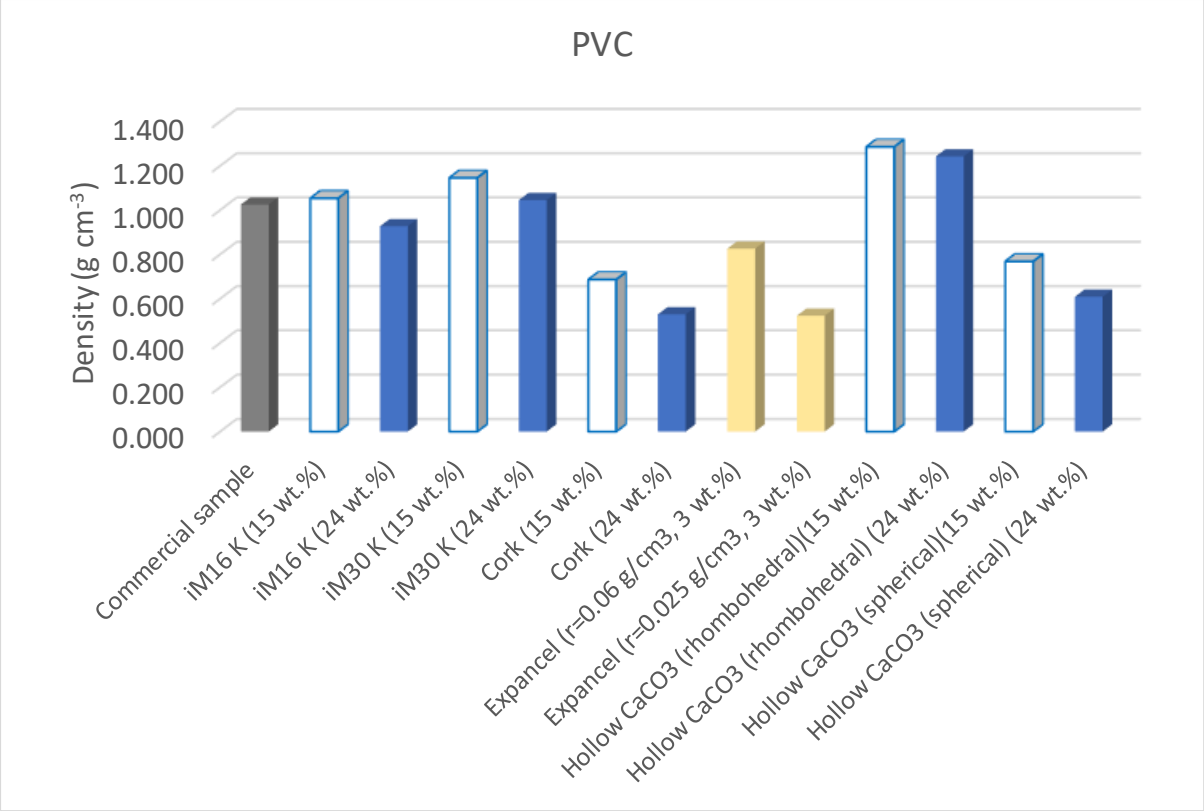

Figure 3.36 Density (g cm^{-3}) of PVC composite with filler levels of 15 wt.% and 24 wt.% (Expancel™ filler at 3 wt.%). Predicted data from a range of sources (commercial specification sheets, matmatch [100], matweb [101])

Some improvements (lower density) are noted, as might be expected, on increase of filler fractions from 0.15 to 0.24. However, the overriding factor in reduction in density is the use of alternative fillers, namely Expancel™ microspheres and cork. Note that for the composites the effect of packing factors (vol. % *c.f.* wt.%) in calculations shows that in practice cork and the expandable microspheres considered here show similar densities at the higher filler level (24 wt.%).

Table 3.4 compares the predicted data with the experimental data to validate the predictive models ('rule of mixtures' equations) used. There is good agreement between the two sets of data.

Table 3.4 Comparison of predicted and experimental data for PVC formulations (see **Table 2.2**) containing hollow calcium carbonate filler (in the range 15-25 wt.%)

	Experimental Density (g cm^{-3})	Predicted Density (g cm^{-3})
Hollow $CaCO_3$ (rhombohedral)	1.330	1.286
iM16 K (15 wt.%)	1.027	1.054
iM16 K (24 wt.%)	0.929	0.927
Commercial sample	1.025	-

Even though there is a good agreement between the predicted and experimental density values in this study, it should be realised that this is for a limited number of samples. In reality, the 'rule of mixtures' equation (Equation 5.1), does not compensate for the crush strength of the hollow particles as a function of shape and fill level (wt. %). From the limited amount of data, for the hollow glass spheres (iM16 K) there is a closer agreement between predicted density and experimental density at 24 wt.% (0.927 g cm^{-3} *c.f.* 0.929 g cm^{-3}) that at 15 wt.% (1.054 g cm^{-3} *c.f.* 1.027 g cm^{-3}). Although it is logical that a higher amount (24 wt.% *c.f*. 15 wt.%) of hollow filler should reduce the density of the final composite, it does not necessarily follow that under given processing conditions the percentage of filler crushed during processing is linear. In addition, the largest deviation between predicted and experimental densities for the hollow $CaCO_3$, which is rhombohedral in shape. An understanding of how shape influences crush density (e.g., spherical versus hollow rods) would refine predictive models.

3.3.4 Thermal Properties

The influence of the glass and calcium carbonate hollow fillers on the thermal stability of PVC is seen in **Figure 3.37** and **Figure 3.38**. PVC is the most thermally sensitive of the major thermoplastic resins. As such, it is subject to degradation during processing and end-use with stability also influenced by the type and level of filler [102-105]. PVC degrades by a two-step process. Dehydrochlorination of the carbon backbone to eliminate HCl takes place, then the HCl catalyses chain-scission and further dehydrochlorination (**Figure 3.37**). To prevent this, stabilisers (calcium and zinc stearates) are added to the formulation to serve as acid scavengers.

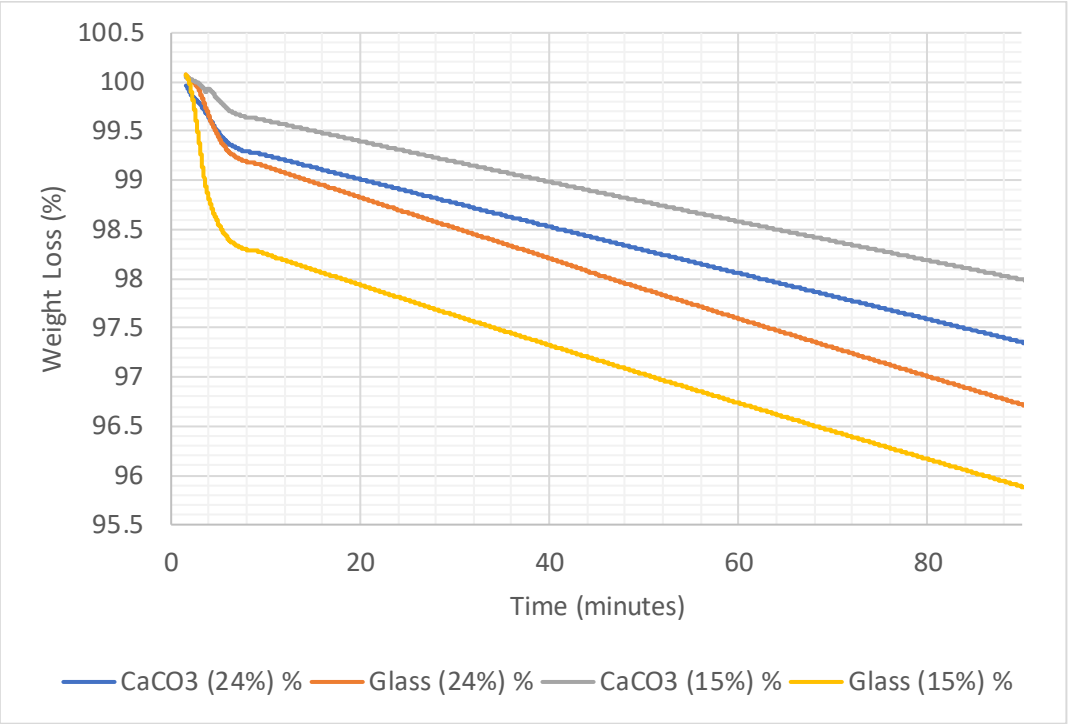

Figure 3.37 Thermogravimetric weight loss (%) for PVC formulations containing hollow glass spheres (15 wt.% and 24 wt.%) and hollow calcium carbonate (15 wt.% and 24 wt.%), under isothermal conditions at 180^{o}C (ramp rate 100^{o}C/min) for 90 minutes under nitrogen

Figure 3.38 illustrates that, compared to hollow glass filler, calcium carbonate as a basic mineral filler can neutralise HCl, so slowing dehydrochlorination and hence thermal degradation of PVC. The two levels of addition 15 wt.% and 24 wt.% show that the rate of weight loss is faster for PVC containing hollow glass microspheres compared with hollow calcium carbonate.

Differences are most pronounced during the initial period of rapid weight loss (0-10 minutes). Thereafter, there is a slower rate of degradation (10-90 minutes) (**Figure 3.37**).

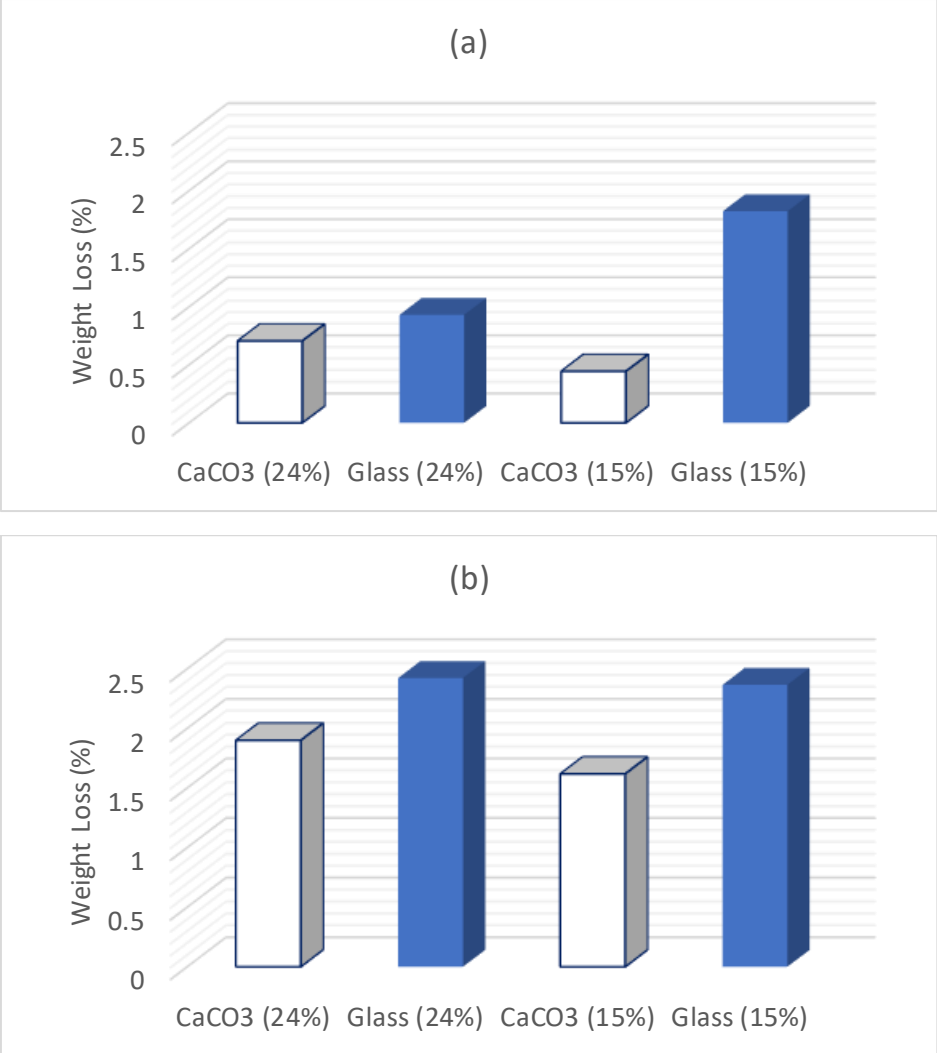

Figure 3.38 Thermogravimetric weight loss (%) for PVC formulations containing hollow glass spheres (15 wt.% and 24 wt.%) and hollow calcium carbonate (15 wt.% and 24 wt.%), under isothermal conditions at 180^{o}C (ramp rate 100^{o}C/min) under nitrogen, at 10 minutes (a) and 10-90 minutes (b).

To measure the thermal conductivity of materials several methods may be employed. Normally thermal diffusivity is measured and then by using heat capacity values of materials the thermal conductivity calculated. Unfortunately, relatively large samples are required to carry out these measurements. More recently DSC has been employed. Here a known mass of material is heated, cooled, or subjected to a controlled temperature and its heat capacity recorded as changes in heat flow. As such, DSC can characterise melting, phase changes, glass transitions, crystallisation,

thermal stability, and heat capacity. To measure thermal conductivity by DSC two methods are adopted. In the first a pure metal is place on top of the material under test and heated to the melting point of the metal. Hence, the thermal conductivity is obtained at the melting point of the metal. In the second, more complex method, thermal sensors are employed to obtain thermal conductivity over a specific temperature range. Other methods have been reported that use an accessory to measure thermal contact resistance and hence thermal conductivity, rather than thermal sensors.

Regrettably, technical issue with the instrument meant that samples could not be run under the required conditions at the time of submission. Hence data has been collected from a variety of resources to allow prediction of thermal conductivity using the 'rule of mixtures', and modified equations (see **Section 3.2.5** for relevant equations).

Here it might be expected that for a given polymer (PVC) the lower the conductivity of the filler (at a specified filler loading) the lower the thermal conductivity of the final composite. **Figure 3.39** shows the predicted thermal conductivity of a range of solid and hollow fillers in PVC at two different levels (15 wt.% and 24 wt.%).

As for composite density (**Figure 3.36**) cork and expandable microspheres show the best performance (lower thermal conductivity). However, the poorer insulation property of calcium carbonate (even the spherical polymorph) is evident. This is expected because the cork and expandable microspheres result in a 'foam-type' structure. Calcium carbonate on the other hand is used to provide some thermal conduction during processing of PVC, so even the production of hollow structures is not sufficient to offset this substantially.

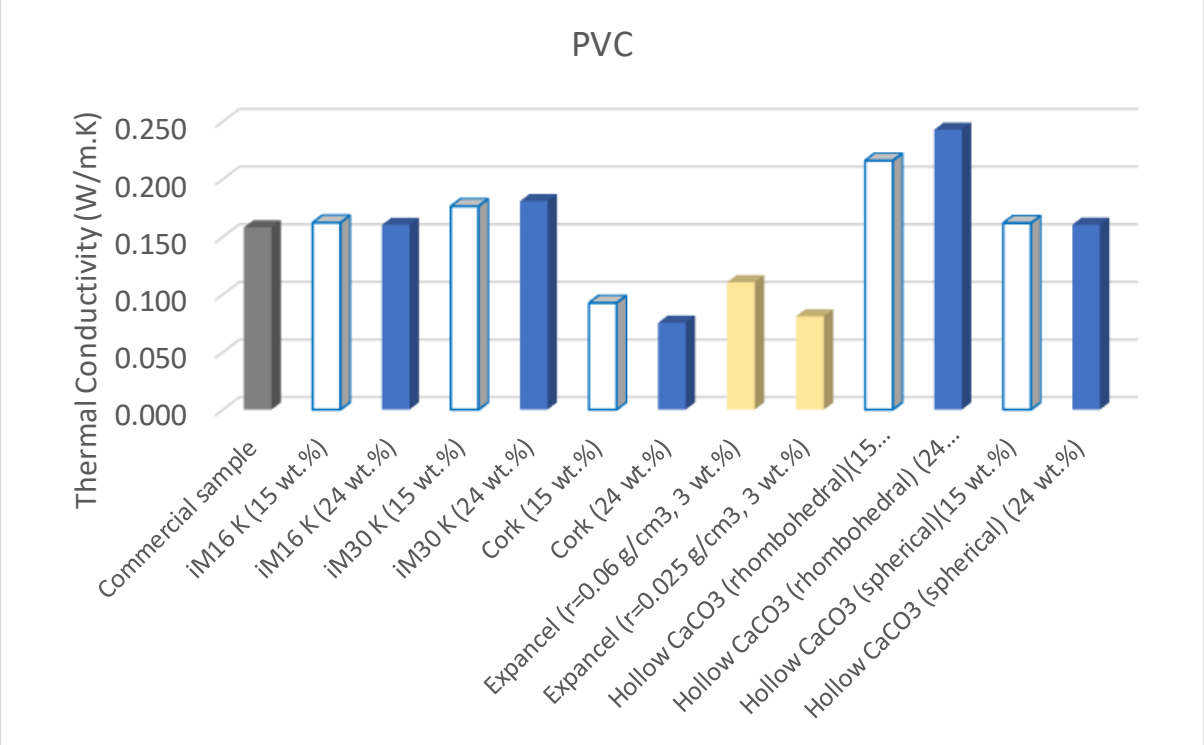

Figure 3.39 Thermal conductivity (W/m.K) of PVC composite with filler levels of 15 wt.% and 24 wt.% (Expancel™ filler at 3 wt.%). Predicted data from a range of sources (commercial specification sheets, matmatch [100], matweb [101])

While modified equations for thermal conductivity used in this study (**Equation 5.3**) give better approximations to experimental conductivities of filled polymers, several factors may result in deviations between predicted and experimental data. Most models indicate that thermal conductivity is linear for spherical particles (on which Equation 5.3 is based), but for cubic/rhombohedral fillers when the volume content is >10% there is an inflection point and percolation threshold. This relates to the influence of filler contacts: the effect of filler contacts for spherical particles being very small. In addition, the influence of crush strength needs to be accounted for. Although manufacturers of hollow particles give data on isostatic crush strengths, limited information is available on how this relates to various polymer processing conditions. An estimation of the fraction of hollow particles crushed under various processing conditions needs to be undertaken in conjunction with the impact of this on physical properties.

3.3.5 Ashby Charts: Thermal Conductivity versus Density

Because mechanical properties (**Section 3.2.2**) were in the region of benchmark values for commercial samples and, because decking is supported such that strength is not a major property of concern in improving the performance of decking materials this has not be considered in this section. Instead, Ashby plots are presented for thermal conductivity versus density for a range of fillers and polymers to assess the benefits of changing materials on composite function.

In this section theoretical calculations have been performed and depicted graphically to facilitate the comparison of a range of alternative fillers and polymer matrices. The figures use the 'Rule of Mixtures' equations or their modifications to predict density (**Equation 5.1**) and thermal conductivity (**Equation 5.2, Equation 5.3)** for a range of potential decking materials. Data for individual polymer (Data derived from a range of commercial specification sheets, matmatch [100] and matweb [101]). Furthermore, prediction of mechanical properties is not presented because there is a good understanding of how addition of filler affects the modulus of a polymer.

Equation 5.1 Density (ρ)

$\rho_c = \left(\frac{\phi_f}{\rho_f} + \frac{1 - \phi_f}{\rho_p}\right)^{-1}$	$\rho_c = composite\ density$ $\rho_f = filler\ density$ $\rho_p = polymer\ density$ $\phi_f = fraction\ filler$

Conversion of weight-fraction to volume fraction of filler:

$$f_v = \frac{f_w}{f_w + (1 - f_w)\frac{\rho_f}{\rho_p}}$$

$f_v = volume\ fraction\ of\ filler$

$f_w = weight\ fraction\ of\ filler$

$\rho_f = filler\ density$

$\rho_p = polymer\ density$

Equation 5.2 Thermal conductivity (*k* or λ)

$k_c = \left(\frac{\phi_f}{k_f} + \frac{1 - \phi_f}{k_p}\right)^{-1}$	$k_c = composite\ thermal\ conductivity$ $k_f = filler\ thermal\ conductivity$ $k_p = polymer\ thermal\ conductivity$ $\phi_f = fraction\ filler$

Equation 5.3 Modified equation for thermal conductivity

$$k_{eff} = \left[\frac{1}{k_p}\left(1 - \frac{6\emptyset_f}{\pi}\right)^{\frac{1}{3}} + 2\left(k_p\left(\frac{4\pi}{3\emptyset_f}\right)^{\frac{1}{3}} + \pi\left(\frac{2\emptyset_f}{9\pi}\right)^{\frac{1}{3}} \times \left(k_g\left(\frac{\rho_s - \rho_a}{\rho_g - \rho_a}\right) + k_a\left(\frac{\rho_g - \rho_s}{\rho_g - \rho_a}\right) - k_p\right)\right)^{-1}\right]^{-1}$$

Potential alternative polymers to PVC and their blends [106-110] are given in **Figures 3.40** (density values) and **Figure 3.41** (thermal conductivity values). Polyester and epoxy resins are included in the data because they are already used as matrices in boat-decking. A range of PVC based polymer blends are included to assess the value of adding elastomeric components (e.g., nitrile rubber, thermoplastic polyurethane (TPU), chlorinated polyethylene (CPE), chlorinated PVC (CPVC). The rationale behind this approach is to improve cushioning underfoot, resistance to staining and potentially replace plasticisers (which migrate from the polymer matrix). In the latter case there are drives to replace or limit the use of plasticisers in current use, due to environmental concerns of health and toxicity. Blends where Polyethylene (PE) has replaced PVC are also included because along with epoxy and polyester resins there are bio-based routes to their production, making them a more sustainable option; though it should be realised that both PVC and PE can be readily recycled.

Polyolefin elastomers (POE) and polyolefin plastomers (POP) are relatively new type of thermoplastic elastomer (TPE) developed in the 1990s. POE/POP are families of homogeneous ethylene-based or propylene-based random copolymer produced from single-site catalysts that bridged the performance gap between conventional polyolefins such as polyethylene and conventional elastomers like ethylene propylene diene monomer (EPDM). The density of POP is typically in the range of density of 0.886 to 0.912 g/cm3. Copolymer resins with lower density are called POE. Ethylene-

based POE/POP have 65–91% ethylene and 9–35% linear alpha-olefin (LAO). LAO such as butene-1, hexene-1, or octene-1 are used. Propylene-based POE typically have 70–90% propylene, 10–30% ethylene or butene. Most of these copolymers are produced by solution processes. POE/POP have garnered attention because of their low density, chemical resistance, processing advantages, good resilience without permanent deformation, applications in plastic recycling, and relatively low cost. Demand for POE/POP has grown at a significant rate. POE/POP's unique properties make them desirable for extruded products, and elastomeric foamed compound.

TPU is an attractive material because it imparts not only good elasticity to a polymer blend but good stain and abrasion resistance.

To establish range of performance of the blends data has been presented for fractions of polymer-to-elastomer at 80:20 and 20:80.

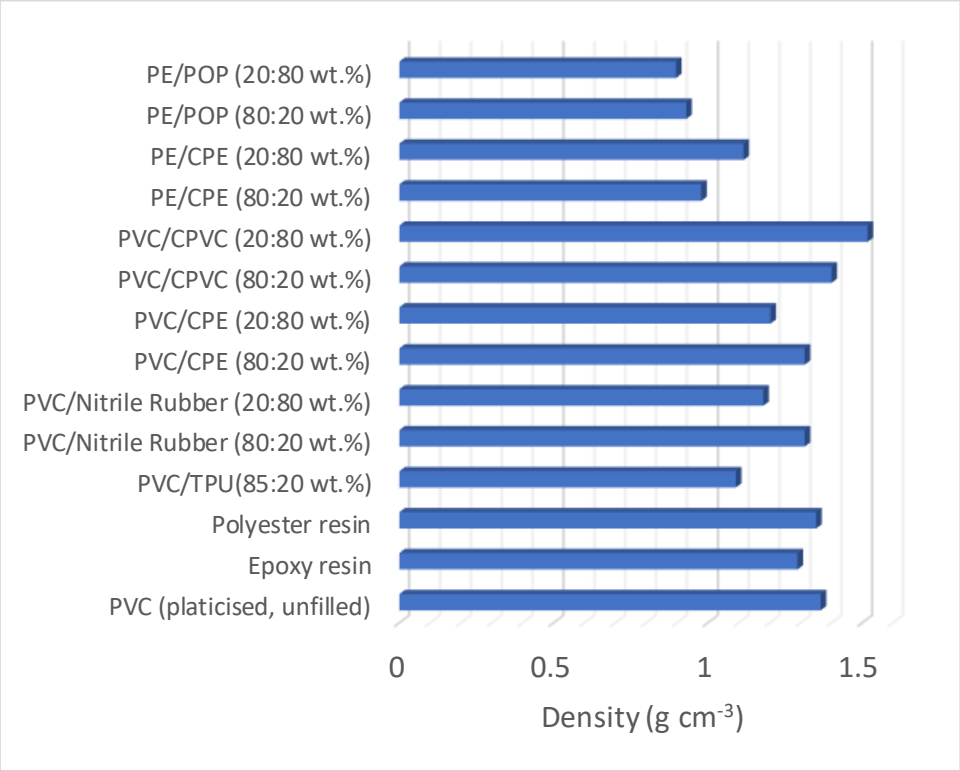

Figure 3.40 Density (g cm^{-3}) of polymers and polymer blends. Data obtained from a range of sources (commercial specification sheets, matmatch [100], matweb [101])

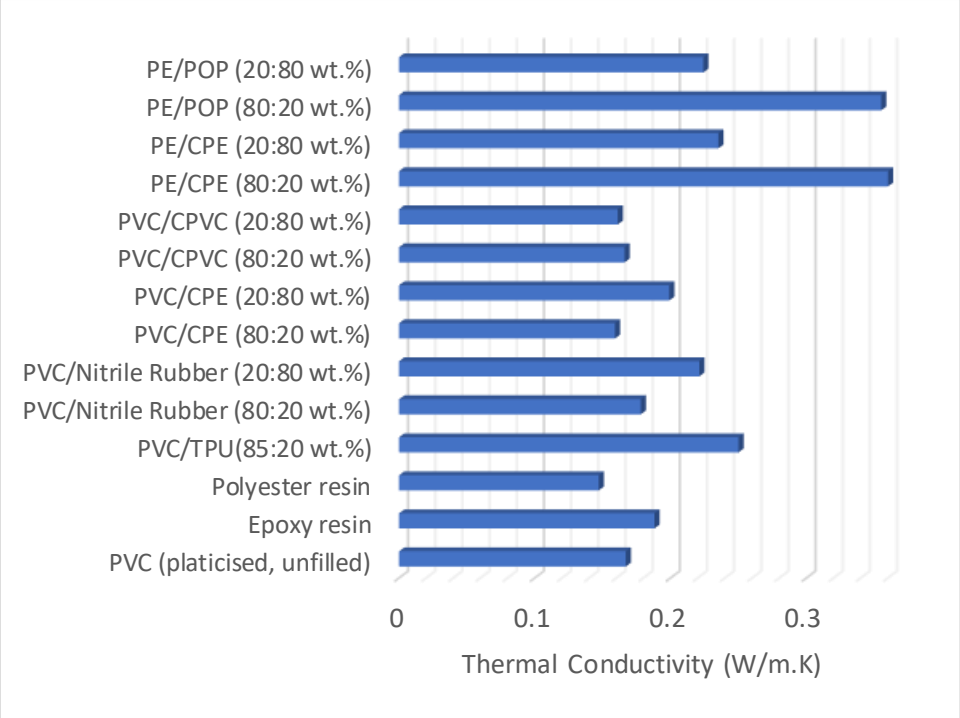

Figure 3.41 Thermal conductivity (W/m.K) of polymers and polymer blends. Data obtained from a range of sources (commercial specification sheets, matmatch [100], matweb [101])

The Ashby plots in subsequent figures map thermal conductivity against density.

A colour key to the data points is given below for **Figure 3.42**. The same trend in data points is observed in other figures so colour coding is not shown, except for the commercial PVC sample containing hollow glass spheres (red).

	PVC (commercial sample)
	PVC (lab sample)
	Epoxy resin
	Polyester resin
	PVC/TPU(85:15 wt.%)
	PVC/Nitrile Rubber (80:20 wt.%)
	PVC/Nitrile Rubber (20:80 wt.%)
	PVC/CPE (80:20 wt.%)
	PVC/CPE (20:80 wt.%)
	PVC/CPVC (80:20 wt.%)
	PVC/CPVC (20:80 wt.%)
	PE/CPE (80:20 wt.%)
	PE/CPE (20:80 wt.%)
	PE/POP (80:20 wt.%)
	PE/POP (20:80 wt.%)

Figure 3.42 and **Figure 3.43** illustrate that for IM16K there is a closer correlation between the samples made in the laboratory and commercial samples at 15 wt.% c.f. 24 wt.% addition. This suggests that the commercial samples, known to contain hollow glass microspheres, represent loadings skewed towards 15 wt.% of filler. As stated earlier for a given filler the same trend in the data for the range of polymers evaluated is seen. This is not surprising, given that 'rule of mixtures' was applied. Although data points demonstrate the range of properties for a given polymer matrix between 80:20 and 20:80 wt.% of polymer/elastomer, in reality practicable use is more likely to be at the 80:20 level. PE/POP and PE/CPE blends, irrespective of filler show a lower density but this is at the expense of higher thermal conductivity.

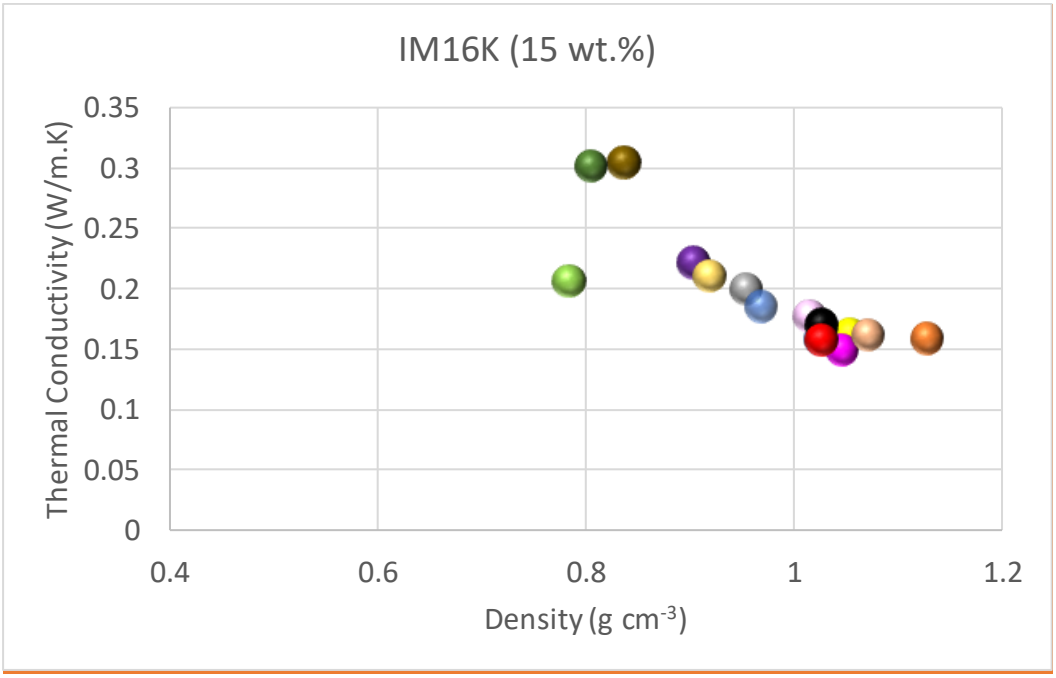

Figure 3.42 Thermal conductivity (W/m.K) versus density (g cm^{-3}) for composite polymers (listed in **Figs. 3.40 and 3.41**) with filler (IM16K) at 15 wt.%. Predicted data using from a range of sources (commercial specification sheets, matmatch [100], matweb [101])

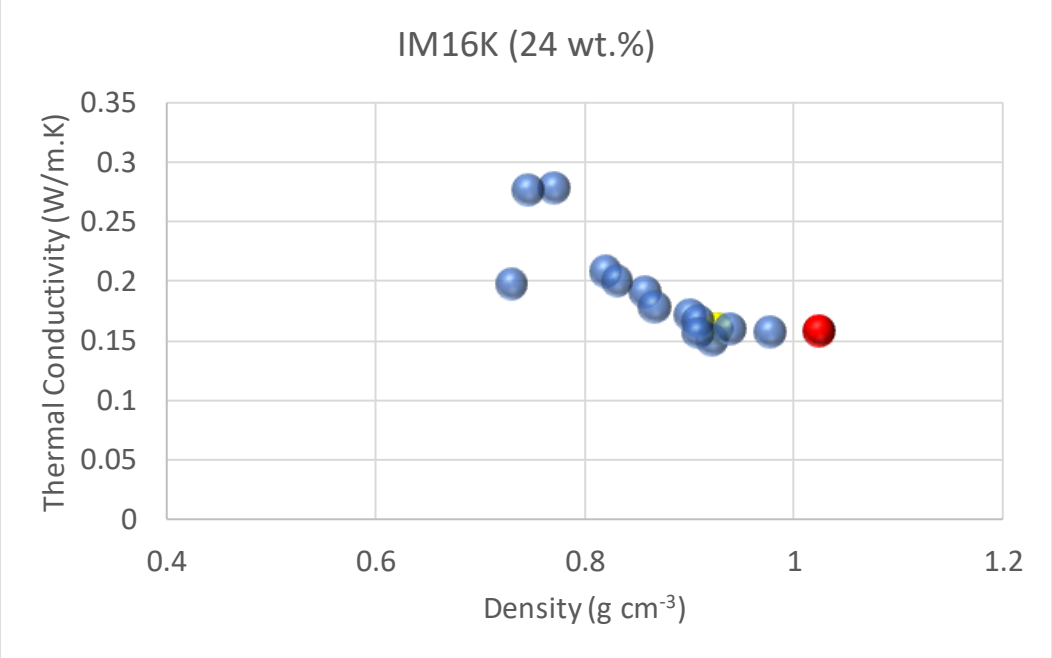

Figure 3.43 Thermal conductivity (W/m.K) versus density (g cm^{-3}) for composite polymers (listed in **Figs. 3.40 and 3.41**) with filler (IM16K) at 24 wt.%. Predicted data using from a range of sources (commercial specification sheets, matmatch [100], matweb [101])

Figure 3.44 shows that the data curves for larger particle, thinner wall hollow calcium carbonate are shifted to lower density *c.f.* hollow glass spheres (**Figure 3.42** and **Figure 3.43**), though the thermal conductivities are similar. Although it should be remembered that the crush strengths of the hollow spheres should be considered before further inferences are made.

Cork gives significantly improved properties (lower density and thermal conductivity) compared with most hollow fillers in this study (**Figure 3.45**). It has been reported that cork filled polyurethane composites (≤ 15 wt.%) of the type currently used in boat decking, have good wear resistance, and exhibit an increase in Youngs' modulus but decrease elongation at break. [111]. Although this material can be recycled it is more likely to be used in a secondary manufacturing process [112].

The Ashby plots for expandable microspheres are shown in **Figure 3.46** and **Figure 3.47**. At the lower density (0.025 g cm^{-3}) the expandable spheres exhibit a shift in both thermal conductivity and density to significantly lower levels. The value of expandable microspheres, such as those with a poly(acrylonitrile-*co*-methacrylonitrile) shell and a hydrocarbon core (blowing agent), has also been reported in the literature [113]. Such

plastic microspheres are commercially available so may present a short-term solution to achieve property gains and enhanced recyclability (while effective commercial scale inorganic hollow fillers are developed).

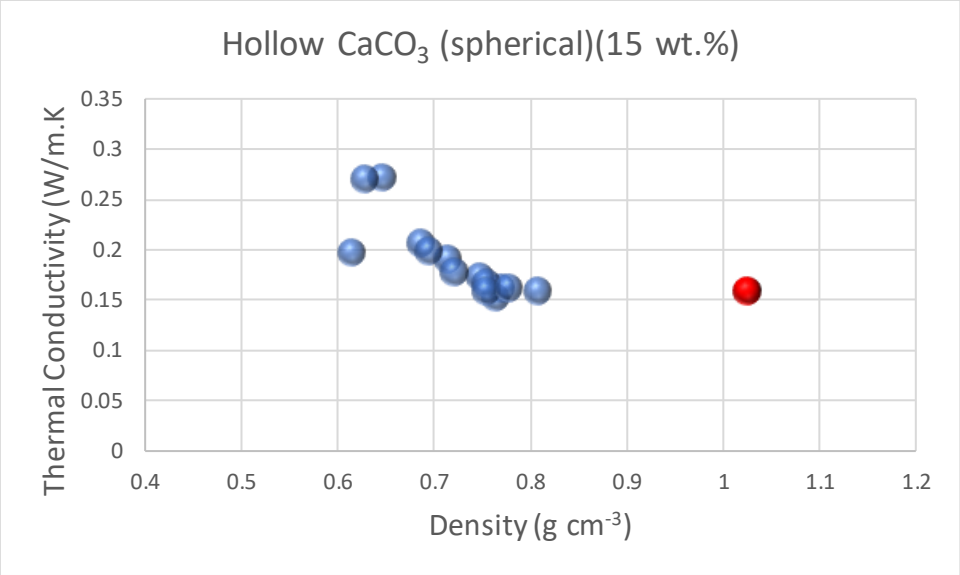

Figure 3.44 Thermal conductivity (W/m.K) versus density (g cm^{-3}) for composite polymers (listed in **Figs. 3.40 and 3.41**) with filler (spherical, hollow calcium carbonate) at 15 wt.%. Predicted data using from a range of sources (commercial specification sheets, matmatch [100], matweb [101])

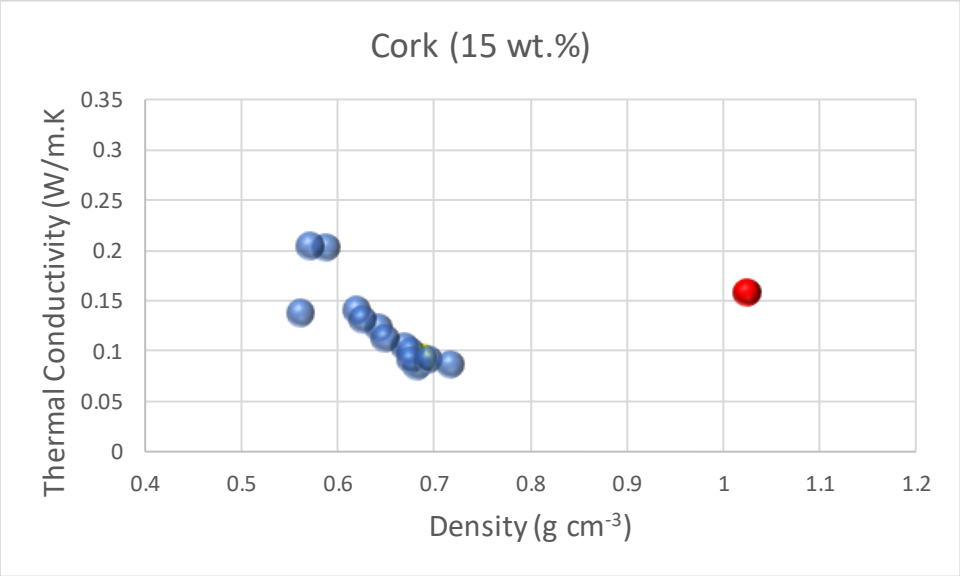

Figure 3.45 Thermal conductivity (W/m.K) versus density (g cm^{-3}) for composite polymers (listed in **Figs. 3.40 and 3.41**) with filler (cork) at 15 wt.%. Predicted data using from a range of sources (commercial specification sheets, matmatch [100], matweb [101])

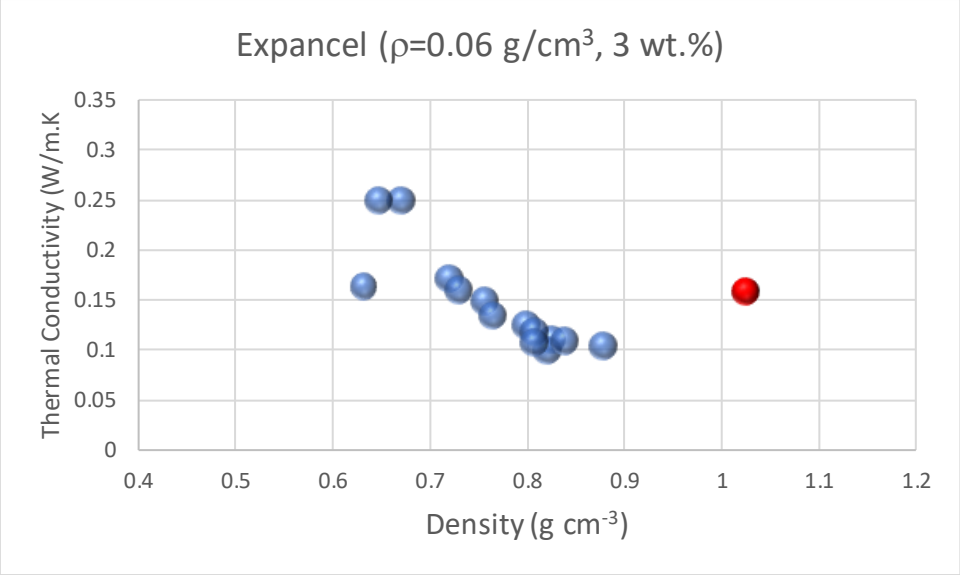

Figure 3.46 Thermal conductivity (W/m.K) versus density (g cm^{-3}) for composite polymers (listed in **Figs. 3.40 and 3.41**) with filler (Expancel (ρ=0.06 g/cm^3) at 3wt.%. Predicted data using from a range of sources (commercial specification sheets, matmatch [100], matweb [101])

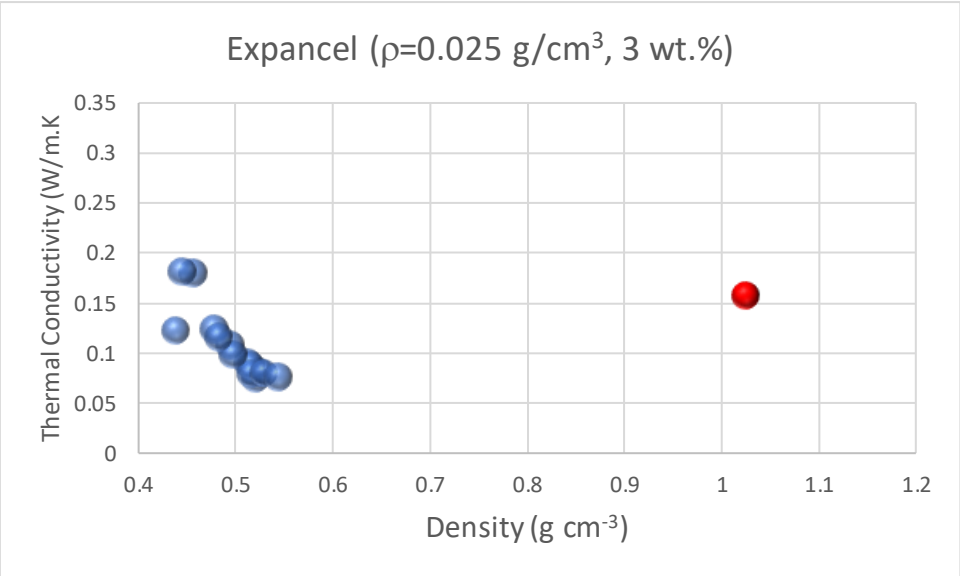

Figure 3.47 Thermal conductivity (W/m.K) versus density (g cm^{-3}) for composite polymers (listed in **Figs. 3.40 and 3.41**) with filler (Expancel (ρ=0.025 g/cm^3) at 3wt.%. Predicted data using from a range of sources (commercial specification sheets, matmatch [100], matweb [101])

4.0 Conclusions

In this study selected hollow fillers in several polymers and polymer blends were evaluated for use in composite boat decking. The focus of the study was to evaluate hollow calcium carbonate as an alternative to hollow glass microspheres, which are difficult to recycle and abrasive on processing equipment. Because hollow calcium carbonate is not in widespread commercial production, the hollow calcium carbonate was synthesised by templating with high molecular weight (400000-500000 g mol^{-1}), cationic polymer (PDADMAC or PDDA) to direct 3D assembly of hollow structures.

$CaCO_3$ microparticles were successfully synthesised by application of a high molecular weight 400,000-500,000 g mol^{-1}) PDDA as a molecular template. By controlling temperature, mixing time, and concentrations of components the precipitation reaction could be optimised to generate hollow particles with micron-sized dimensions (2-4 μm). It was inferred that the particles have hollow cavities from SEM images, though this requires further confirmation from TEM (transmission electron microscopy). The SEM images do support the presence of hollow 'apple core' cavities, which suggest that the vaterite and calcite polymorphs (spherical and rhombohedral) have a relatively thick, porous shell. Microspheres subjected to calcination for 4 hours at 550°C, formed the thermodynamically stable calcite phase (hollow rhombohedral crystals, 4-6 microns diameter).

Inclusion of the calcined micron-sized hollow calcium carbonate at 15 wt.% and 24 wt.% in plasticised PVC formulations gave mechanical properties in the range accepted for current commercial formulations containing hollow glass microspheres. Furthermore, the use of calcium carbonate improved the thermal stability of the composites. However, the density of the PVC composite containing the rhombohedral calcite was higher that of PVC composites containing hollow glass spheres (IM16K). Because shell thickness and cavity dimensions influence density, a factorial experimental design is required to synthesise particles with optimal properties (to balance particle size, cavity dimensions, wall thickness and crush density).

The experimental data has been supported by theoretical predictions of density and thermal conductivity values for a range of fillers [spherical and rhomboidal calcium carbonate, hollow glass spheres (IM16K, IM30K), cork and, expandable microspheres

(with densities 0.06 g cm^{-3} and 0.025 g cm^{-3})], polymers and polymer blends [epoxy and polyester resins, nitrile rubber, thermoplastic polyurethane (TPU), chlorinated polyethylene (CPE), chlorinated PVC (CPVC)]. Data was assimilated at 15 wt.% and 24 wt.% additions (except for the expandable microspheres, where data was calculated at the more realistic 3 wt.% levels of addition). Ashby plots of thermal conductivity versus density showed that the most significant improvements in lowering thermal conductivity and density were obtained by the addition of cork and, expandable microspheres. Curves with similar characteristics were obtained for the polymers demonstrating further refinement of properties could be obtained by changing the polymer matrix. This could then provide additional benefits of improved elasticity, stain resistance and reduced abrasion.

Of interest is that theoretical data predicts that hollow spherical calcium carbonate shows intermediate density and thermal conductivity values between the hollow glass spheres, cork, and expanded microspheres. This suggests that combinations of different hollow fillers could be used to improve recyclability. The addition of hollow calcium carbonate, rather than hollow glass spheres, is likely to widen the scope for optimisation of properties of PVC. Because calcium carbonate is the common filler in most PVC applications there is the opportunity balance mechanical properties and density by partially replacing solid particulate calcium carbonate (GCC or PCC) with hollow calcium carbonate. More control to tailor properties could encompass enhanced productivity by faster cooling rates from the melt and lead to better dimensional stability and reduced thermal conductivity. All this could be possible with only minor modifications to existing equipment.

.

5.0 Recommendations for Future Work

Although the hollow calcium carbonate synthesised in this study has revealed its potential as a hollow filler in PVC, when compared with hollow glass spheres, alternative hollow spheres warrant further inspection. Initial experimental results lend value to the data calculated and presented in the Ashby charts. However, this requires further validation. Given the large number of samples that could be screened as potential decking materials, the number of experiments needs limiting by application of factorial experimental design. Here key properties should include hardness and abrasion resistance in addition to thermal conductivity, density, and mechanical properties. In particular, the types of expandable microspheres should be extended to different densities and materials to facilitate incorporation in alternative base polymers to PVC. This would give flexibility in responding to market demands and constraints.

In addition to hollow calcium carbonate, other inorganic hollow spheres have been synthesised and evaluated including SiO_2 [114] and TiO_2 [115]. There would be value in adding these to the list of fillers to be assessed. Coated solid particle titanium dioxide (rutile) is already used in rigid PVC applications (window profiles and pipes). Hence, the possibility to combine hollow TiO_2 for light-weighting, along with the transfer of the hollow calcium carbonate technology to other PVC applications presents itself.

Another possibility is a mixture of glass and plastic microspheres. It has been reported that such hybrid materials can incorporate high filler fractions, which could be cost competitive on a volume basis with those currently used in decking [116]). Furthermore, this would reduce abrasion on processing equipment.

Although hollow calcium carbonate spheres have been synthesised in this project using a templating method a full-cost-benefit analysis should be undertaken, comparing methods of production (e.g., carbon dioxide bubbling). Also, the calcium carbonate incorporated in the PVC formulations was calcined prior to addition. This resulted in a transition from vaterite/calcite spherical particles to rhombohedral calcite. The experiment should be repeated incorporating the calcium carbonate without calcination. Although calcination was undertaken to remove the template or species that had not reacted from the particle core, and to facilitate compatibility with the

polymer matrix, a temperature below the calcination temperature (<550^{o}C) could be used to achieve this.

In addition, increased compatibility between the filler and polymer matrix may be improved by addition of a coupling agent. The experiments could be quickly repeated for the PVC formulations used in this study adding the titanate coupling agents that are used commercially to enhance compatibility between PVC and calcium carbonate (GCC and PCC) fillers. Such coupling agents are also likely to be effective when hollow glass spheres are used.

In summary a preliminary assessment of the potential of alternative decking materials has been achieved in this study, but a more systematic assessment with a view to short term, medium term, and long-term development of the composites in boat decking should be undertaken.

References

1. C. Chen and L. Hu, *Adv. Mater.* 2021, **33**, 28**,** 200289
2. *Ibid.,* Ref 1., 200291
3. M.M.Aung, *Forestry in Myanmar*, Forest Department, Yangon, Myanmar (2000)
4. B. Meakins, *Practical Boat Owner*, March 1, 2016
5. R. Holmes, *Yachting World*, May 7, 2020.
6. K. Crouvisier-Urion, J. Chanut, A. Lagorce, P. Winckler, Z. Wang, P. Verboven, B. Nicolai, J. Lherminier, E. Ferret, R.D.Gougeon, J.-P. Bellat, and T. Karbowiak, *Nature Scientific Reports*, (2019) 9:19682
7. L. Gil, *Frontiers in Materials*, January 2015, Volume 1, Article 38.
8. J. Sierra-Pérez, J. Boschmonart-Rives, X. Gabarrell, *Resources, Conservation and Recycling* 98 (2015) 55–66
9. AquaCork® Marine Decking | Cork Decking with grooves | Jelinek Cork (corkstore.com)
10. C. Woodward, Foam Boat Decking Advantages, *SaltWater Sportsman*, Feb 4, 2022
11. *Ibid.,* Ref 5.
12. G. Wypych, *PVC Formulary* (3rd Edn.), ChemTec Publishing 2020, ch. 4, pp95-363
13. *PVC's physical properties*, PVC Forum: South East Europe (seepvcforum.com), 2010
14. *Particle Shape*, Functional Fillers & Specialty Minerals for Plastics (phantomplastics.com), 2020
15. *Properties of Common Functional Fillers*, Functional Fillers & Specialty Minerals for Plastics (phantomplastics.com), 2020
16. N.A.S. Fernando and N.L. Thomas, *Journal of Vinyl and Additive Technology* 13(2), 2007
17. R.N. Rothon (ed.), *Particulate-Filled Polymer Composites (2nd Edition)*, Rapra Technology, 2003, p.18
18. P.H.T. Vollenberg and D. Heikens, *Polymer*, 1989, **30**, 9, 1656.
19. J. Feng, S.R. Venna, D.P. Hopkinson, *Polymer* 103 (2016) 189 -195

20. Soo-Bok Jeong, Young-Cheol Yang*, Young-Bae Chae and Byoung-Gon Kim, *Materials Transactions*, Vol. 50, No. 2 (2009) pp. 409 to 414

21. R.N. Rothon (ed.), *Particulate-Filled Polymer Composites (2nd Edition)*, Rapra Technology, 2003, p.399

22. P.M. Angelopoulos, M. Taxiarchou, I. Paspaliaris, *3rd International Conference on Competitive Materials and Technology Processes* (IC-CMTP3), IOP Publishing, IOP Conf. Series: Materials Science and Engineering 123 (2016) 012061. doi:10.1088/1757-899X/123/1/012061

23. 3m-glass-bubbles-brochure.pdf, 2018, p10

24. https://multimedia.3m.com/mws/media/625138O/3mtm-glass-bubbles-im30k-hyundai-mobis-appl-info.pdf

25. K. Wood, *Composites World*, 4/1/2008, https://www.compositesworld.com/articles/microspheres-fillers-filled-with-possibilities, updated 3/31/2020

26. S. Shira and C. Buller, in *Hollow Glass Microspheres for Plastics, Elastomers and Adhesive Compounds*, (Eds S.E. Amos and B. Yalcin), Elsevier 2015.

27. S.E. Amos, B. Yalcin, A. D'Souza, and I.S. Gunes, , 3M™ Technical Paper 11835 Glass Bubbles, 3M™ Science Applied to Life, Fig. 5, p.3.

28. https://www.plasticstoday.com/materials/nouryon-will-build-us-polymerization-plant-e

29. M.F. Ashby, *Materials Selection in Mechanical Design*, 5th Edition, Elsevier, 2016.

30. M.F. Ashby*, Granta CES Edupack 2010* (2010), Granta Design Ltd., Cambridge, UK., Chart 3, p8. https://www.grantadesign.com/download/pdf/booklets/Material_and_Process_Property_Charts.pdf

31. https://polymerdatabase.com/polymer%20physics/Stress-Strain%20Behaviour.html

32. https://www.doitpoms.ac.uk/tlplib/polymers/stress-strain.php

33. S. Wu, *J. of Appl. Poly. Sci.*, Vol 46, pages 619-624 (1992)

34. *Ibid.* Ref. 30., Chart 1, p6.

35. *Ibid.* Ref. 30., Chart 2, p7.

36. *Ibid.* Ref. 30., Chart 9, p14.

37. Y. Agari and T. Uno, *Journal of Applied Polymer Science*, Vol. 32, 5705-5712 (1986)

38. S. Zhai, P. Zhang, Y. Xian, J. Zeng, B. Shi, *International Journal of Heat and Mass Transfer* 117 (2018) 358–374

39. *Ibid.* Ref. 30., Chart 10, p15.

40. *Ibid.* Ref. 30., Chart 14, p19.

41. *Ibid.* Ref. 30., Chart 15a, p20.

42. Ibid. Ref 5.

43. A. Barrett, *Bioplastics News*, October 23, 2019

44. K. Hong, Q. Sun, X. Zhang, L. Fan, T. Wu, J. Du, and Y. Zhu, *ACS Sustainable Chem. Eng*. 2022, 10, 1036−1046

45. Solmaz Maleki Dizaj, Mohammad Barzegar-Jalali , Mohammad Hossein Zarrintan , Khosro Adibkia , Farzaneh Lotfipour , *Pharmaceutical Sciences*, March 2015, **20**, 175-18, Figure 1 page 176.

46. P. Bots, L.G. Benning, J.-D. Rodriguez-Blanco, T. Roncal-Herrero, S. Shaw, *Cryst. Growth Des.* **2012**, 12, 3806–3814.

47. R. Salomão, L.M.M. Costa, G.M. Olyveira, *Adv. Tissue Eng. Regen. Med.,* **2017**, 3.

48. Y. Boyjoo, V.K. Pareek, and J. Liu, *Journal of Materials Chemistry A,* Issue 35, 2014

49. J. Aizenberg, G. Lambert, S. Weiner, and L. Addadi, Vol. 124, No. 1, 2002, *J. Am. Chem. Soc.* 32-39

50. G. W. Yan, J. H. Huang, J. F. Zhang and C. J. Qian, *Mater. Res. Bull.*, 2008, 43, 2069–2077.

51. L. Qi, J. Li and J. Ma, *Adv. Mater*., 2002, 14, 300.

52. X. Ji, G. Li and X. Huang, *Mater. Lett.*, 2008, 62, 751–754.

53. L. Zhao and J. Wang, *Colloids Surf. A*, 2012, 393, 139–143.

54. J. Yu, X. Zhao, B. Cheng and Q. Zhang, *J. Solid State Chem.*,2005, 178, 861–867.

55. J. T. Han, X. Xu and K. Cho, *J. Cryst. Growth*, 2007, 308, 110–116.

56. A. W. Xu, Q. Yu, W. F. Dong, M. Antonietti and H. C¨olfen, *Adv. Mater.*, 2005, 17, 2217–2221.

57. T. Zheng, H. Yi, S. Zhang and C. Wang, *Journal of Crystal Growth*, 549 (2020) 125870

58. *Ibid.,* Ref 57.

59. *Ibid.*, Ref 57.

60. Y. Kojima, T. Yasue, J. Soc. Inorg. Mater. Jpn. 10 (2003) 78 (in Japanese).

61. H. Watanabe, Y. Mizuno, T. Endo, X. Wang, M. Fuji and M. Takakashi, *Advanced Powder Technology*, 20 (2009) 98-93

62. G. Hadiko, Y.S. Han, M. Fuji, M. Takahashi, *Materials Letters* 59 (2005) 2519 – 2522

63. *Ibid*., Ref 62, Figure 4

64. *Ibid*., Ref 62, Figure 1

65. Y. Wang, Y. X. Moo, C. Chen, P. Gunawan and R. Xu, *J. Colloid Interface Sci*., 2010, 352, 393–400.

66. H. Tang, J. Yu, X. Zhao and D. H. L. Ng, *J. Alloys Compd*., 2008, 463, 343–349.

67. S.C. Huang and Y. Chujo, *Polymer Journal*, Vol. 40, No.2, pp 154-162 (2008)

68. *Ibid.*, 67

69. M. Lei, W. H. Tang, L. Z. Cao, P. G. Li and J. G. Yu, J. *Cryst. Growth*, 2006, 294, 358–366.

70. P. Bots, L.G. Benning, J.-D. Rodriguez-Blanco, T. Roncal-Herrero, S. Shaw, *Cryst. Growth Des*. **2012**, 12, 3806–3814.

71. D.B. Trushina, T.V. Bukreeva, M.V. Kovalchuk, M.N. Antipina, *Mater. Sci. Eng. C* **2014**, 45, 644–658.

72. R. Sevcik, P. Sasek, and A. Viani, *J Mater Sci* (2018) 53:4022–4033

73. G. Wypych, Handbook of Fillers (Fourth Edition), ChemTec Publishing, 2016, Pages 303-371, ch. 5 - Physical Properties of Fillers and Filled Materials, 5.1. Density

74. *Ibid*., 5.7. Porosity

75. P.J. Yoo, N.S. Zacharia, J. Doh, K.T. Nam, A.M. Belcher, P.T. Hammond, *ACS Nano* 2008, 2, 561–571.

76. Guo, Y.; Geng, W.; Sun, J. *Langmuir* 2009, 25, 1004–1010.

77. K. Tang, N.A.M. Besseling, *Soft Matter* 2015, 12, 1032–1040.

78. S. Fujita, S. Shiratori, *Nanotechnology* 2005, 16, 1821–1827

79. J. Fu, J.B. Schlenoff, *J. Am. Chem. Soc.* 2016, 138, 980–990.

80. M. Akhondi, E. Jamalizadeh, *Ceramics International* 47 (2021) 851–857

81. D.J. Belton, S.V. Patwardhan, V.V. Annenkov, E.N. Danilovtseva, and C.C. Perry, *PNAS*, 2008, vol. 105, no.165963–5968,

82. Q. Meng, S. Xiang, K. Zhang, M. Wanga, Xinyuan Bu, P. Xue, L. Liu, H. Sun, B. Yang, *Journal of Colloid and Interface Science* 384 (2012) 22–28

83. D. Konopacka-Łyskawa, B. Koscielska, J. Karczewski, A. Gołabiewska, *Materials Chemistry and Physics* 193 (2017) 13-18

84. A. L. Goodwin, F. M. Michel, B. L. Phillips, D. A. Keen, M. T. Dove and R. J. Reeder, *Chem. Mater.*, 2010, **22**, 3197–3205

85. F. Manoli, S. Koutsopoulos, E. Dalas, *Journal of Crystal Growth* 182 (1997) 116-124

86. M. Suzuki, H. Nagasawa, and T. Kogure, *Crystal Growth & Design*, Vol. 6, No. 9, 2006

87. J. Chen, S.R. Kline, Y. Liu, *J Chem Phys*, 2015 Feb 28;142(8):084904

88. B. Myszka, M. Schußler, K. Hurle, B. Demmert, R. Detsch, A.R. Boccaccini, and Stephan E. Wolf, *RSC Adv*., 2019, 9, 18232–18244

89. J.D. Rodriguez-Blanco, S. Shaw, and L.G. Benning, *Nanoscale*, 2011, 3, 268

90. N. Nassrallah-Aboukaïs, J. Jacquemin, C. Decarne, E. Abi-Aad, J.F. Lamonier and A. Aboukaïs, *Journal of Thermal Analysis and Calorimetry*, 74(1), 21-27, 2003

91. T.S. Chow, *Journal of Materials Science*, 1980, **15**, 8, 1873.

92. G. Gibson in *Polypropylene Structure Blends and Composites*, *Volume 3: Composites*, Ed., J. Karger-Kocsis, Chapman and Hall, London, UK, 1995,

93. H. Roshanaei, F. Khodkar, M. Alimardan, *Iranian Polymer Journal* (2020) 29:901–909

94. K.B. Bommegowda, N.M. Renukappa, and J. Sundara Rajan Techno-Societal 2020 pp 637–648, Springer

95. P.H.T. Vollenberg and D. Heikens, *Polymer*, 1989, **30**, 9, 1656.

96. B. Pukánsky, J. Kolarik and F. Lednicky, *Polymer Composites: Proceedings of the 28th Microsymposium on Macromolecules*, Prague, Czechoslovakia, 1985, **67**, 553.

97. H.P. Schreiber and F. St.Germain in *Acid-Base Interactions: Relevance to Adhesion Science and Technology*, (Eds., K.L. Mittal and H.R. Anderson, Jr.), VSP, Utrecht, The Netherlands, 1991, 273.

98. J.-Z. Liang, *Macromol. Mater. Eng*. 2002, 287(9), 588–591

99. L. Nicolais, M. Narkis,Polym. Eng. Sci.1971,11, 194.

100. https://matmatch.com; How to Use Matmatch - User Guide

101. Online Materials Information Resource - MatWeb

102. George Wypych, *PVC Degradation and Stabilization*, 3rd Edn., ChemTec Publishing, 2013

103. N. Guermazi, N. Haddar, K. Elleuch, H.F. Ayedi, Polymer Composites, 2016, 2171 – 2183

104. J. Tomaszewska, T. Sterzynski, and D. Walczak, *Polymers 2021*, 13, 2057. https://doi.org/10.3390/polym13132057

105. Jean C. Chauffoureaux, Pure & Appi. Chem., Pergamon Press Ltd. 1979, Vol. 51, pp.1123—1147

106. M. Rusu and D. Rusu, Handbook of Polymer Blends and Composites. Vol. 4a (pp.73-119), 2003, RAPRA Technology Press (Eds: C. Vasile, A.K. Kulshereshtha)

107. R.D. Maksimov, T. Ivanova, J. Zicans, S.N. Negreeva, and E. Plume, *Materials Research Innovations,* **volume 7**, pages326–330 (2003)

108. G.M. Shashidhara, K.G. Pradeepa, R. Goel, R. Bharath, A D. Rao, and R. Abhilash**,** *Material Science Research India* Vol. 7(2), 457-466 (2010)

109. N.L. Thomas and R.J. Harvey, *Progress in Rubber, Plastics and Recycling Technology*, Volume 17, Issue 1, 2001.

110. M. Bani-Hani, D. Banu, J. Campanelli, D. Feldman, *Journal of Applied Polymer Science*, Vol. 74, 1156–1168 (1999)

111. S. Oprea, *Journal of Composite Materials*, Volume 42, Issue 25, 2008.

112. B. Malchiodi, R. Marchetti, L. Barbieri and P. Pozzi, *Appl. Sci*. 2022, 12, 3844.

113. M. Jonsson, O. Nordin, A. Larsson Kron, E. Malmstrom, *Journal of Applied Polymer Science*, Vol. 117, 384–392 (2010)

114. M. Fuji, Y.S. Han and C. Takai, *KONA Powder and Particle Journal*, No. 30 (2013)

115. Y. Bao, Q.L. Kanga, J.Z. Maa, C. Liu, *Ceramics International* 43 (2017) 8596–8602

116. M.E. Curd, N.F. Morrison, M.J.A. Smith, P. Gajjar, Z. Yousaf, W.J. Parnell, *Composites Part B* 223 (2021) 108952.

Appendix

(a)

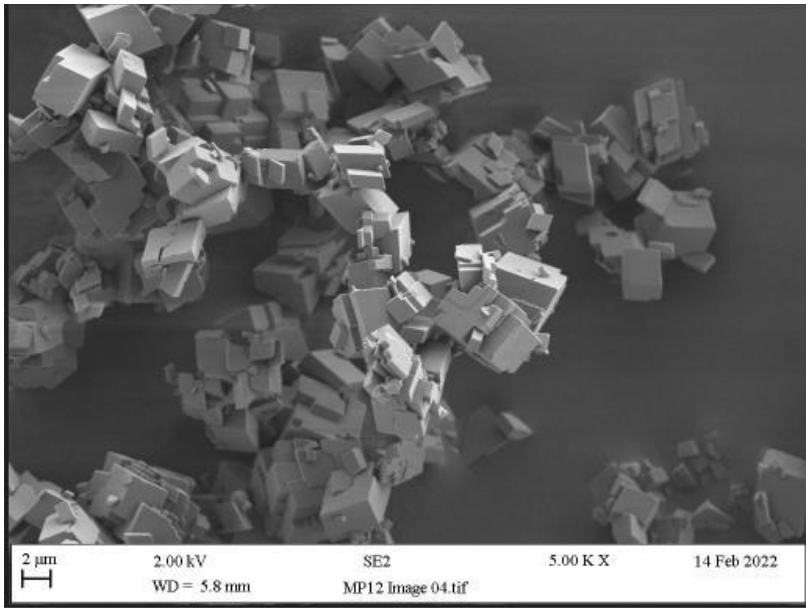

(b)

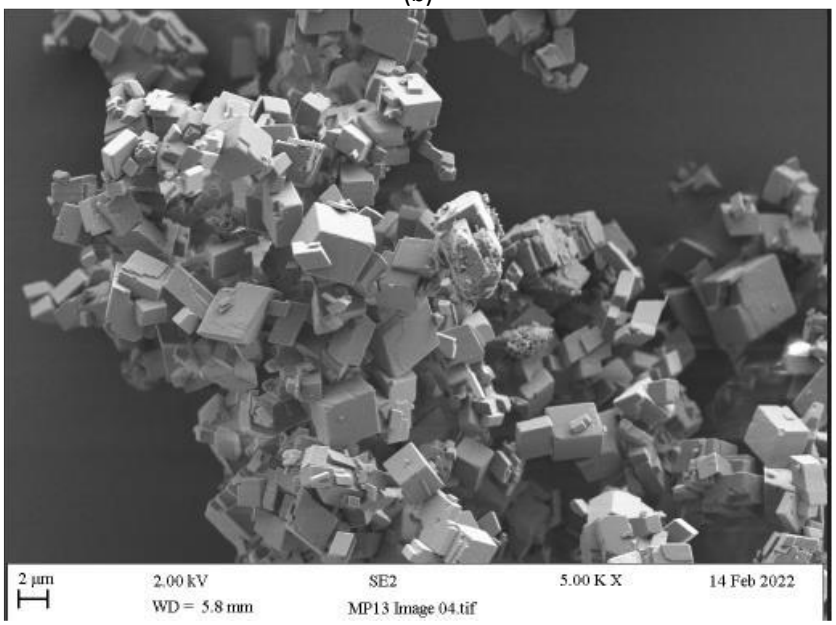

Appendix 1 SEM images of samples **MP12** (a) and **MP13** (b) (see **Table 2.1**)